9-1-2001

Analytical Investigation of Assumptions used to Design the SR 33 Lehigh River Bridge

Brian J. Santosuosso

Stephen P. Pessiki

Follow this and additional works at: http://preserve.lehigh.edu/engr-civil-environmental-atlss-reports

ANALYTICAL INVESTIGATION OF ASSUMPTIONS USED TO DESIGN THE SR 33 LEHIGH RIVER BRIDGE

by

Brian J. Santosuosso

Stephen Pessiki

ATLSS Report No. 02-08

September 2002

ANALYTICAL INVESTIGATION OF ASSUMPTIONS USED TO DESIGN THE SR 33 LEHIGH RIVER BRIDGE

by

Brian J. Santosuosso
Graduate Research Assistant
Civil and Environmental Engineering

Stephen Pessiki
Associate Professor
Civil and Environmental Engineering

ACKNOWLEDGEMENTS

TABLE OF CONTENTS

v

LIST OF TABLES

LIST OF FIGURES

xiii

ABSTRACT

The SR 33 Lehigh River Bridge located in eastern Pennsylvania is a composite deck truss structure. The truss chords were provided with shear studs to allow composite action with the rest of the deck structure. This construction technique is unique to this bridge. Researchers at Lehigh University's Center for Advanced Technology for Large Structural Systems conducted a series of experimental controlled load tests on this bridge. In the current work, a series of analyses were performed on the bridge structure. The design assumptions, experimental results, and analytical results are correlated to better understand the actual behavior of the bridge, and to evaluate the validity of the design assumptions. This research resulted in three main findings. First, the AASHTO distribution factors used to determine the lateral load distribution on the bridge deck were found to be conservative with respect to the stringers incorporated into the composite bridge deck structure. Second, local out-of-plane bending stresses exist in the diagonal truss members of the SR 33 Lehigh River Bridge. The stresses are low in magnitude, but are significant relative to the live load in-plane bending and axial stresses, sometimes representing as much as 50% of the axial stress value. Finally, the entire composite deck structure in the negative moment region of the truss system above Pier 2 was found to be effective in carrying global load cases placed at the center of Span 2. This was observed as an evenly distributed tension strain and the resulting stress distribution on all members in the cross-section.

1

CHAPTER 1
INTRODUCTION

1.1 INTRODUCTION

The Lehigh River Bridge was erected in eastern Pennsylvania as part of a three-mile extension of SR 33, connecting the roadway to I-78. The bridge is a deck truss construction containing two truss lines. The bridge was opened to traffic in January 2002. Figure 1.1 is a photograph of the completed bridge.

URS Corporation designed the structure in a unique fashion, connecting the reinforced concrete deck to the upper chords of the trusses with shear studs to cause the deck to act compositely with the trusses. Other aspects of the design were the same as for other structures.

Researchers at Lehigh University's Center for Advanced Technology for Large Structural Systems (ATLSS) conducted controlled load testing on the structure to gather data on the bridge's behavior.

This report describes a series of analyses that were performed on the bridge structure. The design assumptions, experimental results, and analytical results are compared in order to better understand the actual behavior of the structure and to evaluate the validity of the design assumptions. This will allow designers to more efficiently design similar bridges in the future.

1.2 OBJECTIVE

The objective of this research is to evaluate some of the key assumptions used in the design of the SR 33 Lehigh River Bridge and report on their validity. This is accomplished by comparing the design assumptions used by URS Corporation, the results of experimental controlled load testing performed by researchers at the ATLSS Center, and the results of analytical studies performed in this research.

1.3 APPROACH

This research compares two major design assumptions and offers conclusions about the same. The first design assumption concerns the lateral distribution of loads placed on the bridge deck and the effects that these loads have on the supporting stringers and upper chord members of the trusses. This relates to the issue of lateral load distribution factors. The analytical work related to this topic is presented in Chapters 4 and 5. A comparison among the design assumption, experimental results, and analytical work is presented in Chapter 6.

The second design assumption concerns the use of a two-dimensional truss model for the design of the truss structure. Two ramifications of this design assumption are studied. The first relates to out-of-plane bending stresses in the diagonal truss members. The analytical work related to this topic is presented in Chapter 5. A comparison among the design assumption, experimental results, and analytical work is presented in Chapter 6.

The second ramification concerns the global participation of the composite deck and stringers positioned over the bridge piers in the negative moment

region of the truss. This relates to the issue of effective deck width. The analytical work related to this topic is presented in Chapter 5. A comparison among the design assumption, experimental results, and analytical work is presented in Chapter 6.

1.4   SUMMARY OF FINDINGS

This research resulted in three main findings. First, the AASHTO distribution factors used to determine the lateral load distribution on the bridge deck were found to be conservative with respect to the stringers incorporated into the composite bridge deck structure. Second, local out-of-plane bending stresses exist in the diagonal truss members of the SR 33 Lehigh River Bridge. The stresses are low in magnitude, but are significant relative to the live load in-plane bending and axial stresses, sometimes representing as much as 50% of the axial stress value. Finally, the entire composite deck structure in the negative moment region of the truss system above Pier 2 was found to be effective in carrying global load cases placed at the center of Span 2. This was observed as an evenly distributed tension strain and the resulting stress distribution on all members in the cross-section.

1.5   OUTLINE OF REPORT

Chapter 2 presents background information, including a further description of the design assumptions that are addressed, and a description of the bridge geometry and layout. A discussion of important controlled load test experimental results is presented in Chapter 3. Chapter 4 describes in detail the construction of the analytical *lateral load distribution model.* A convergence study regarding finite element mesh refinement and the number of deck sections required to accurately produce local results is also presented. Chapter 4 also presents the results obtained from the lateral load distribution model. The analytical model presented in Chapter 4 is referred to in this report as the *lateral load distribution model.* Chapter 5 describes in detail the construction of the analytical *full bridge model.* It also contains a comparison of results between the lateral load distribution model and the full bridge model. Lastly, Chapter 5 contains the results from the full bridge model that are related to the design assumptions presented in Chapter 2. The analytical model presented in this chapter is referred to in this report as the *full bridge model.* Chapter 6 revisits each design assumption and compares the design assumption, experimental results, and analytical results. Chapter 7 presents the conclusions of this research and provides a list of topics for future work.
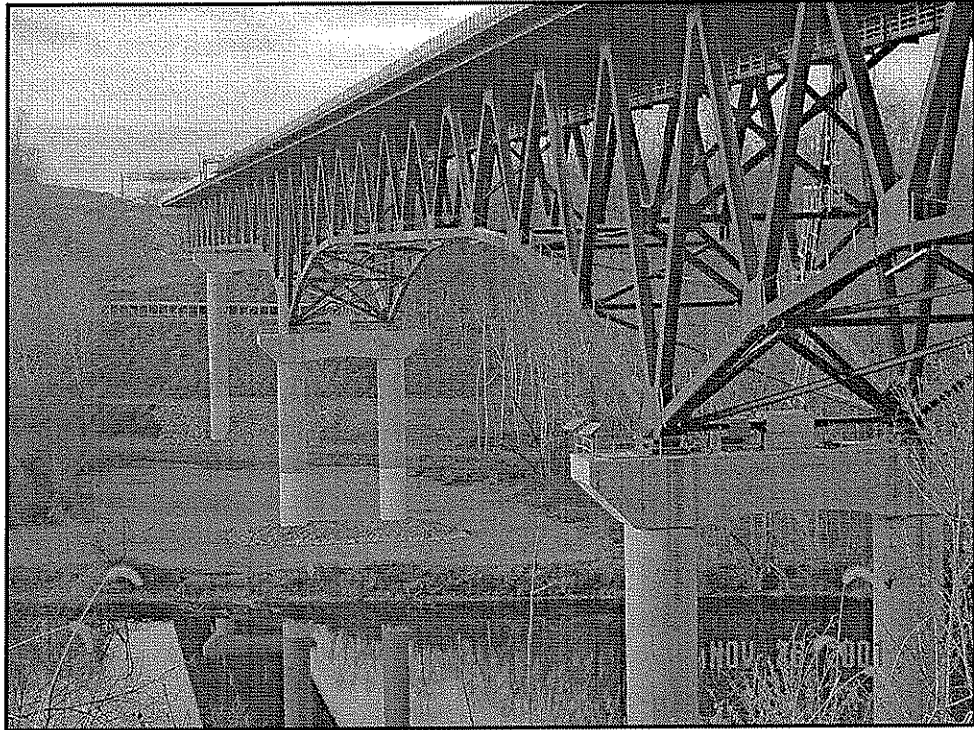
Figure 1.1. Photograph of the completed SR 33 Lehigh River Bridge – view looking north.

4

CHAPTER 2
BACKGROUND

2.1   INTRODUCTION

This chapter contains background information related to this research. Section 2.2 describes the geometry of the SR 33 Lehigh River Bridge. This is followed by Section 2.3, which discusses the key assumptions used to design the bridge and studied in this research. Section 2.4 reviews previous research regarding how to model composite action of a bridge deck using finite elements. Finally, Section 2.5 describes the specific capabilities of the finite elements used in this research. This chapter is intended to describe the bridge and deck superstructure, discuss the major design assumptions incorporated into this structure, give a brief overview of previous finite element models pertinent to this research, and explain the capabilities of the specific finite elements used in the analyses presented in this report. This is the foundation upon which the rest of the report is built.

2.2   DESCRIPTION OF THE BRIDGE

The SR33 Lehigh River Bridge is a four-span continuous deck truss comprised of two longitudinal weathering steel trusses (running in the north-south direction) and a reinforced concrete deck. Figure 2.1 is a photograph of the bridge looking north. This view shows the west truss as the near truss and the east truss as the far truss. Traffic flows toward the north on the east side of the bridge and toward the south on the west side of the bridge. The closest pier in the photograph is Pier 2. Piers 3 and 4 can be seen in the distance, numbered sequentially as distance from the viewer increases.

Figure 2.2 is an elevation drawing of the bridge looking west. From south to north (left to right), Spans 1 and 3 are both 432 ft. long, Span 2 (the main span over the Lehigh River) is 594 ft. long, and Span 4 is 270 ft. long. Each panel point, or point of intersection among truss members, is 54 ft. in distance from the next panel point longitudinally. Upper panel points are described with notation beginning with a U and lower panel points are described with notations beginning with an L. For instance, U1 is an upper panel point, and L1 is a lower panel point. The depth of truss between the upper and lower panel points varies from 36 ft. at the center of the spans to 72 ft. at Piers 2 and 3. The bridge's southern approach is also depicted in this figure as the span between Abutment 1 and Pier 1A. This short approach span is not considered in any portion of this report but is shown in the figure for completeness. Piers 1A and 1B are shown in the same location because they are separate structures but are directly adjacent to each other.

Figure 2.3 is a cross-section view of the bridge. The bridge is 80 ft.-10½ in. wide for Spans 2 through 4, and for most of Span 1. This width provides for a 4 ft. inside shoulder, two 12 ft. lanes, and a 10 ft. outside shoulder in each traveling direction. Reinforced concrete parapet walls divide traffic in the center

5

and protect traffic on the bridge's sides. Figure 2.4 contains photographs and labels for most bridge components.

The bridge's superstructure is made up of many different shapes and sizes of members, each constructed from Grade 50 weathering steel. The upper and lower chords of the two trusses are primarily composed of built-up welded box sections. These boxes are of varying height, width, and wall thickness at various locations throughout the bridge. Consistent with the terminology customarily used in steel truss design, the top and bottom plates of the box sections are referred to as web plates, and the side plates are referred to as flange plates. This is shown in Figure 2.5. Some lower chord members are made from built-up H sections with accompanying redundancy plates. These members are located near Piers 1B and 5.

The primary diagonal members connecting the upper and lower panel points are composed of built-up welded H and box sections. These members are of varying flange and web size and thickness at various locations throughout the truss. The diagonal sway and cross bracing that connects the two longitudinal trusses in an east to west fashion is composed of hot rolled wide flange I shapes.

The deck is composed of reinforced concrete with a specified 28-day concrete compressive strength of 4500 psi. Wide-flange steel stringers support the deck. The reinforcement is coated with epoxy and has a specified yield strength of 60 ksi. Shear connectors are welded to each of the stringers, the floorbeams, and the upper chord sections in order to provide composite action between the deck and the structural steel. Figure 2.6 is a photograph of shear studs welded to the upper chord, floorbeam, and stringer sections.

The bridge extends from south to north across two active rail lines, the Lehigh River, and a municipal bike path. The southern approach span connects the bridge to I-78. This transitional section of roadway is rather short, and required a slight widening of the bridge, resulting in a mild taper (in plan view) in the truss lines from U1 to U10. The taper (1 ft. of widening to 60 ft. of length) of the bridge on the southern end of Span 1 was implemented in order to better accommodate traffic connecting to or from I-78. This variation in width is not considered in this report as it has little effect on stresses in the area of interest, which are discussed in more detail in Chapter 4. The lateral pitch of the roadway, i.e. the slight increase in elevation of the center of the bridge deck relative to its sides, was also not considered. This report primarily focuses on the members positioned between U16 and U30. More specifically, Chapter 4 focuses on members located between U16 and U18. Chapter 5 focuses on members located between U18 and U30.

2.3   DESIGN ASSUMPTIONS

URS Corporation designed of the SR 33 Lehigh River Bridge. The bridge was designed using the AASHTO Guide Specification for Strength Design of Truss Bridges (Load Factor Design) 1985, and the AASHTO Standard Specifications for Highway Bridges 1992 (Macioce, Tarquinio, and Connor, 2002). These are referred to as the *AASHTO Specifications* in this report. Two

main design assumptions made by the firm are addressed in this report (John Tarquinio, 2002).

The first design assumption concerns the design of the steel stringers supporting the reinforced concrete deck. Table 2.1 contains excerpted information from the AASHTO Specifications used to design these members. The interior stringers were designed in accordance with distribution factors found in Table 3.23.1 of the AASHTO Specifications (1992). The exterior stringers were designed in accordance with AASHTO distribution factors found in Section 3.23.2.3.1.5 of the AASHTO Specifications (1992). The distribution factors are essentially multiplication factors that are applied to wheel loads, which are defined by the AASHTO Specifications to be the load resulting from a rear wheel and a front wheel in line with each other (1985, 1992).

The upper chord box sections of the truss were not designed using distribution factors attained from a table in the AASHTO Specifications. Information relating to the design of upper chord members is taken from personal correspondence with John Tarquinio from September, 2002. For the upper chord member design, the deck was assumed to act as a simple beam with an overhang at each support. The truss chords were treated as the supports. This transferred the entire load on the deck to the upper chord members using a simple span distribution. The resulting couple developed on the two upper chord members in the cross-section was maximized using various positions of trucks. The upper chord members were designed for this load case.

The lateral load distribution factors affecting a deck cross-section is determined analytically by first determining the moment imposed on all members in the cross section by a wheel load. The moment value found in a particular member is then divided by the total moment value found in the entire cross-section. The result of this computation is the percentage of the total moment imposed on that particular member. This is the distribution factor for that particular member for the one wheel loading applied. In order to capture the distribution factor for an all-lanes-loaded condition, the process described above for one wheel load must be carried out for all possible wheel loads. The distribution factors in a particular member due to each wheel load are then added, producing the distribution factor for an all-lanes-loaded condition.

Figure 2.7 illustrates what the bending moment distribution factor equations presented in Table 2.1 are intended to capture. These equations represent an upper-bound value of the distribution factors for the worst-case design load, namely an all-lanes-loaded condition. Figure 2.7(a) presents a qualitative lateral distribution for a truck in Lane 1. Figure 2.7(b) presents a qualitative lateral distribution for a truck in Lane 2. When the two distributions are added, they form the distribution shown in Figure 2.7(c). The stringers underneath the bridge deck in the figures should be designed for the lateral distribution presented in Figure 2.7(c), as this appears to be the worst load case for the structure.

However, an analysis of a structure such as the one presented in the figure is complicated. Therefore, the AASHTO Specification allows designers to

simply use a conservative equation, such as the ones from Table 2.1, to empirically calculate the worst-case distribution factors for each stringer. The experimentally and analytically determined lateral load distribution factors for each member in the section of the bridge between U16 and U18 are compared to this design assumption in Chapter 6.

The second design assumption concerns the use of a two-dimensional model to design the diagonal truss members. For this bridge, each truss line was considered with a 112 in. section of reinforced concrete deck acting compositely with the upper chord members of the truss. The concrete was not considered to act in tension. However, the continuous longitudinal reinforcement was considered for tension forces. This was in accordance with AASHTO Specifications (1985, 1992).

The second design assumption has two distinct ramifications that are studied in this research. First, the experimentally and analytically determined structural behavior of the diagonal members of the truss is compared to this design assumption (in Chapter 6). The diagonal members were not considered for out-of-plane bending due to the two-dimensional design model.

Second, the experimentally and analytically determined structural behavior of the composite deck structure is compared to this design assumption (in Chapter 6). Only the upper chord of the truss and the continuous longitudinal reinforcement within the 112 in. effective width of the concrete deck were considered to carry tensile forces in the negative moment region of the truss. The steel stringers were considered only for local action, and were designed in accordance with AASHTO specifications as mentioned above. They were not considered to act globally.

2.4   PREVIOUS COMPOSITE BRIDGE DECK MODELS

The reinforced concrete deck and supporting structural steel of the SR33 Lehigh River Bridge were provided with composite action through the addition of shear studs as shown in Figure 2.6. This type of construction has been modeled in the past using various finite element modeling techniques. This section provides a brief overview of some the finite element modeling methods employed by other researchers for this type of construction. The method chosen for this report is discussed in detail in Chapter 4.

While conducting research on wheel load distribution for I-girders supporting highway bridges, Tarhini and Frederick (1992) modeled the composite action of steel girders and a reinforced concrete deck. A conceptual view of this model is shown in Figure 2.8(a). They modeled the concrete deck with isotropic brick elements whose bottom surface nodes coincided with those of shell elements representing the top flange of the girder. The bottom flange and web of the girder were also modeled with shell elements.

Mabsout, Tarhini, Frederick, and Kesserwan (1999) employed a different model during their research on wheel load distribution for I-girder bridges. A conceptual view of this model is shown in Figure 2.8(b). They modeled the girders using frame elements and the reinforced concrete deck using shell

8

elements. The composite action of these two structural components was modeled by setting the centroid of the shell elements and the frame elements in the same location. This approach was found to effectively model the transverse distribution of load.

Mourad and Tabsh (1999) took yet a different approach while studying integral abutment bridges. A conceptual view of this model is shown in Figure 2.8(c). They modeled the reinforced concrete deck using shell elements. The top and bottom flanges of the girders were modeled using frame elements and the web of the girders was modeled using shell elements. The composite action of the steel and concrete components was modeled by attaching the deck shell elements to the top flange frame elements with a shear link stiff enough to force plane sections to remain plane.

Cao and Shing (1999) used still another element variation during their investigation of a simplified analysis procedure for highway bridge decks. A conceptual view of this model is shown in Figure 2.8(d). They modeled the reinforced concrete deck as plate elements. The girders were modeled as frame elements. These components were forced into composite action by shear links connecting the centroid of the frame elements to the plate element nodes above.

The last approach discussed in this report (although other variations exist) is that of O'Connell and Dexter (2001) during their fatigue study of steel trusses. They modeled composite action by using shear links with a high stiffness value. A conceptual view of this model is shown in Figure 2.8(e). For their study, stiff stub-columns were provided as the connection between a frame element grillage representing the reinforced concrete deck and the truss system. The truss system was also made of frame elements.

Table 2.2 presents a summary of the features of the above-described models. Four main features of these models are evaluated: the model's ability to capture the full moment of inertia (I) of the cross-section; the model's ability to account for membrane rotation in the deck structure; the model's ability to easily provide element stress results at locations important in this research (such as the longitudinal stress results from the bottom flange of deck stringers); and the model's inclusion of elements that are able to be manipulated in the particular software package used in the current study. SAP 2000 (see Section 2.5) was the finite element analysis program used in this research. The lateral load distribution model used in this research (presented in Chapter 4) is a variation of the models described above. As will be explained, the approach taken in this research includes all of the features listed in Table 2.2.

2.5 SUMMARY OF SAP 2000

SAP 2000 version 7.44 was used to conduct the finite element analyses described in this report (CSI Inc., 2000). This versatile program includes a graphical user interface that allows for three-dimensional views of any model as it is being constructed. This ability is extremely important, because it allows for easy identification of mistakes that can be corrected before the model is analyzed. Another advantage of this program it that using the graphical user

9

interface, it is user friendly. Structure geometry, material properties, section properties, etc. are all easily defined using this interface.

SAP 2000 is equipped with a wide variety of finite element types that can be chosen to suit the user's needs. Each of the elements and their capabilities used to conduct this research are described briefly. A more comprehensive description can be found in the SAP 2000 user manuals (CSI, Inc., 2000). The following is a paraphrase of sections of this manual.

The frame element is an element that connects two nodes. The primary uses for frame elements are to model beams and beam-columns. In SAP 2000, the elements do not have to be prismatic. There are usually six degrees of freedom (DOFs) that describe the possible motion of each frame element, but these DOFs can be restrained or released in a number of ways, including constraints and restraints. Frame elements may be loaded in any direction and in any loading configuration.

The shell element is an area element that connects either three or four nodes. These nodes do not have to be planar. The primary uses for shell elements are to model two and three-dimensional slabs and tank structures. Like the frame element, there are six DOFs available at each node. These DOFs can be modified by the user's definition of constraints and restraints. Shell elements may be loaded in any direction at their defining nodes or may be loaded by a pressure load on either the positive or negative face of the element.

The analytical work for this report was performed using the two element types described above – frame and shell elements. These two element types were used to discretize the structure and produce results that were in reasonable agreement with the controlled load tests conducted on the structural system. Specific descriptions of the finite element models created for this research are presented in Chapters 4 and 5 of this report.

Interior Stringers[1]		
Kind of Floor	Bridge Designed for One Traffic Lane	Bridge Designed for Two or More Traffic Lanes
Concrete: On Steel I-Beam Stringers[g] and Prestressed Concrete Girders	$\dfrac{S}{7.0}$ If S exceeds 10 ft. use note f.	$\dfrac{S}{5.5}$ If S exceeds 14 ft. use note f.
Exterior Stringers[2]		
Kind of Floor	S < 6 ft.	6 ft. < S < 14 ft.
Concrete: Supported by Four or More Steel Stringers	$\dfrac{S}{5.5}$	$\dfrac{S}{4 + .25(S)}$ If S exceeds 14 ft. use note f.

Excerpted Notes
S = average stringer spacing in feet.
f.   In this case the load on each stringer shall be the reaction of the wheel loads, assuming the flooring between the stringers to act as a simple beam.
g.   "Design of I-Beam Bridges" by N. M. Newmark – Proceedings, ASCE, March 1948.

General Notes
1.   Section excerpted from AASHTO Specification Table 3.23.1 (1985)
2.   Section excerpted from AASHTO Specification Section 3.23.2.3.1.5 (1985)

Table 2.1. Excerpted AASHTO specifications providing lateral load distribution stipulations.

Previous Models	Ability to Capture the Full Moment of Inertia?	Ability to Account for Deck Membrane Action?	Ability to Account for Deck Plate Action?	Ability to Easily Capture Element Stress Results at Key Locations for this Research?	Ability to Manipulate All Elements Using SAP 2000 Graphical User Interface?
Tarhini and Frederick (1992)	Yes	Yes	Yes	Yes	No
Mabsout, Tarhini, Frederick, and Kesserwan (1999)	No	Yes	Yes	No	Yes
Mourad and Tabsh (1999)	Yes	Yes	Yes	No	Yes
Cao and Shing (1999)	Yes	No	Yes	No	Yes
O'Connell and Dexter (2001)	Yes	No	Yes	No	Yes

Table 2.2. Features of previous composite bridge deck models.
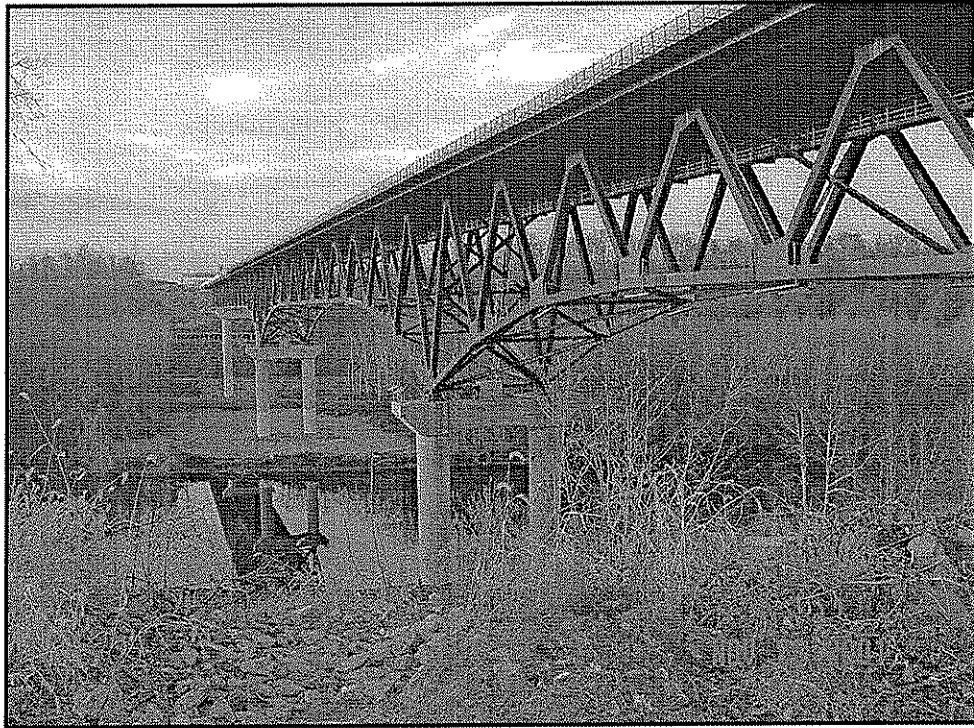
Figure 2.1. Photograph of the SR33 Lehigh River Bridge looking north.
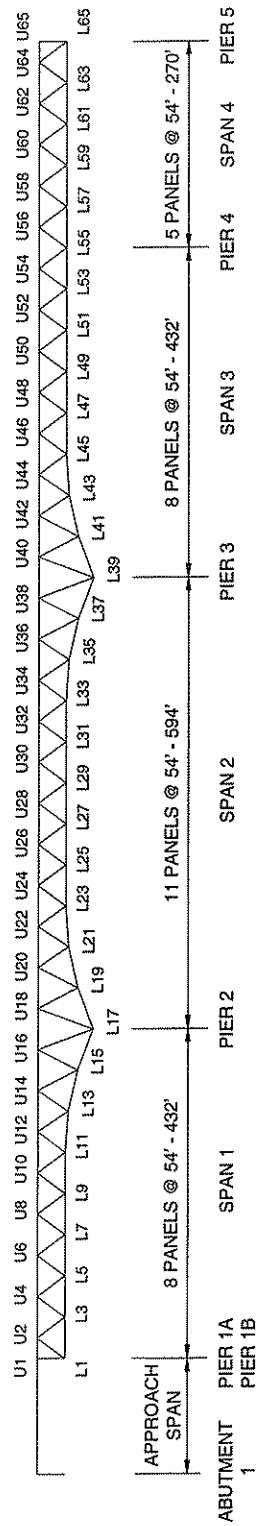
Figure 2.2. Elevation drawing of the SR33 Lehigh River Bridge looking west.

14
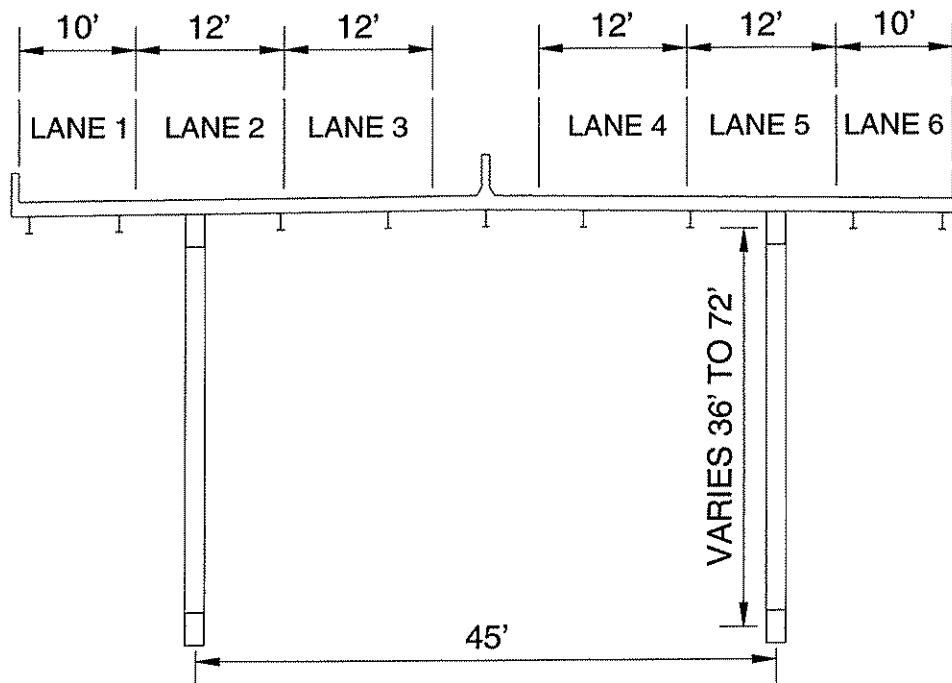
Figure 2.3. Cross-section drawing of the SR33 Lehigh River Bridge looking north.

15

FLOORBEAM   LOWER   SWAY   STRINGER   CROSS   UPPER
                    CHORD   BRACING   BRACING   CHORD

DIAGONAL

BRIDGE PIERS   CONCRETE   PARAPET
                                          DECK
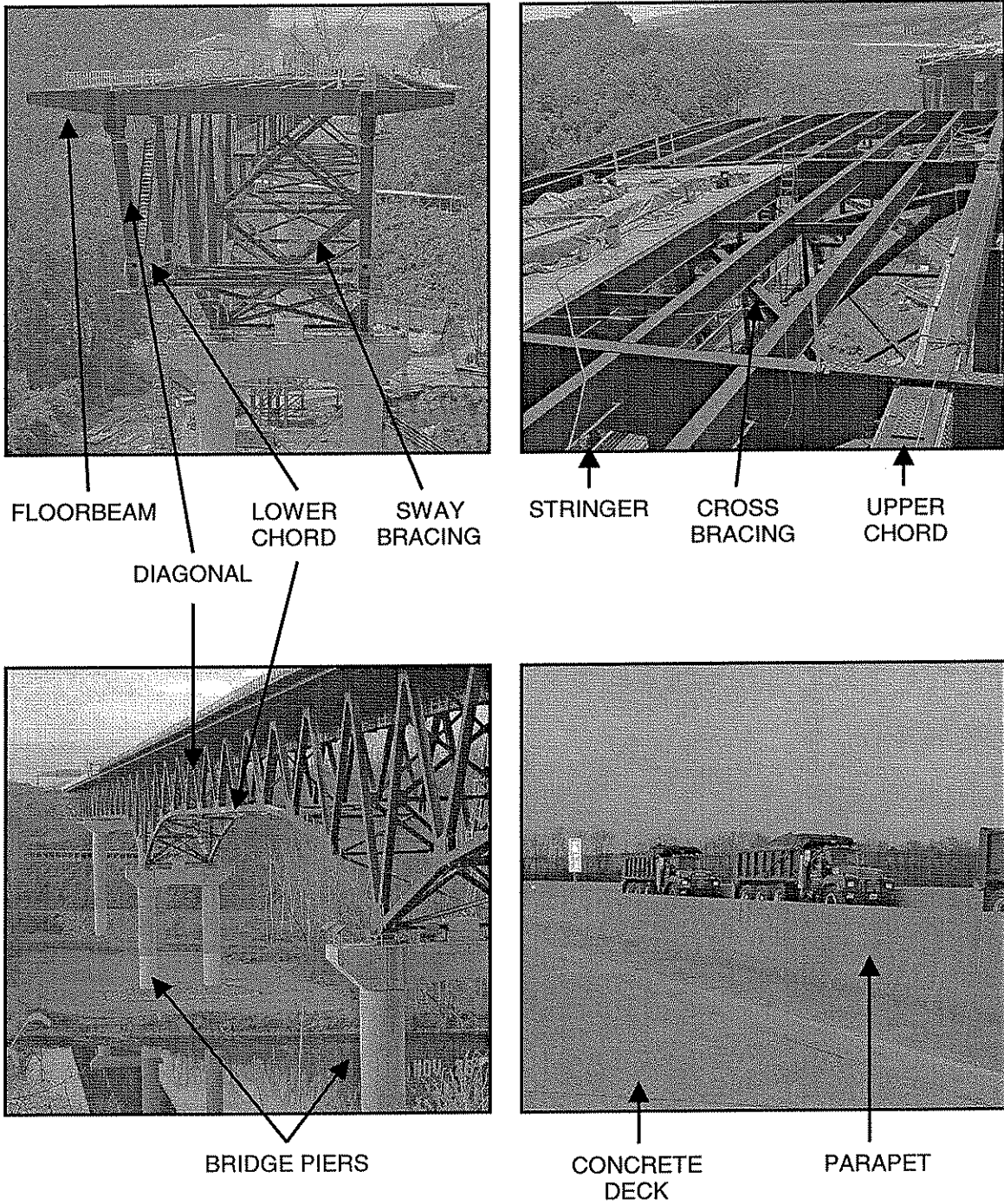
Figure 2.4. Photographs of various main bridge components.

16
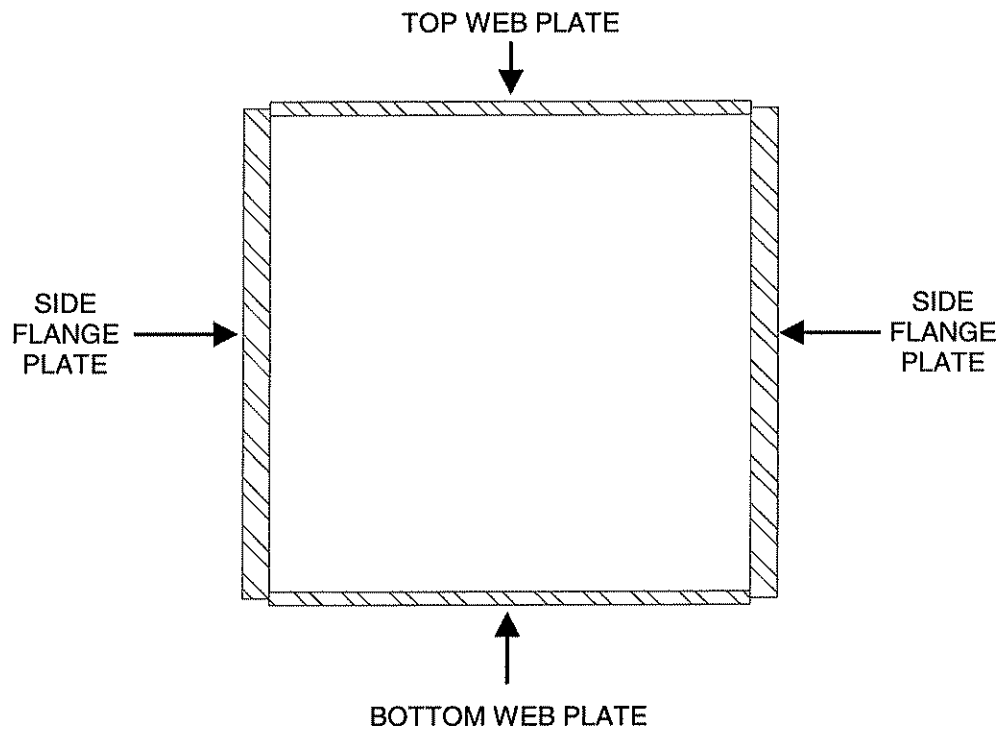
Figure 2.5. Terminology used in steel box truss design.
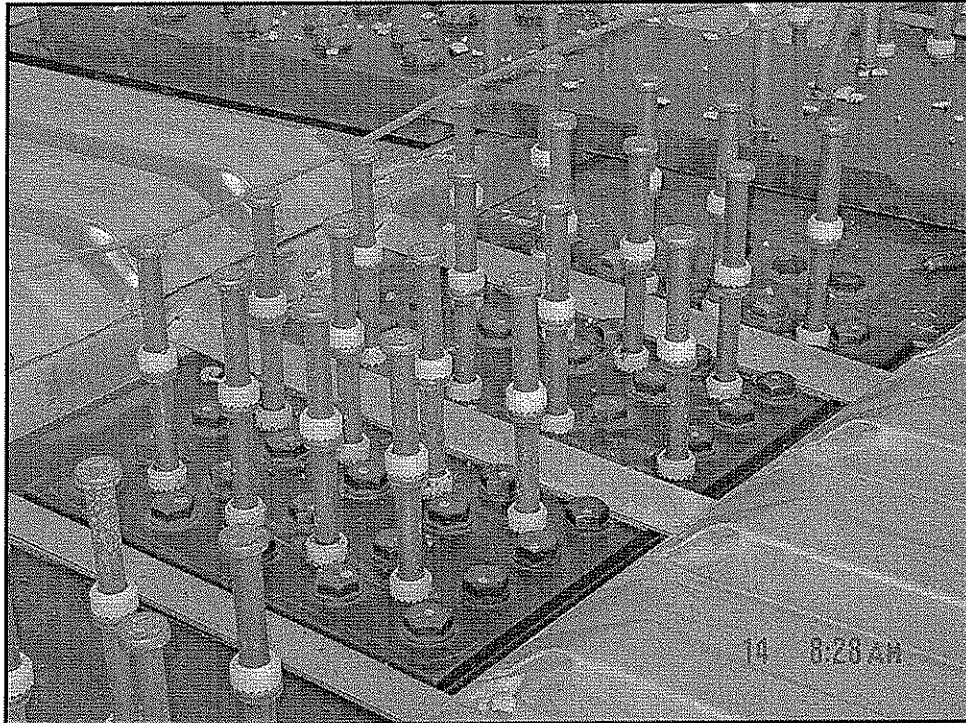
Figure 2.6. Photograph of shear studs installed on the upper chord before the reinforcement was placed or the concrete was poured.
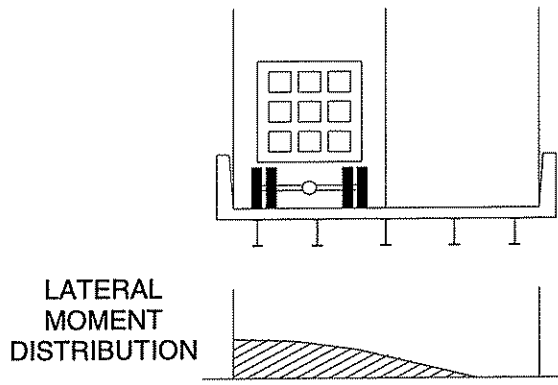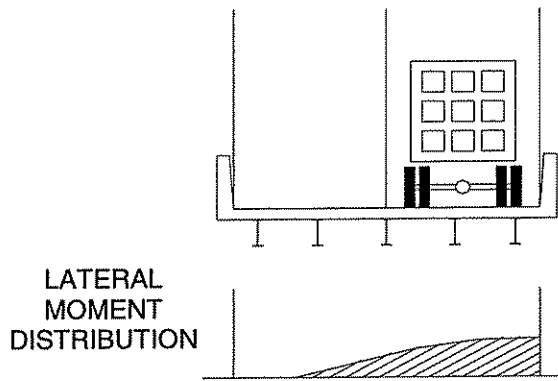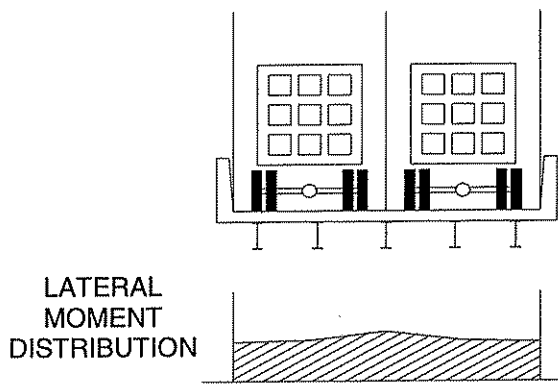
Figure 2.7. Illustration of what is captured by AASHTO Specifications distribution factors: (a) 1 truck load in left lane; (b) 1 truck load in right lane; (c) 1 truck load in each lane (design distribution).

19

BRICK
ELEMENTS

SHELL
ELEMENTS

(a)

FRAME
ELEMENTS

SHELL
ELEMENTS
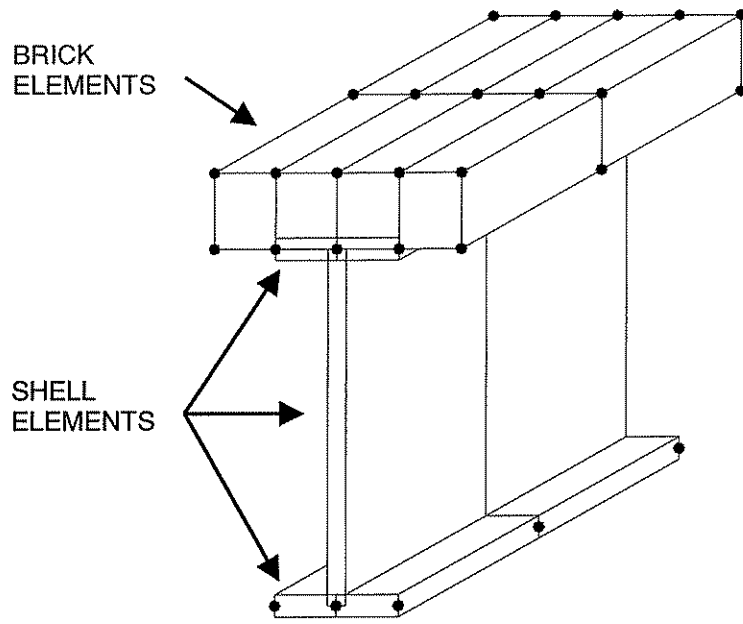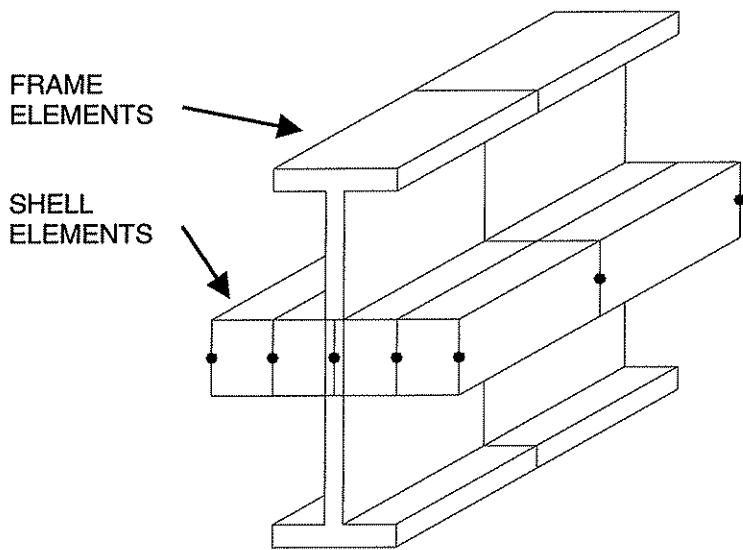
(b)

Figure 2.8. Previous finite element arrangements used to model composite
action between a reinforced concrete deck and supporting steel girders:
(a) Tarhini and Frederick (1992); (b) Mabsout, Tarhini, Frederick, and Kesserwan
(1999).
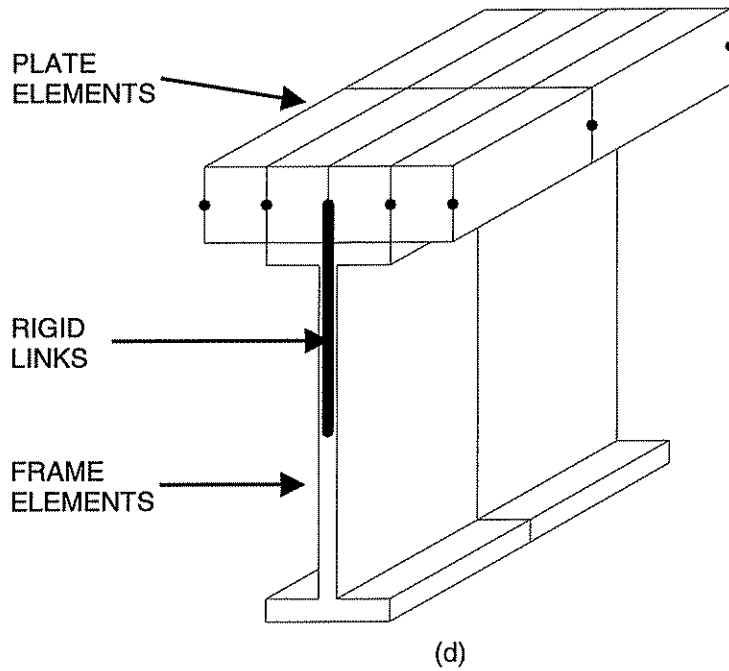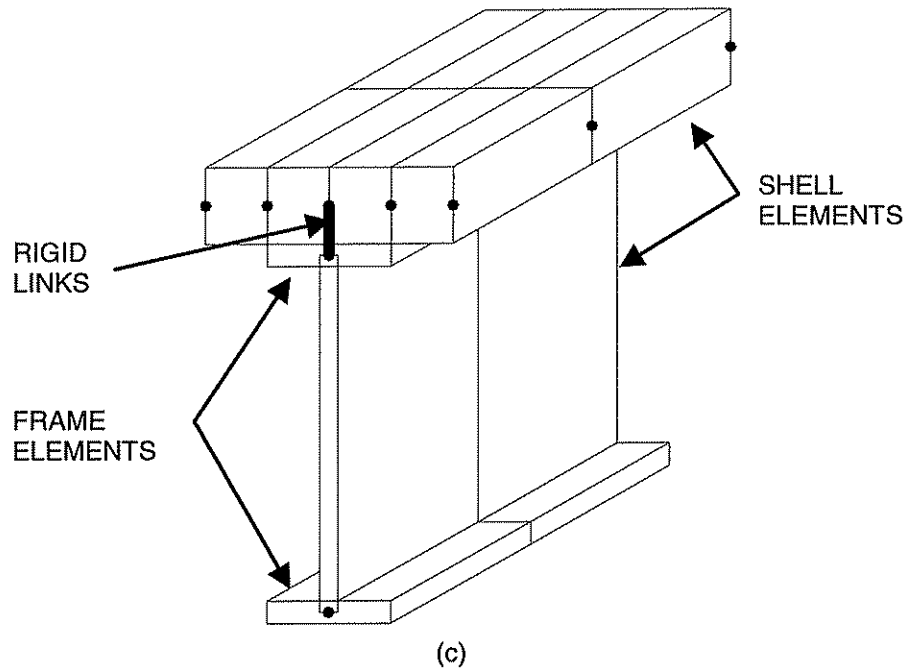
RIGID
LINKS

SHELL
ELEMENTS

FRAME
ELEMENTS

(c)

PLATE
ELEMENTS

RIGID
LINKS

FRAME
ELEMENTS

(d)

Figure 2.8 (Cont.). Previous finite element arrangements used to model
composite action between a reinforced concrete deck and supporting steel
girders: (c) Mourad and Tabsh (1999); (d) Cao and Shing (1999).
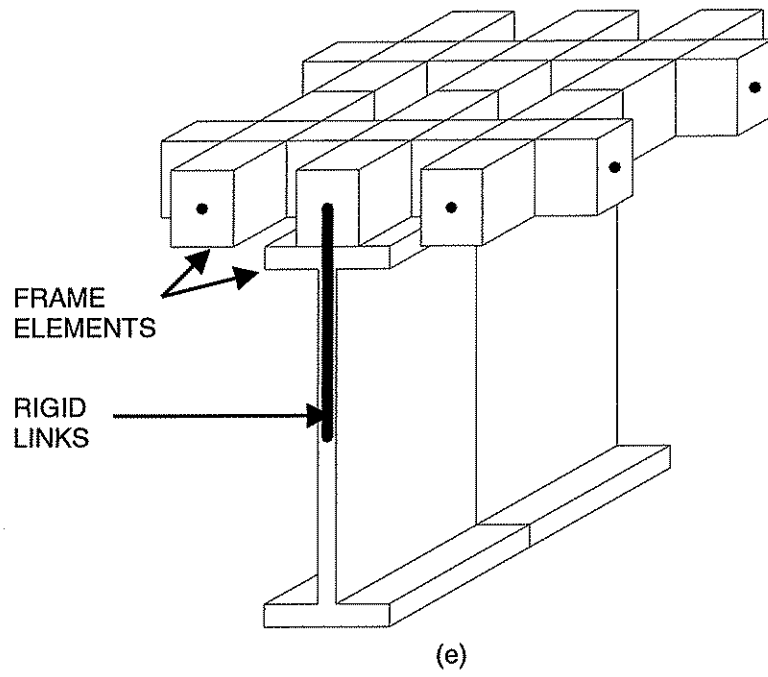
21

FRAME
ELEMENTS

RIGID
LINKS

(e)

Figure 2.8 (Cont.). Previous finite element arrangements used to model composite action between a reinforced concrete deck and supporting steel girders: (e) O'Connell and Dexter (2001).

CHAPTER 3
SUMMARY OF CONTROLLED LOAD TESTING

3.1   INTRODUCTION
This chapter summarizes the controlled load experiments conducted by the ATLSS researchers. Section 3.2 is a summary of the instrumentation from which the data was collected. This section also contains a description of where the instrumentation was attached to the bridge. Section 3.3 contains a description of the controlled load test vehicle utilized to produce the experimental results pertinent to this research. Section 3.4 contains a summary of the controlled load test methodology used during the experiments. Section 3.5 contains a summary of the pertinent park test experimental data gathered during the controlled load tests. Lastly, Section 3.6 contains a summary of the pertinent crawl test experimental data gathered during the controlled load tests. This chapter is intended to give the reader an overview of the tests conducted on the bridge. The park test results are directly compared to analytical results while the crawl test results are utilized as an indication of bridge behavior.

The information presented in the following sections is taken from ATLSS Report 02-07 (Connor and Santosuosso, 2002). A more comprehensive description of the tests and results can be found in this reference.

3.2   INSTRUMENTATION AND GAGE PLANS
Two types of strain gages were used to collect data from the bridge – vibrating wire strain gages and electrical resistance strain gages. Both types of gages are characterized as uniaxial and spot weldable. They were installed at various locations throughout the truss and reinforced concrete deck of the bridge structure to monitor strains during construction and beyond. Vibrating wire strain gages were installed to monitor the long-term effects of stress and strain related to steel erection, and the creep and shrinkage of the composite reinforced concrete deck. Electrical resistance strain gages were installed to monitor much faster events, such as the load imposed by the passage of heavy trucks. Figure 3.1 is a photograph of a typical vibrating wire and a resistance strain gage mounted to the steel truss. Figure 3.2 is a photograph of a typical set of gages installed in the reinforced concrete deck.

This report treats only live load data generated by controlled load tests of the bridge that occurred on 4 January 2002. Therefore, while the vibrating wire strain gages are included in Figures 3.1 and 3.2, they did not provide any data for this research. The electrical resistance strain gages were utilized to gather the pertinent data.

The strain gages utilized to provide data for this research are shown in Figures 3.3 through 3.9. Each gage is named according to its location in reference to the panel points of the bridge truss and what type of structural member it is either mounted on or to which it is adjacent. For example, the gage location BU1618EW indicates that is on a box member (B) located on the upper chord of the truss (U) between panel points 16 and 18 (1618) on the east side of

the bridge (E) and on the west side of the member (W). All gages are named in a similar fashion.

Most gages mounted on the steel truss were installed at the centerline of the face of the member. A small offset (less than 1-1/4") was necessary to install the vibrating wire gages and the uniaxial resistance gages side-by-side. An example of this offset is shown in Figure 3.1. The centerline of the member face is the dark line drawn between the gages.

The gages that were mounted on the steel stringers supporting the reinforced concrete deck were installed in a somewhat different configuration due to the location of the deck pans. The bottom gages were installed on the bottom of the bottom flange similar to those on the steel truss. The top gages were installed on the bottom of the top flange with a 2-7/8" offset from the web. This location was chosen to allow for proper gage installation and to avoid any local strain concentrations at the web - flange interface. A section view of these gages is shown in Figure 3.6.

The embedded gages were placed in the reinforced concrete deck. The uniaxial electrical resistance strain gages were spot welded to the center of a section of reinforcement sized to provide proper development length. These were then tied to the existing reinforcement cage.

3.3   LIVE LOAD TEST VEHICLE

A triaxle dump truck was used as the loading vehicle during the controlled load tests. It was loaded beyond its specified road rating to cause an overloaded condition on the roadway. This truck is referred to in this report as Truck #80. Its total weight was measured as 84.75 kips. Figure 3.10 contains truck weight and geometry data.

3.4   CONTROLLED LOAD TEST METHODOLOGY

This section details the methodology behind the types of controlled load tests, focusing on information relevant to this research. Two types of tests were conducted – park tests and crawl tests.

3.4.1   Park Test Methodology

The controlled load tests conducted that produced results related to the upper chord members and the steel stringers for this research are termed as park tests. This set of tests was conducted above Pier 2 in the span between U16 and U18 of the bridge. In order to appropriately manage truck placement, a series of roadway marks were placed in each lane at 18 in. north of U16 and at 27 ft. north of U16 to mark each loading position. Truck #80 was slowly driven to each loading position, stopped for a period of about 10 seconds, and then slowly driven in the same manner to the next loading position. These tests were conducted in Lanes 2 through 6.

3.4.2 Crawl Test Methodology

The controlled load tests conducted that produced results related to the steel stringers, the diagonal members, and embedded gages are termed as crawl tests. The three data sets pertaining to this research were recorded from crawl tests conducted in Lanes 4, 5, and 6 of the roadway. In order to conduct a crawl test, the test truck was driven at a slow rate of speed (about 5 mph). These tests were considered quasi-static because they occurred with the truck traveling at such a slow rate of speed. This means that any dynamic effect the moving truck might have had on the bridge was considered negligible. The results of a crawl test can be utilized as a scaled influence line because they show exactly what the effect of a slowly moving load was on any instrumented member.

3.5 PERTAINENT MEMBER TEST RESULTS FOR PARK TESTS

This section presents the relevant experimental park test results collected during the controlled load testing of the bridge. A full description of the results for all controlled load tests is presented in ATLSS Report 02-07. Measured strains were converted to stresses using E = 29,000 ksi.

The results of the experimental park tests are compared directly to analytical data gathered from the finite element models presented in following chapters.

3.5.1 Upper Chord Member Test Results

Figure 3.3 shows the locations of the strain gages installed on the east and west upper chords of the truss. On each upper chord box member, uniaxial strain gages were installed on the centerline of the bottom web plate. Gages were also installed on the centerline (i.e., mid-depth) of each of the two side flange plates. All gages were located between panel points U16 and U18. They were positioned to measure any axial force or bending moment at mid-span. This research focuses on the results obtained from the bottom plates of the upper chord box members.

Figures 3.11 and 3.12 show typical responses of the upper chord to an 85 kip (rounded up from measured value of 84.75 kips) triaxle truck traveling in Lanes 2 and 3 respectively. In both tests the truck was facing north. These figures contain a couple of important characteristics that must be noted. First, the figures show that a load placed on the west side of the bridge deck had little effect on the upper chord members on the east side of the bridge deck. Only a slight rise in stress was seen in the east upper chord member presented.

The most notable feature of the two figures is the two plateaus. The first plateau represents the static placement of the back axles of the truck over the strain gages located 18 in. north of U16. The second plateau represents the static placement of the back axles of the truck over the strain gages located at 27 ft. north of U16. All park test plots exhibited these two plateaus.

This and the remaining experimental data that are compared to the analytical results of later chapters are presented in Figures 3.13 through 3.22. These figures contain a plot of stress data gathered from the bottom flanges of

each instrumented stringer and the bottom web plate of each upper chord member in the cross-section 27 ft. north of U16. The data points are positioned to graphically line-up with the appropriate member in the cross-section view below the plots. The plan view below the cross-section view contains a graphic representation of where the truck axles were positioned during the experiment. It is important to note that the results presented in the plots all come from the cross-section 27 ft. north of U16, no matter what the truck position.

The data is plotted over two domains. The tests conducted with the back axles of the truck 18 in. north of U16 are plotted over a domain of –0.4 ksi to 1.0 ksi. The tests conducted with the back axles of the truck 27 ft. north of U16 are plotted over a domain of –1.0 ksi to 4.0 ksi.

3.5.2 Steel Stringer Test Results

Figure 3.6 shows the locations of the strain gages installed on the stringers of the bridge. Uniaxial strain gages were installed on the centerline of the bottom flange plate and the bottom of the top flange plate at the center of the span. The gages were located near the edge of the top flange so as not to be sensitive to local stresses caused by the web – flange interface. All gages were located between panel points U16 and U18. They were positioned in this fashion to experimentally measure any axial force or bending moment at mid-span. This research focuses on the results obtained from the bottom flange gages on the stringer sections.

The data gathered from the bottom flange gages is compared to analytical data in later chapters. This data is plotted along with the upper chord data in Figures 3.13 to 3.22. The importance of these plots is that they demonstrate the lateral distribution of deck loading to adjacent chords and stringers and therefore are helpful in evaluating the designer's assumptions stated in Section 2.3.

The data points presented for the stress in the bottom flange of Stringer S9 in Figures 3.13 through 3.22 are not included in the comparison to analytical data. This is the case because the gage at this location is thought to have provided erroneous results. The measured values from this gage are consistently smaller in magnitude than the analytical data by a factor of roughly five. The data points are included in the Figures 3.13 through 3.22 for completeness.

3.6   PERTINENT MEMBER TEST RESULTS FOR CRAWL TESTS

This section contains an overview of the relevant experimental crawl test results collected during the controlled load testing of the bridge. A more comprehensive description of the results for all controlled load tests is presented in ATLSS Report 02-07. Measured strains were converted to stresses using E = 29,000 ksi.

It should be noted that the results of the experimental crawl tests are taken as an indication of the bridge's structural behavior. This data will not be directly compared to analytical data. Instead, the data is viewed to give insight into analytical load cases that can be used to recreate the noted structural

behavior. Comparisons between the model results provided by URS Corporation and model results obtained from analytical work done for this research are compared, rather than direct comparison to experimental data. Chapter 5 contains the analytical results of the full bridge analytical model related to these topics. A comparison among the design assumption, experimental results, and analytical results is presented in Chapter 6.

3.6.1 Steel Stringer Test Results

Figure 3.23 contains plots of the upper chord, lower chord, and stringer response to Truck #80 in Lane 5 traveling north. The importance of this figure is that it shows that as a load traveled out to midspan, shown as the peak in the lower chord response, the gages on the stringers exhibited a similar amount of axial stress as did the upper chord gages. This means that all of the steel in the composite deck structure worked together in tension to carry a load at midspan. This result was typical of all tests and all gages in the same cross-section. ATLSS Report 02-07 provides a more comprehensive set of stringer data.

3.6.2 Diagonal Member Test Results

Figures 3.4 and 3.5 show the locations of the strain gages installed on the east and west diagonals of the truss. Uniaxial strain gages were installed on the centerline of the east and west flange plates of each instrumented diagonal member. All gages were located between panel points U18-L19 and U20-L21.

Figure 3.24 shows the response of the instrumented east diagonals to Truck #80 traveling north in Lane 5. The response of the east upper chord bottom is also plotted to put the member response in perspective. The most important feature of this plot is it clearly shows that when the traveling load was placed above one of the truss lines, the primary diagonal response was an axial loading. This action was expected of the truss diagonal elements.

Placing the load outside of the trusses produced a different result. Figure 3.25 shows the response of the instrumented east diagonal members to Truck #80 in Lane 6 headed north. This plot demonstrates that when the load is placed outside of the longitudinal truss lines, a bending component appears in the diagonal response. In this case for the east truss with the load placed to the east, the gage on the west side of the members went directly into tension as expected, producing no reversal. The gage on the east side of the members, however, showed a significant compression reversal. This means that the upper panel point of the truss rotated out of plane, causing a bending stress in the diagonal member. The phenomenon is local because after the load passed the panel point in which it caused the rotation, the member response reverted to axial tension. This response was typical of all similar tests. This observation is important because of the way the trusses were designed, as described in Section 2.3. For a more comprehensive data set the reader should refer to ATLSS Report 02-07.

3.6.3 Embedded Gage Test Results

Figure 3.7 shows the locations of the strain gages installed on rebar embedded in the bridge deck. Each gage was spot welded to a section of rebar long enough to provide the necessary development length. The reinforcement bar sections were obtained from stock at the site. All gages were located between panel points U16 and U18 and were positioned parallel to the longitudinal upper cage reinforcement in the deck. The gages located on either side of the instrumented stringers were set at a distance east or west of three feet, while those located on either side of the upper chords were set at a distance east or west of four feet.

Figure 3.26 is a plot of typical embedded gage response to a crawl test in Lane 5 with Truck #80 traveling north. In the figure, the lower chord response is plotted for reference. The peak of this plot line occurs when the truck is at midspan of Span 2. The other two plot lines clearly show that there is global tension present in the deck reinforcement when a load is placed in the span. This information is important because it shows that the deck exhibits global tension although this was not considered in the composite deck design.

3.6.4 Global Deck Test Results

Table 3.1 contains experimental results from the cross-section at the midspan between U16 and U18. These data were gathered from a crawl test in Lane 5 with Truck #80 positioned at midspan of Span 2. The position of Truck #80 was determined roughly by noting the peak stress response in lower chord member L27-L29. For reference, a similar response plot for L27-29 is shown in Figure 3.23.

The data are reported in terms of steel stress and were calculated as the average from a linear stress distribution across the cross-section of each member. This allowed any local bending influence to be subtracted from the results. The data show that there is global tension in the stringers, upper chord box members, and deck reinforcement in each of the composite sections reported in Table 3.1. It should be noted that experimental data was not available for all members in the cross-section between U16 and U18. Therefore only results from the East and West Upper Chords and Stringers S6, S7, and S8 are reported in the table.

The importance of this data is that global tension exists in the composite deck structure and that the stress caused by this tension is distributed rather evenly to each member in the cross-section. For this test, the load was applied directly to the east truss line. Therefore, it was expected that the members on the east side of the bridge deck exhibited a higher stress than those on the west side of the deck. The stress values reported are low, but do exist.

28

Member	Global Tension Stress (ksi)
WUC	0.02
S6	0.03
S7	0.03
EUC	0.05
S8	0.05

Table 3.1. Stress results from the composite deck cross-section at the centerline of U16-U18 due to Truck #80 in Lane 5 positioned at the center of Span 2.
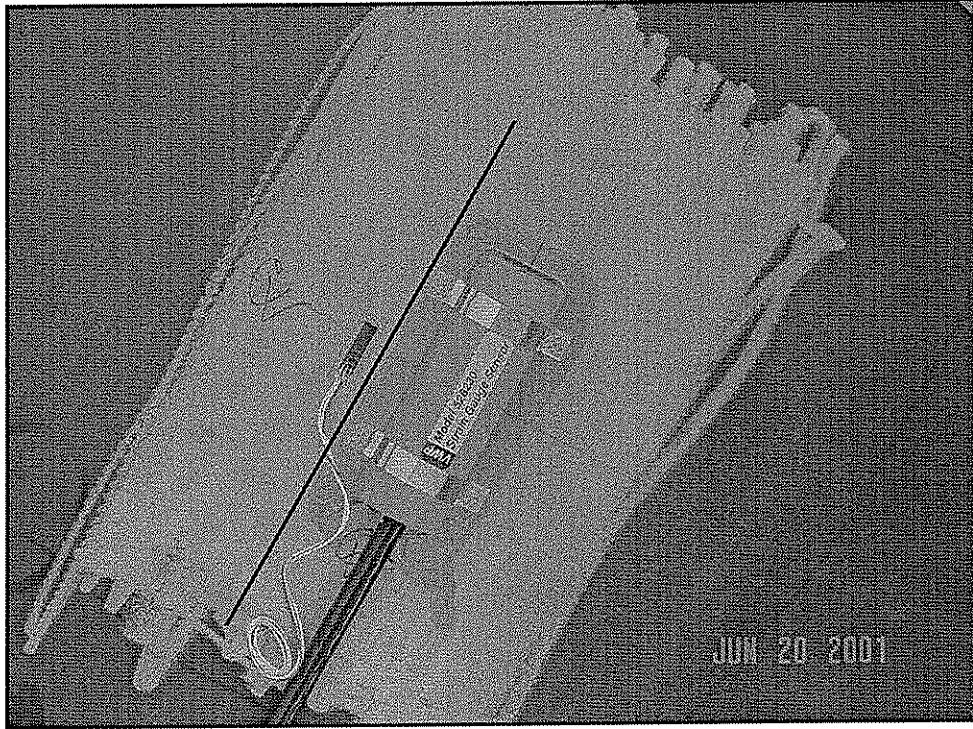
Figure 3.1. Typical strain gage location with an electrical resistance strain gage on the left and a vibrating wire strain gage on the right.
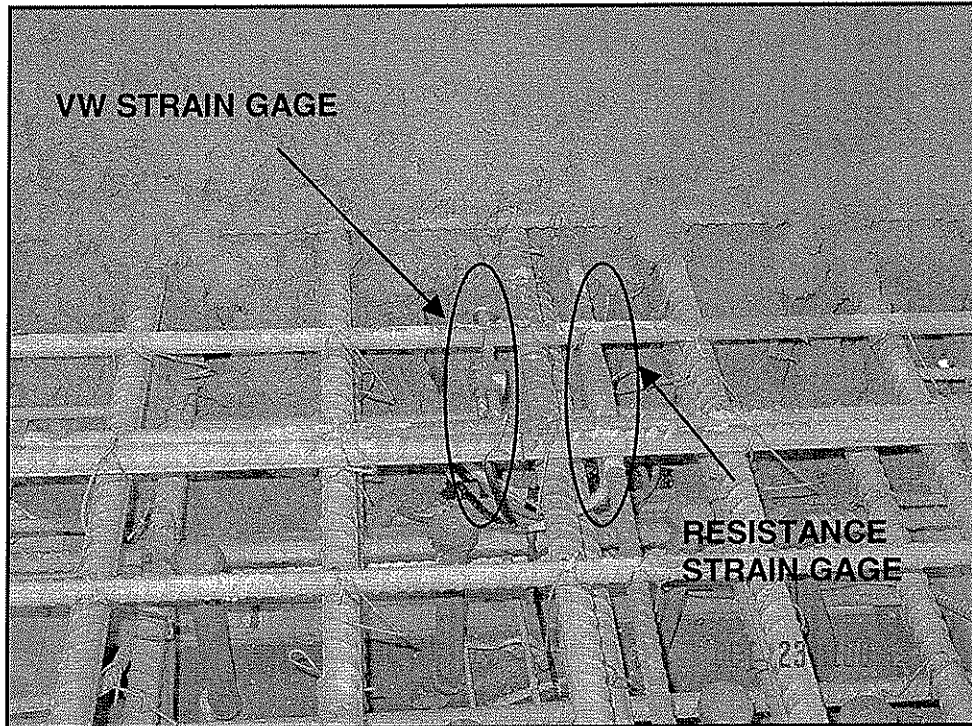
Figure 3.2. Typical embedded strain gage view as the concrete is being poured. The electrical resistance strain gage is spot welded to a length of reinforcement bar as shown in the figure.
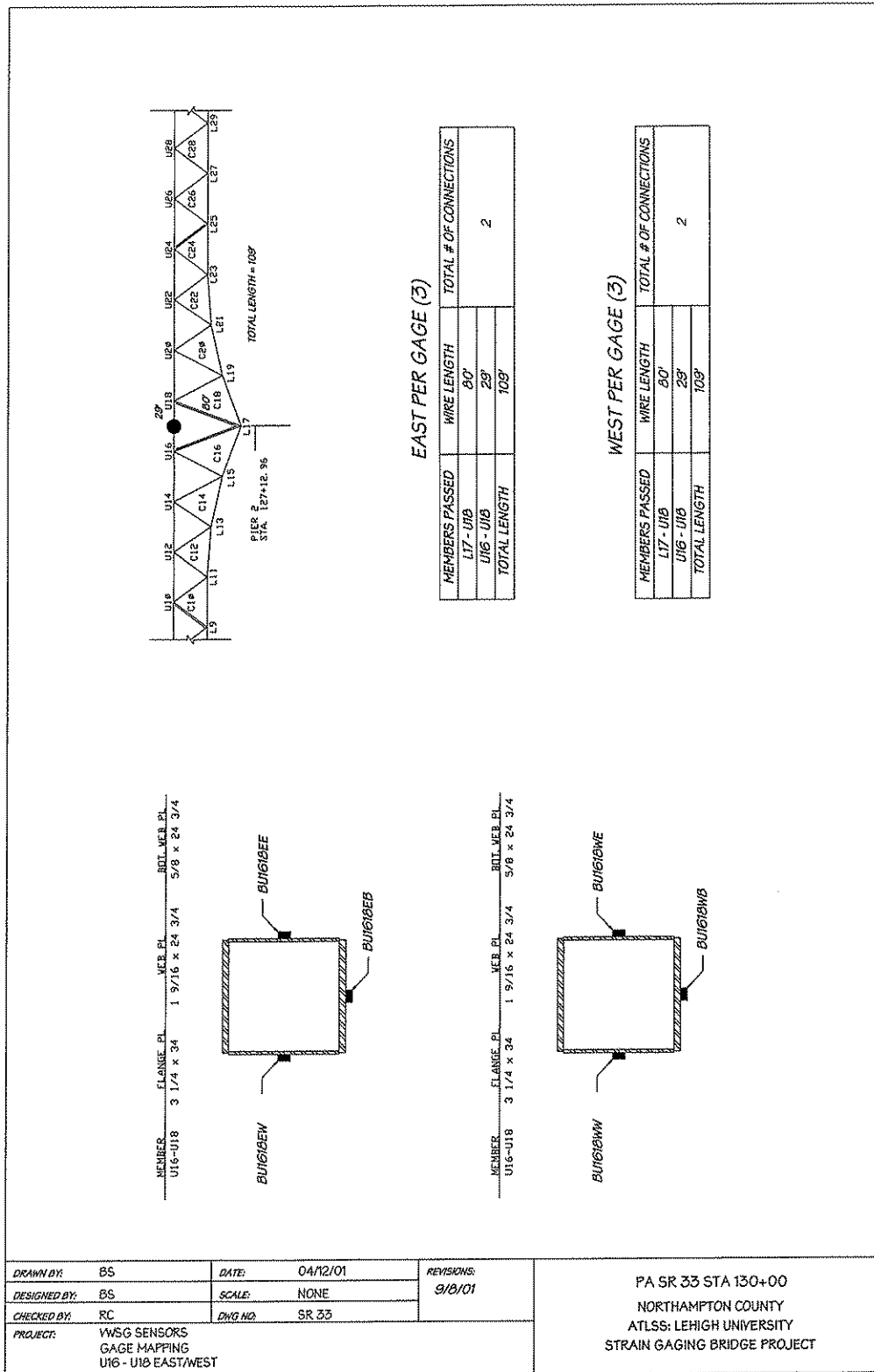
Figure 3.3. Strain gage layout on the upper chord between U16 and U18.
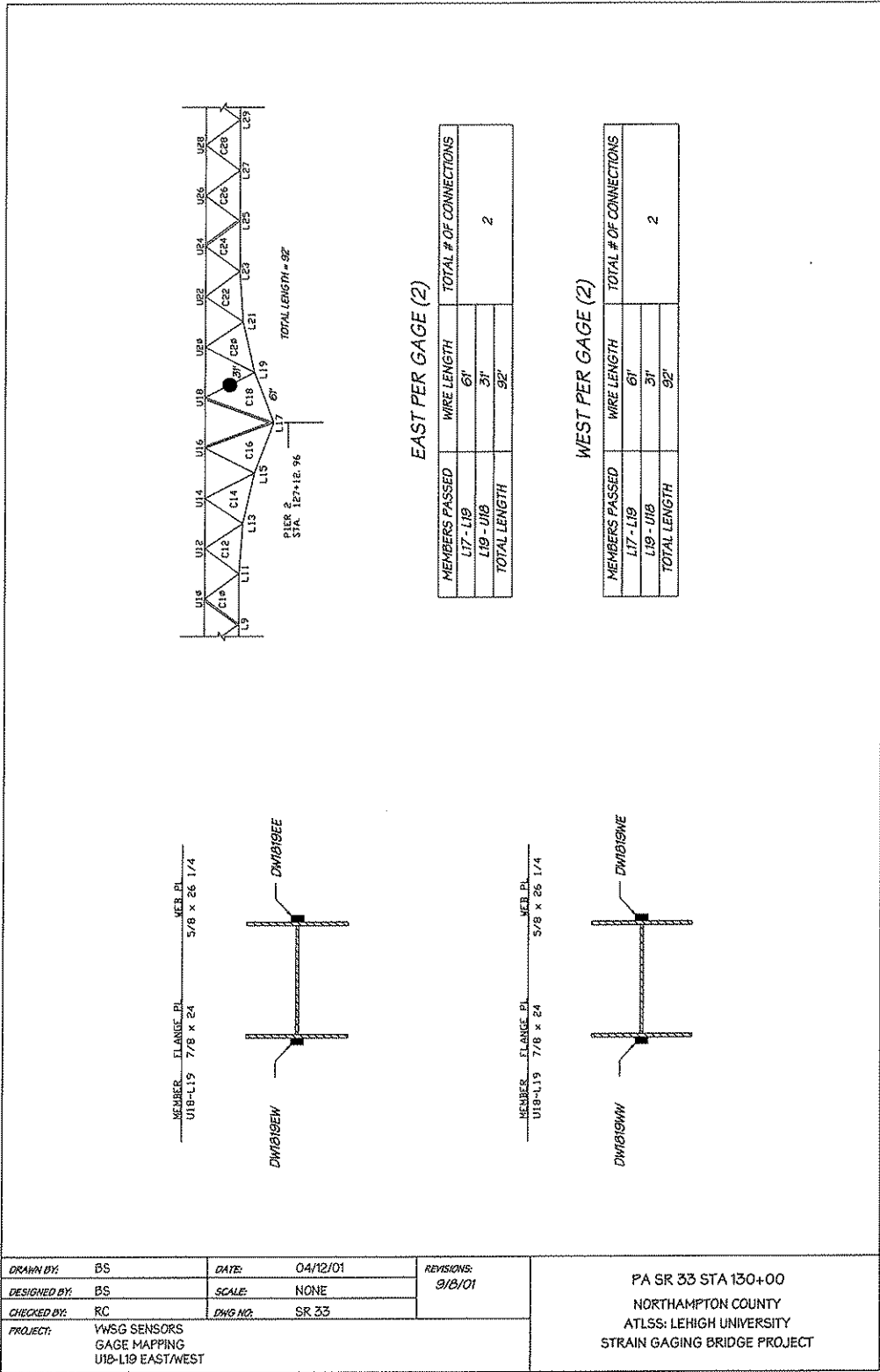
Figure 3.4. Strain gage layout on the diagonal members between U18 and L19.

EAST PER GAGE (2)

MEMBERS PASSED	WIRE LENGTH	TOTAL # OF CONNECTIONS
L17 - L19	6'	3
L19 - L21	58'	
U20 - L21	26'	
TOTAL LENGTH	145'	

WEST PER GAGE (2)

MEMBERS PASSED	WIRE LENGTH	TOTAL # OF CONNECTIONS
L17 - L19	6'	3
L19 - L21	58'	
U20 - L21	26'	
TOTAL LENGTH	145'	

TOTAL LENGTH = 145'

PIER 2
STA. 127+12. 96

U10 U12 U14 U16 U18 U20 U22 U24 U26 U28
L9 L11 L13 L15 L17 L19 L21 L23 L25 L27 L29
C10 C12 C14 C16 C18 C20 C22 C24 C26 C28

MEMBER FLANGE PL WEB PL
U20-L21 7/8 x 26 11/16 x 26 1/4
DW2021EW DW2021EE

MEMBER FLANGE PL WEB PL
U20-L21 7/8 x 26 11/16 x 26 1/4
DW2021WW DW2021WE

DRAWN BY:	BS	DATE:	04/12/01	REVISIONS:
DESIGNED BY:	BS	SCALE:	NONE	9/8/01
CHECKED BY:	RC	DWG NO:	SR 33	
PROJECT:	VWSG SENSORS GAGE MAPPING U20-L21 EAST/WEST			

PA SR 33 STA 130+00
NORTHAMPTON COUNTY
ATLSS: LEHIGH UNIVERSITY
STRAIN GAGING BRIDGE PROJECT

Figure 3.5. Strain gage layout on the diagonal members between U20 and L21.
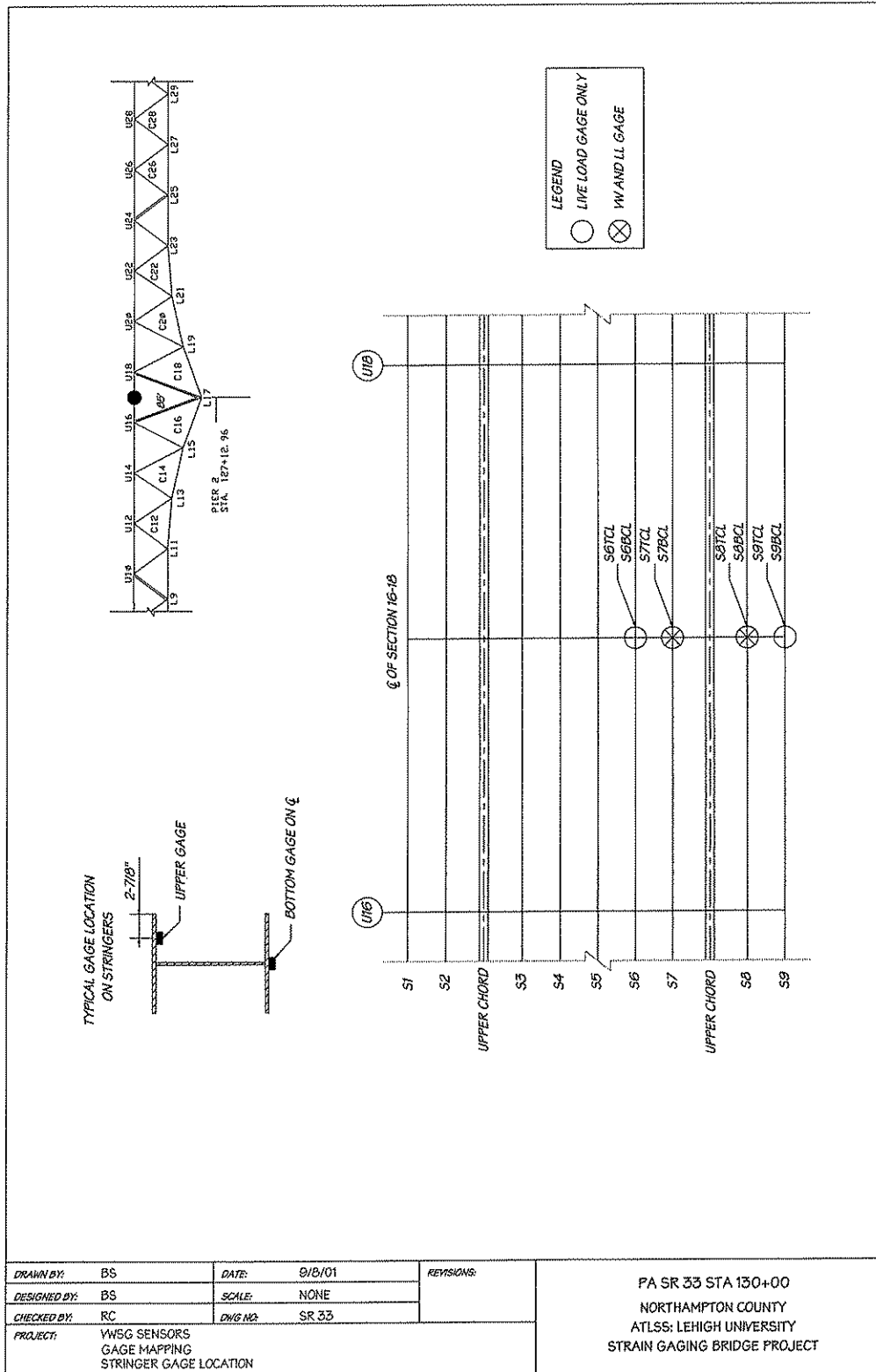
Figure 3.6. Strain gage layout on the stringers between U16 and U18.

35
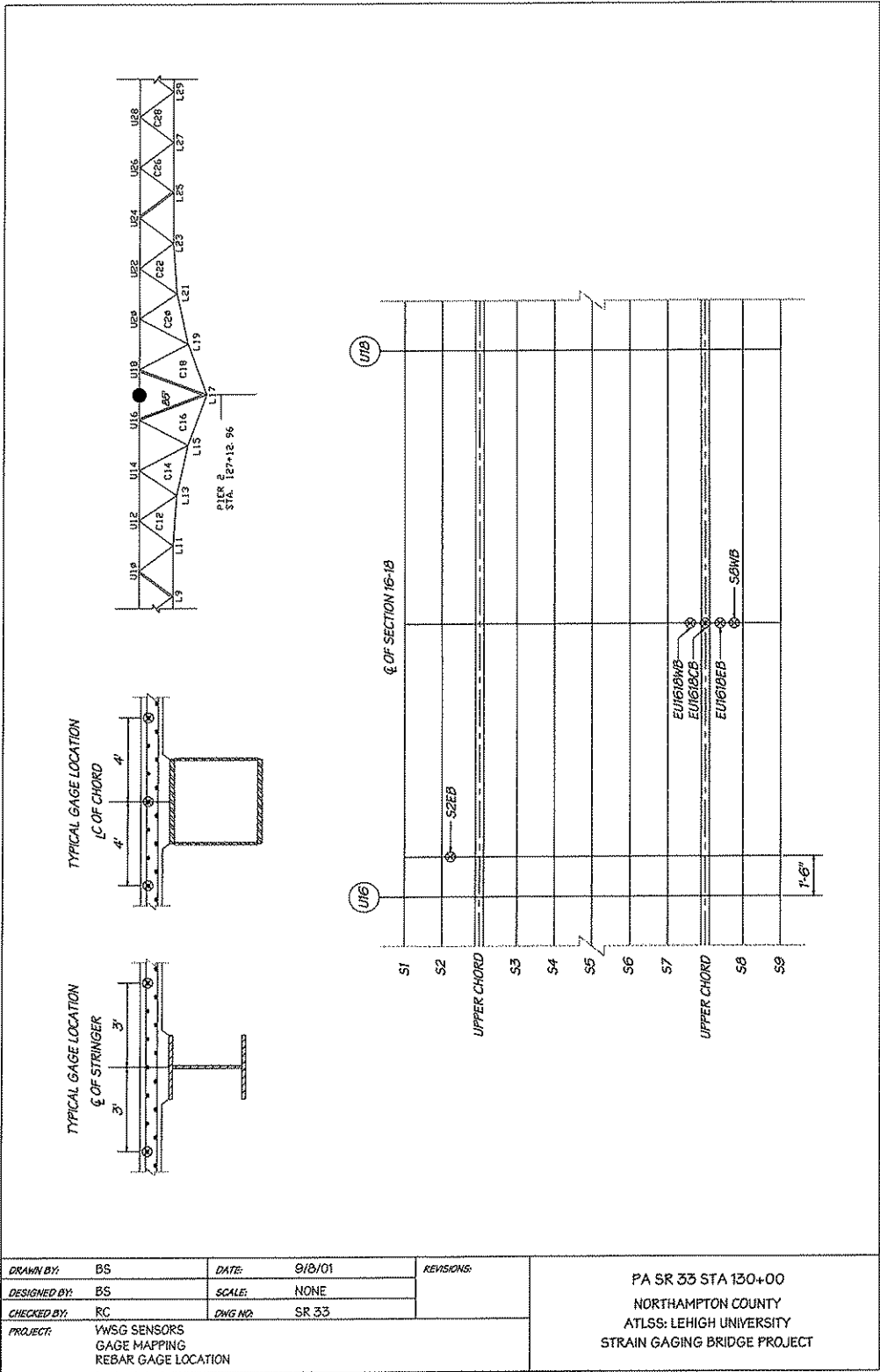
Figure 3.7. Strain gage layout on the reinforcing bar embedded in the deck.

36
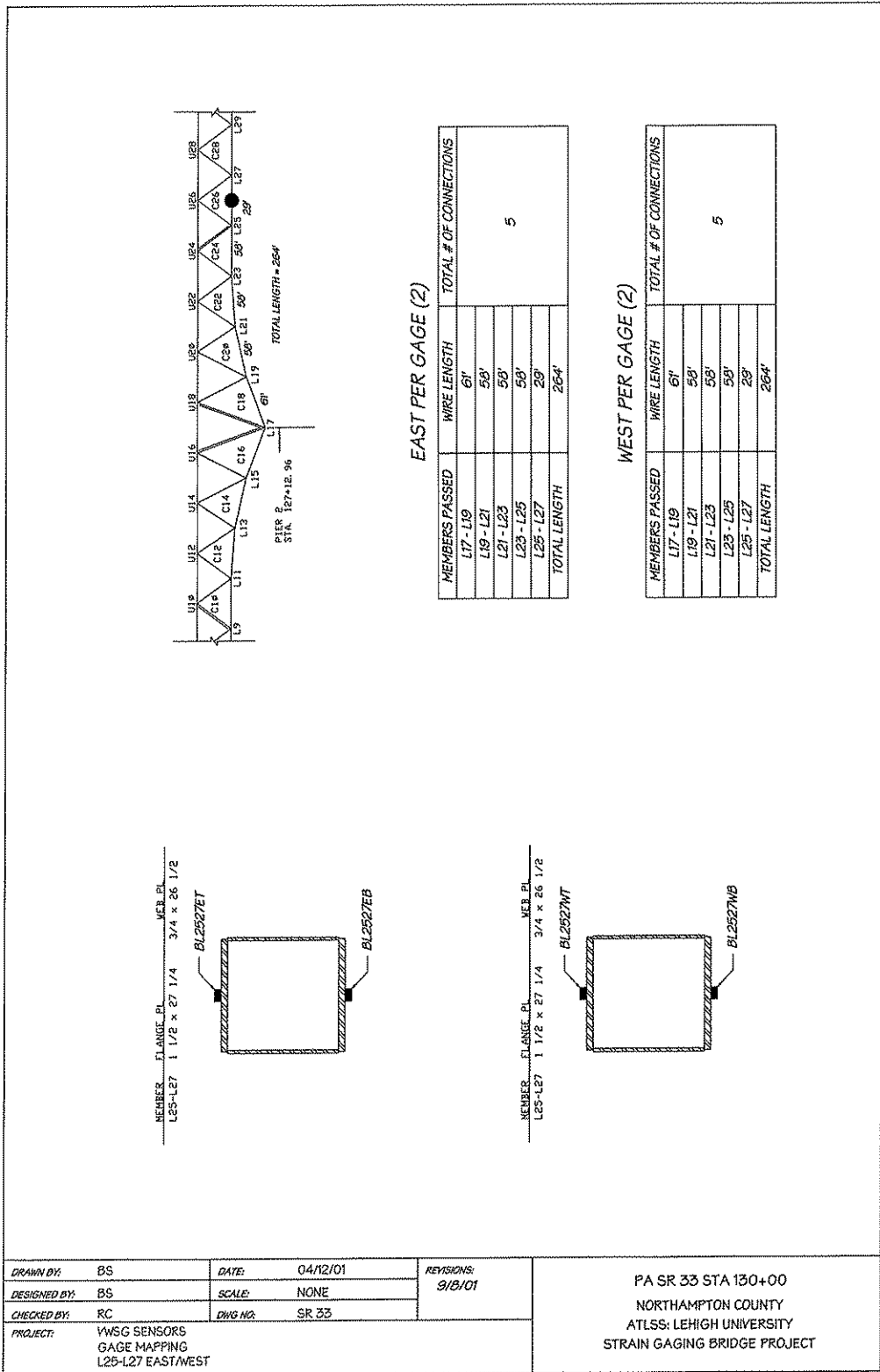
Figure 3.8. Strain gage layout on the lower chord between L25 and L27.
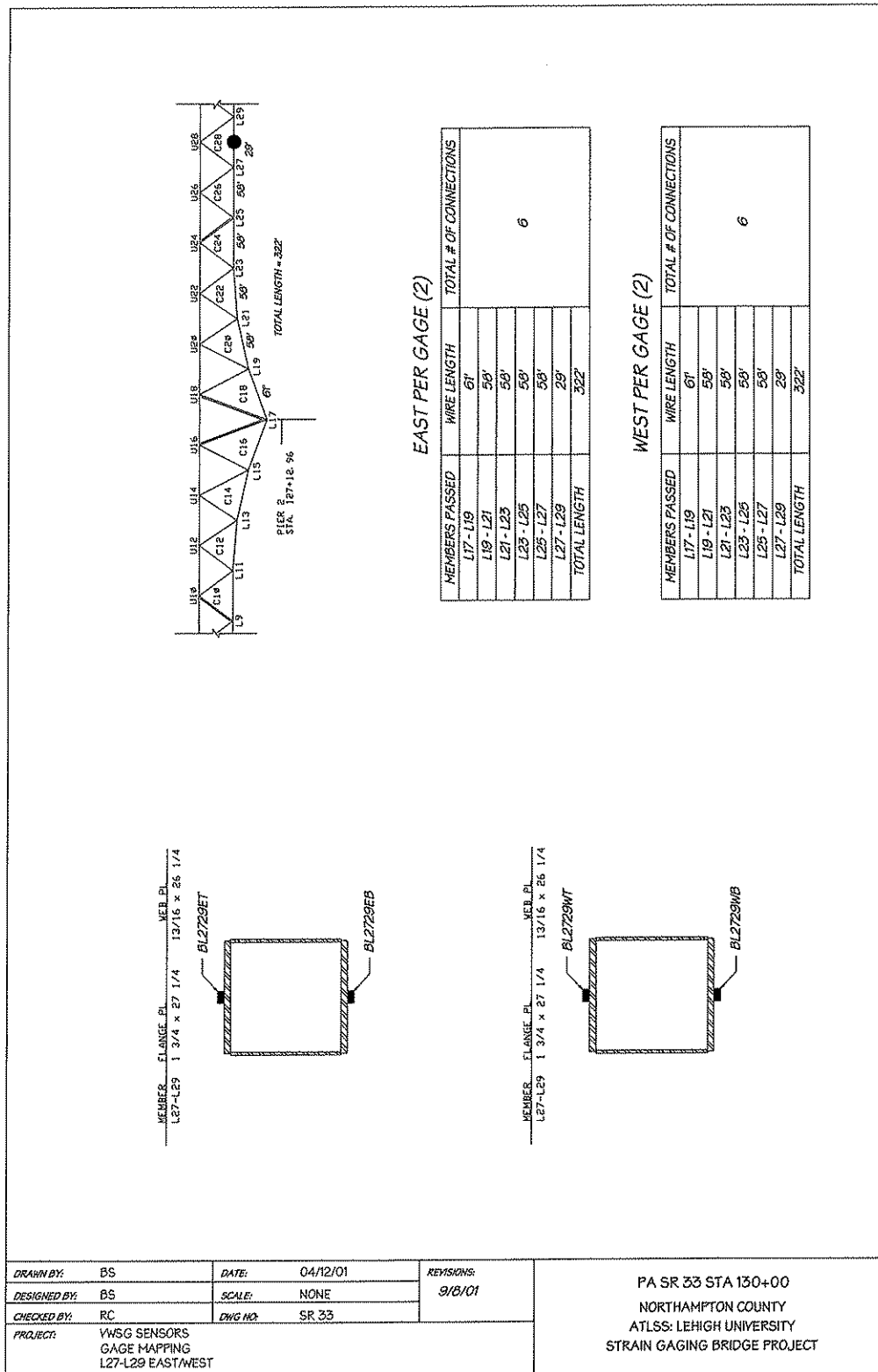
Figure 3.9. Strain gage layout on the lower chord between L27 and L29.

Test Description	Rear Axle Type	Front Axle Load (lb)	First Rear Axle Load (lb)	Second Rear Axle Load (lb)	GVW[1] (lb)	Truck #
Controlled Load Tests	Tandem[2]	17,450	33,250	34,050	84,750	80

Notes
1. GVW=Gross Vehicle Weight
2. Truck had a floating third rear axle that was in the "up" position for all tests.

Truck #	L1 (in)	L2 (in)	Wf (in)	Wr (in)	A[1] (in)	B (in)	C (in)	D[1] (in)	E (in)
Truck #80[2]	193	56	81.5	71.5	-	9.0	22.0	-	9.0

Notes
1. This dimension was not measured.
2. Truck had a floating third rear axle that was in the "up" position for all tests.
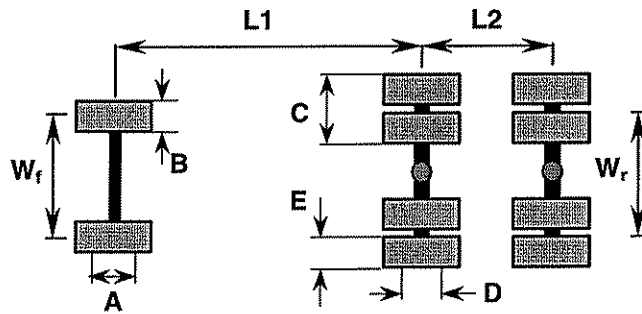
Figure 3.10. Controlled load truck information.
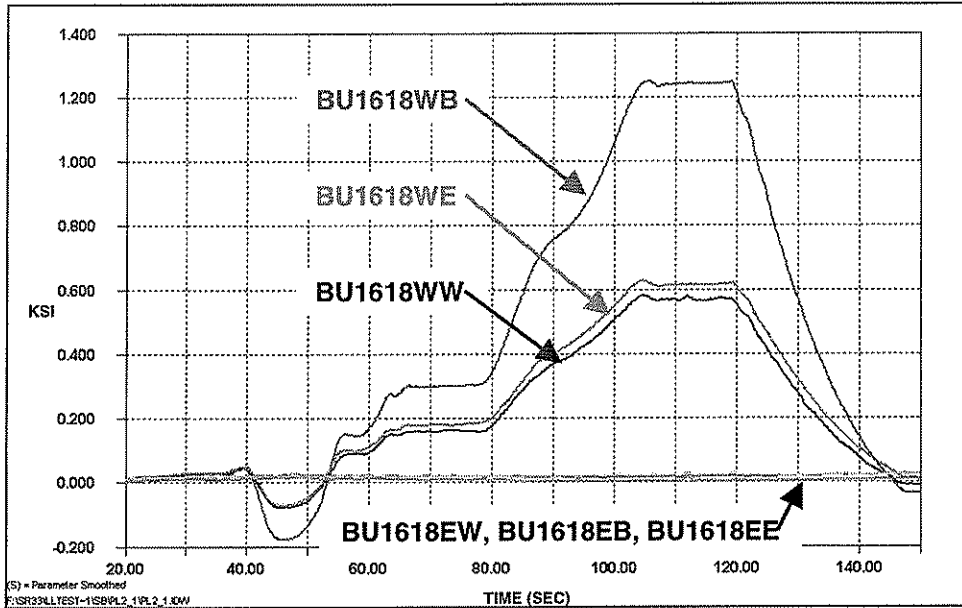
Figure 3.11. Typical upper chord response to a park test in Lane 2 (Truck #80 in Lane 2 headed north).
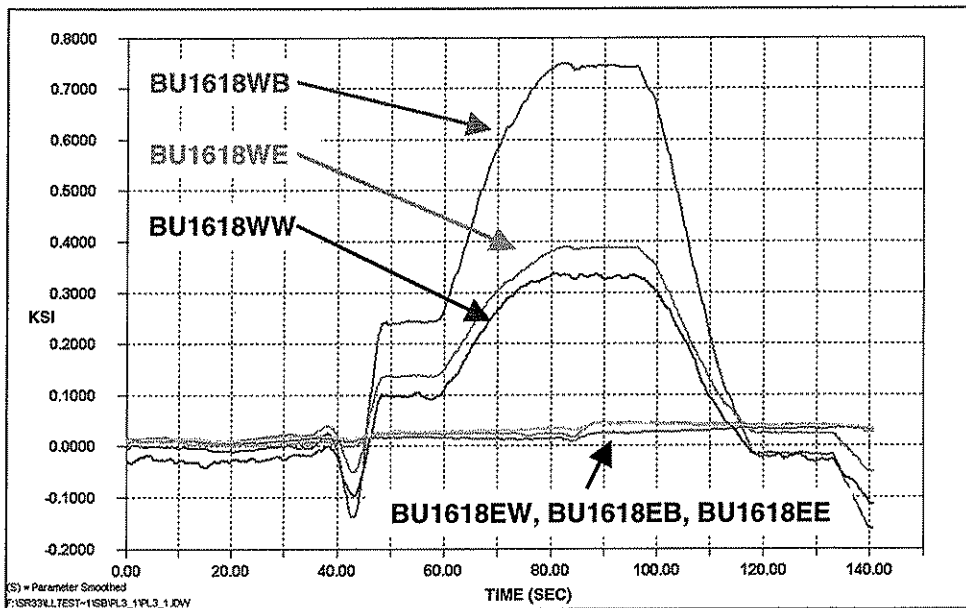
Figure 3.12. Typical upper chord response to a park test in Lane 3 (Truck #80 in Lane 3 headed north).

40
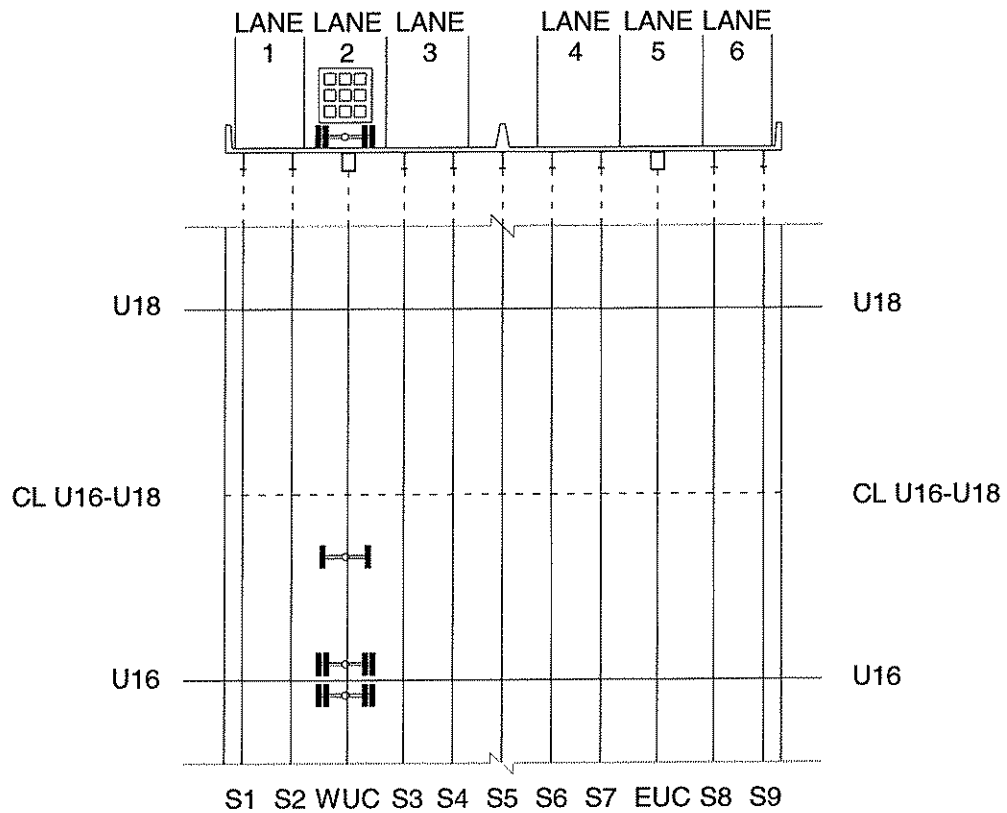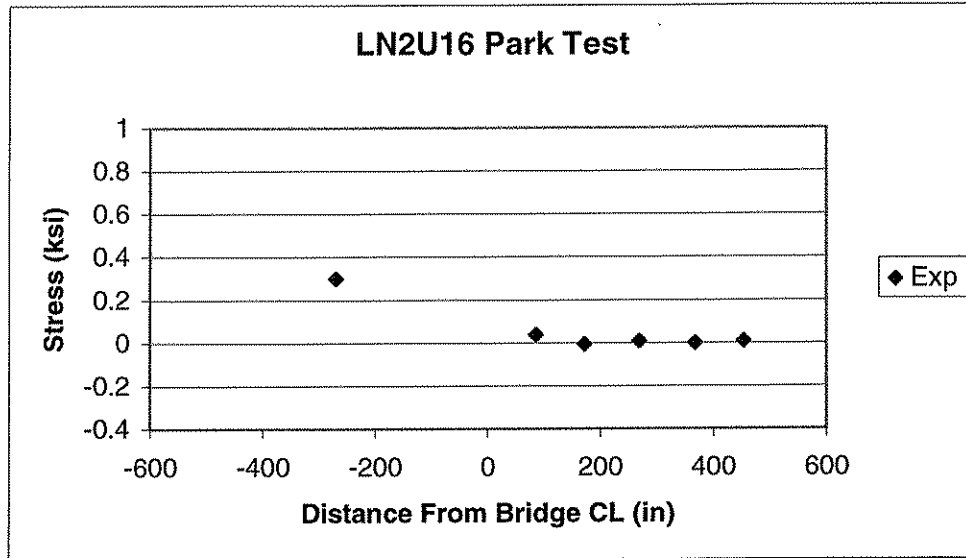
Figure 3.13. Experimental – Stringer bottom flange and upper chord bottom web results presented for a park test in Lane 2 with the centerline of the truck's back axles centered 18 in. north of U16.
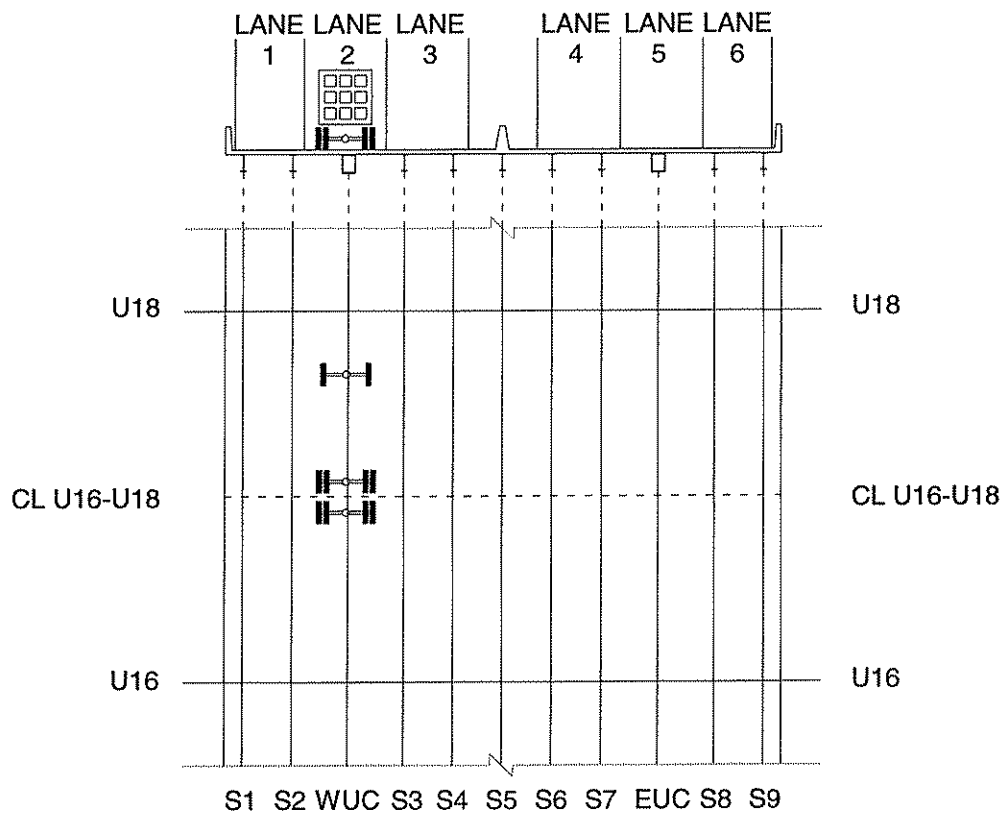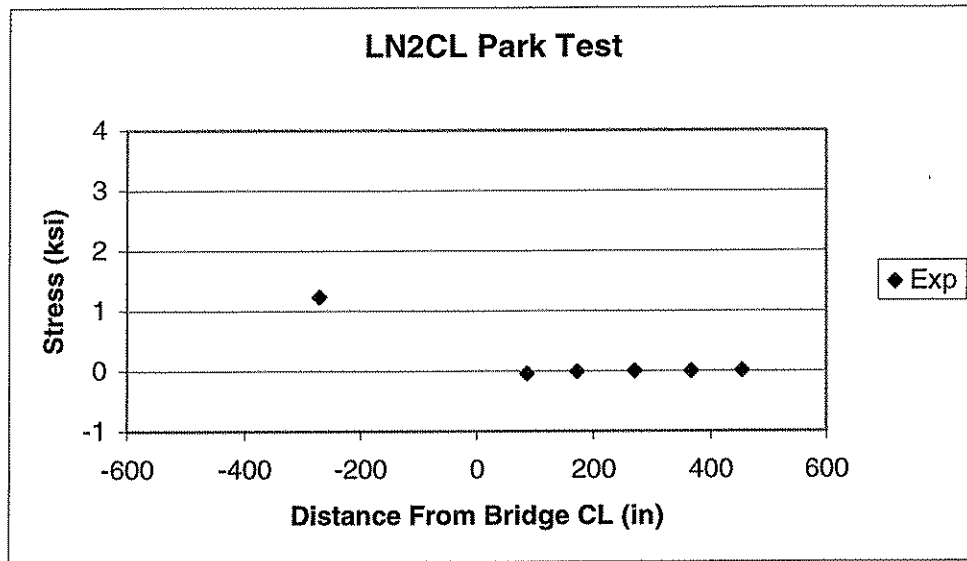
Figure 3.14. Experimental – Stringer bottom flange and upper chord bottom web results presented for a park test in Lane 2 with the centerline of the truck's back axles centered over the center of span between U16 and U18.
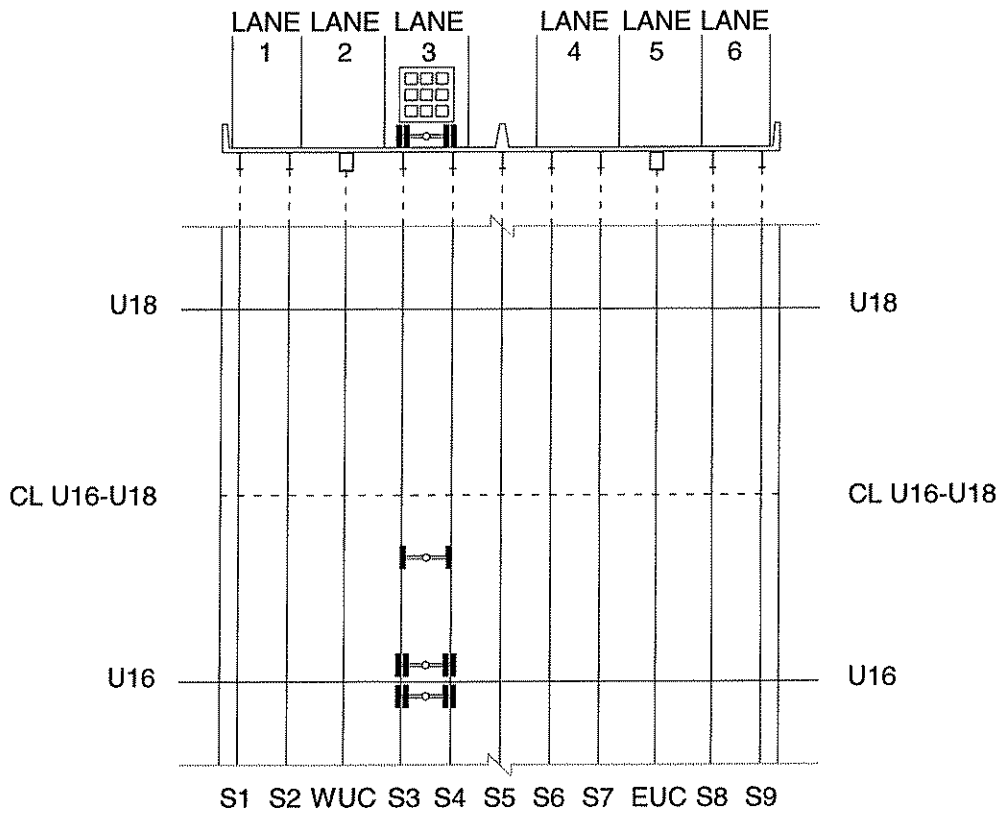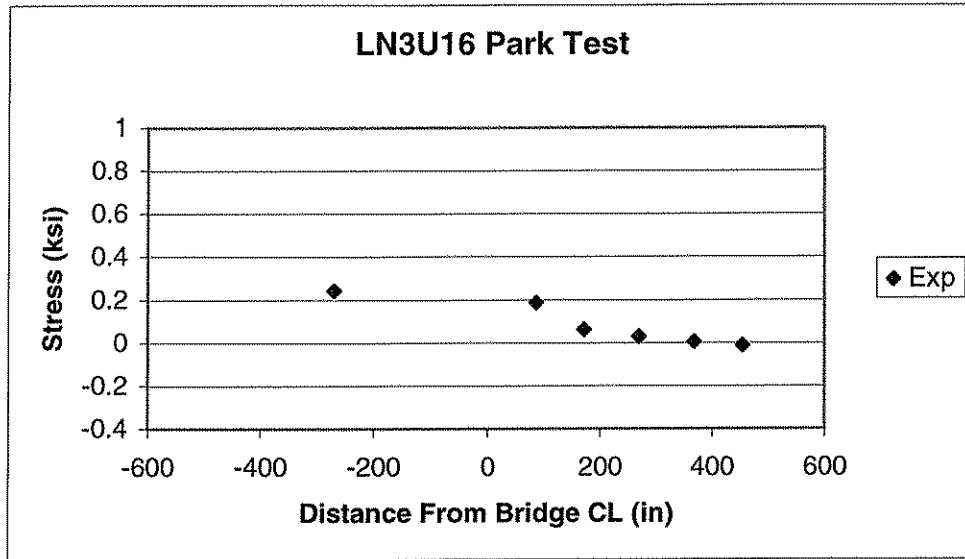
Figure 3.15. Experimental – Stringer bottom flange and upper chord bottom web results presented for a park test in Lane 3 with the centerline of the truck's back axles centered 18 in. north of U16.
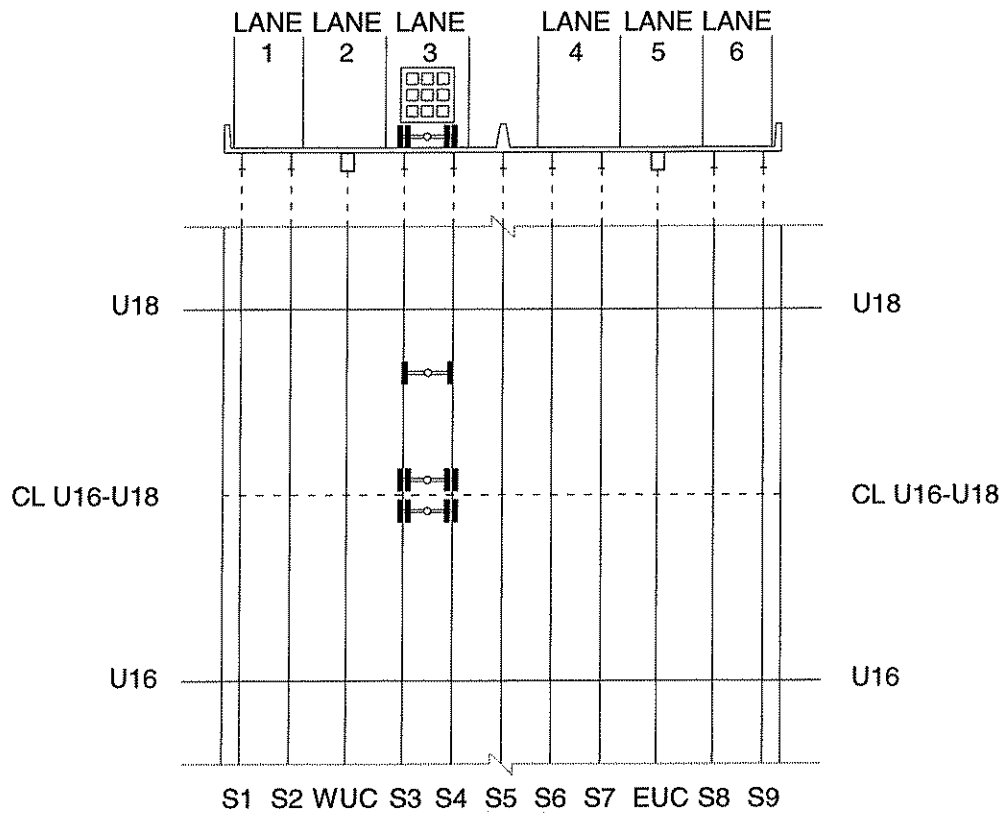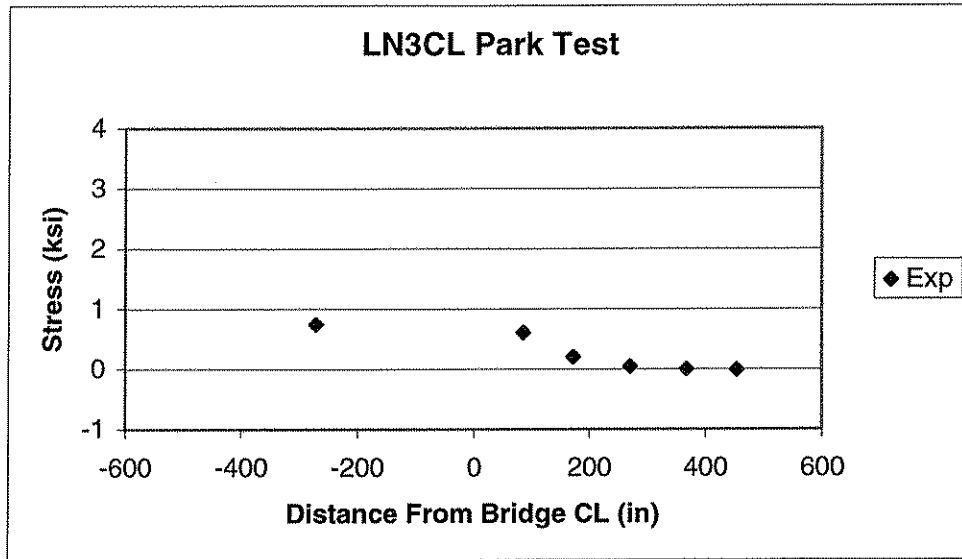
Figure 3.16. Experimental – Stringer bottom flange and upper chord bottom web results presented for a park test in Lane 3 with the centerline of the truck's back axles centered over the center of span between U16 and U18.

44
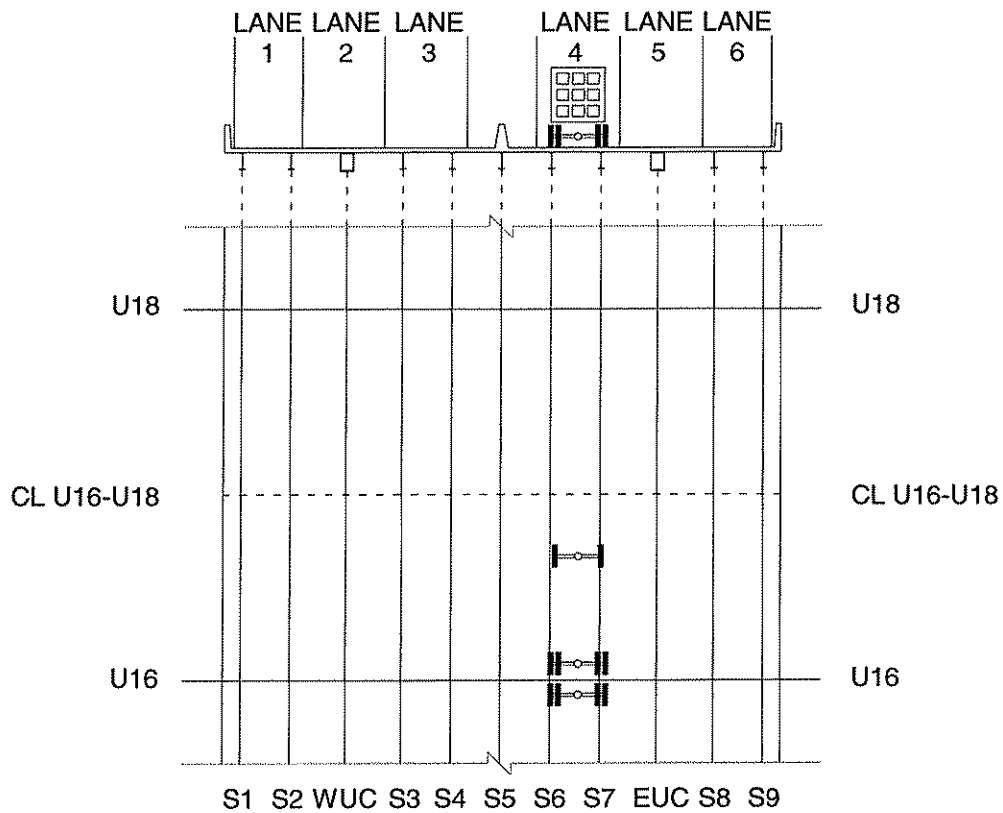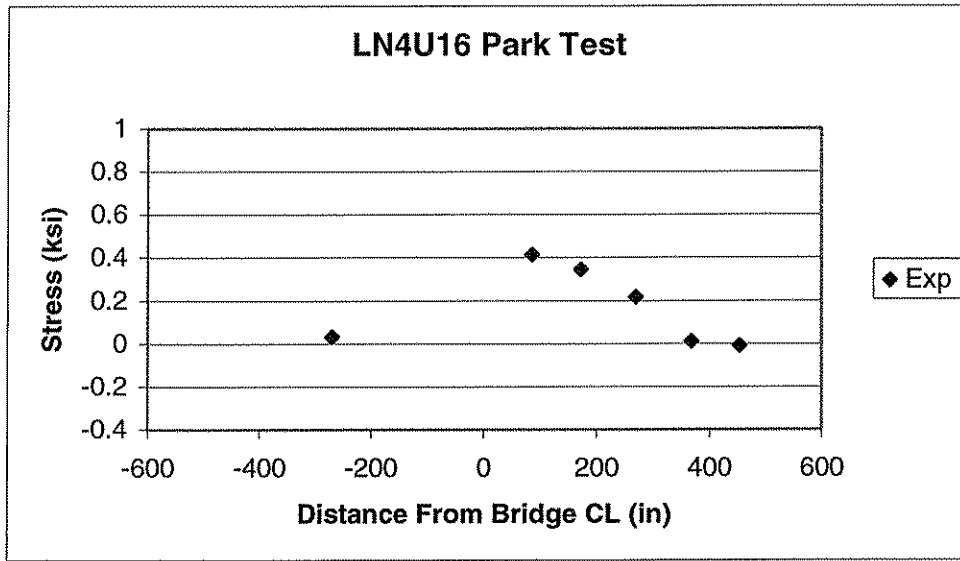
Figure 3.17. Experimental – Stringer bottom flange and upper chord bottom web results presented for a park test in Lane 4 with the centerline of the truck's back axles centered 18 in. north of U16.

45
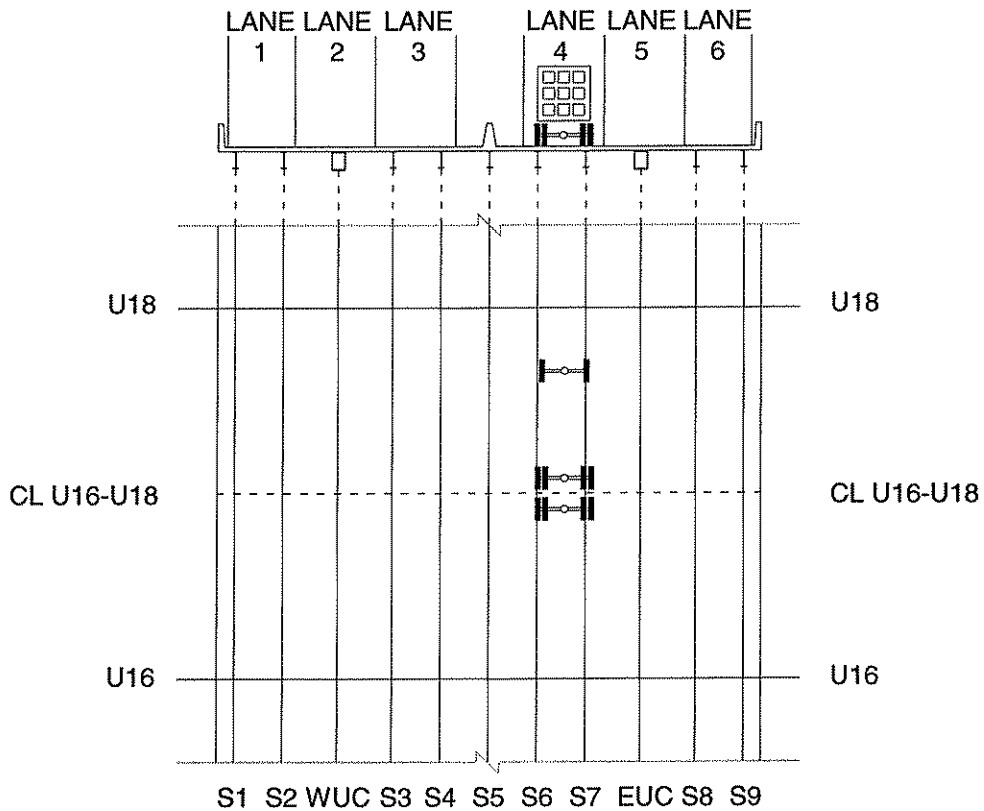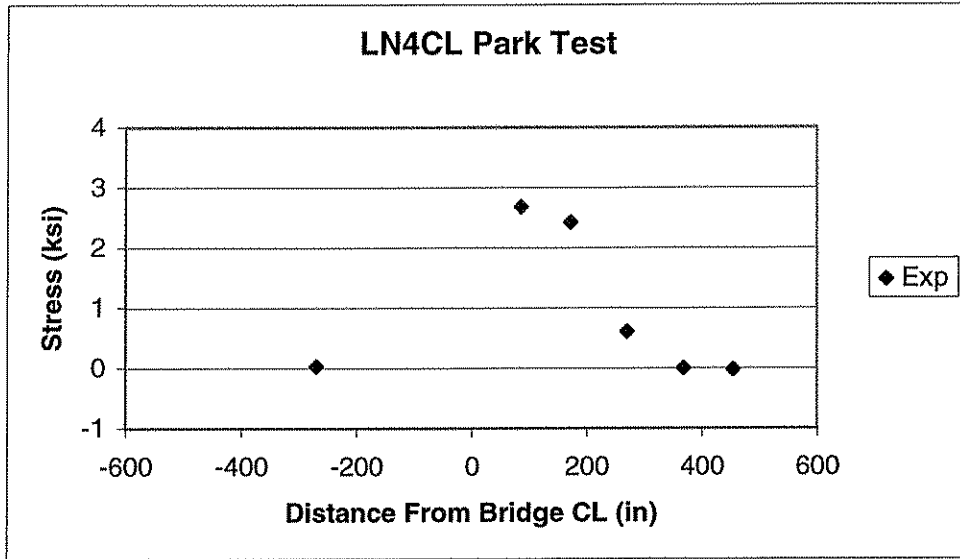
Figure 3.18. Experimental – Stringer bottom flange and upper chord bottom web results presented for a park test in Lane 4 with the centerline of the truck's back axles centered over the center of span between U16 and U18.

46
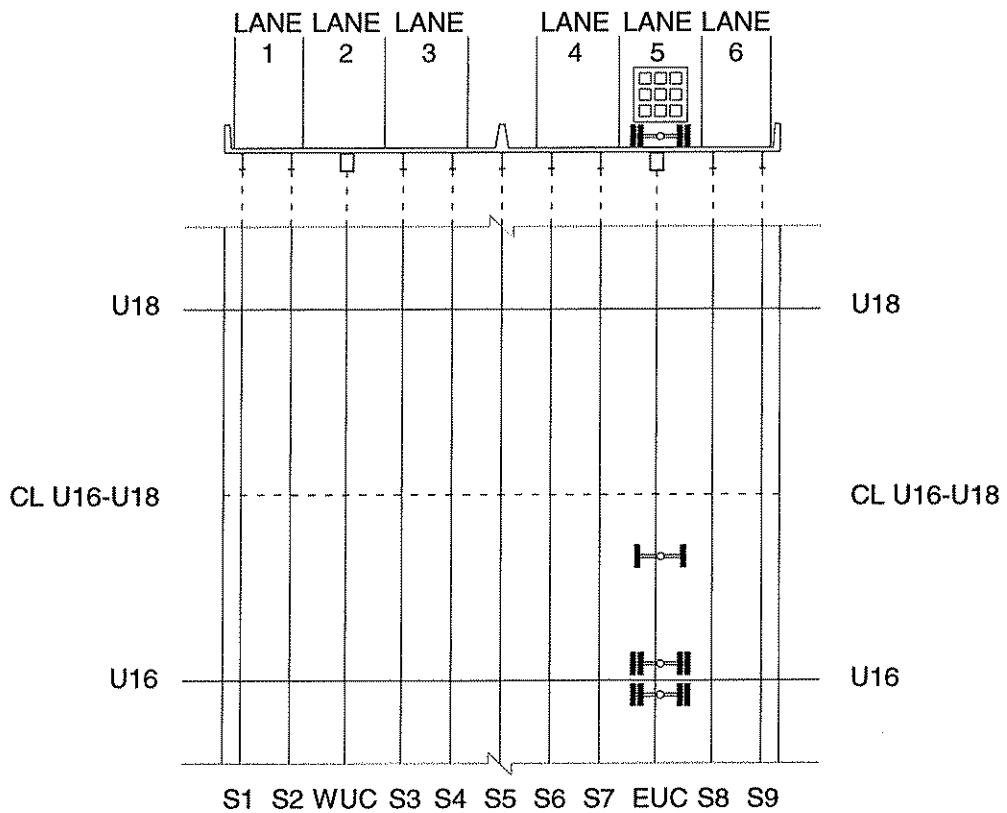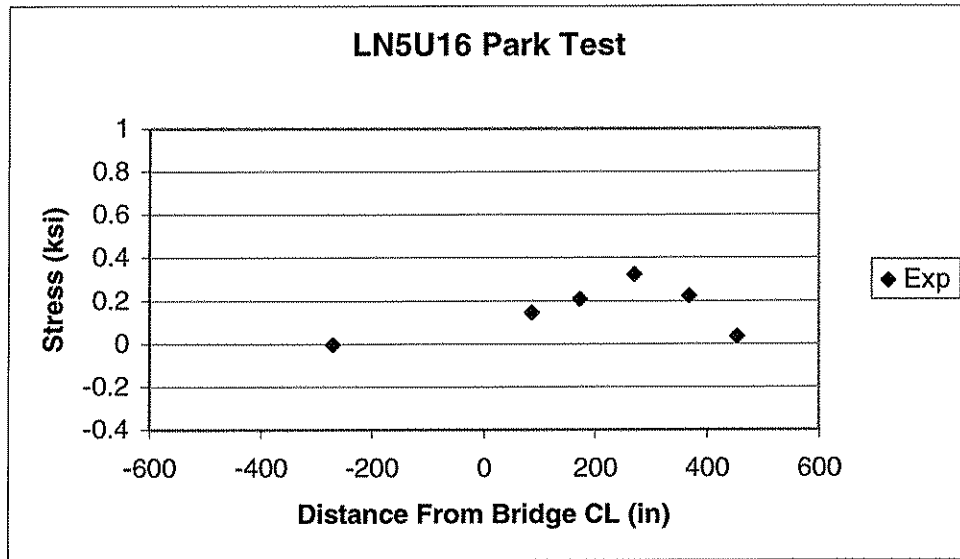
Figure 3.19. Experimental – Stringer bottom flange and upper chord bottom web results presented for a park test in Lane 5 with the centerline of the truck's back axles centered 18 in. north of U16.

47
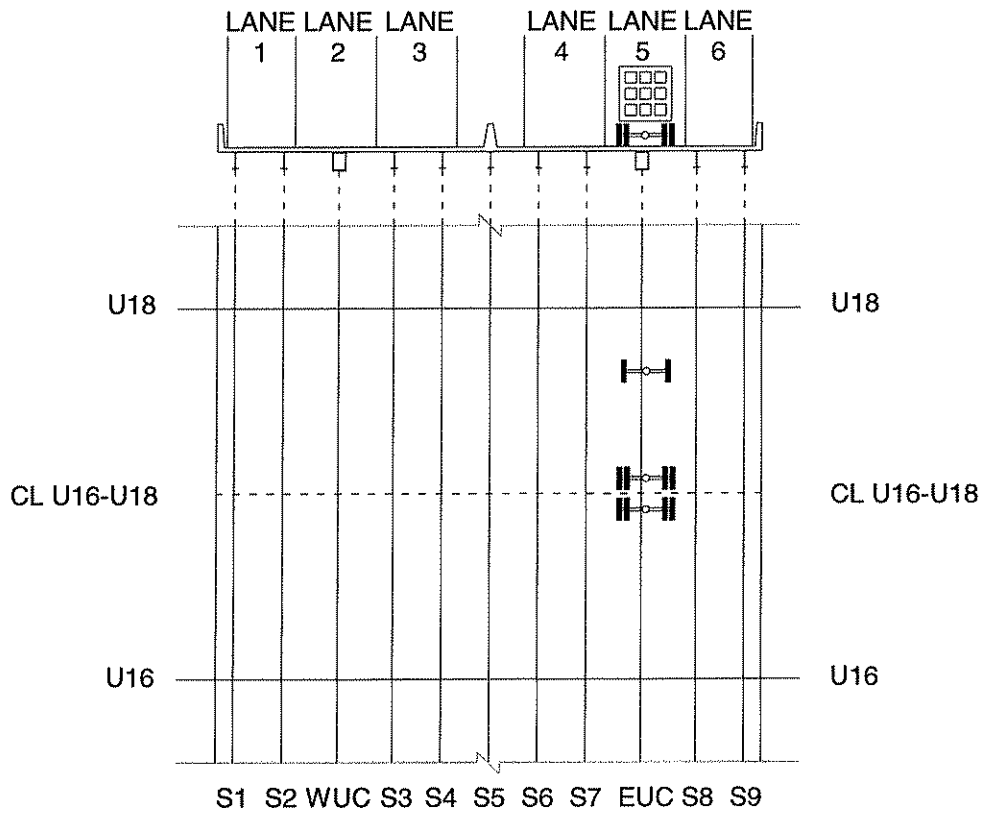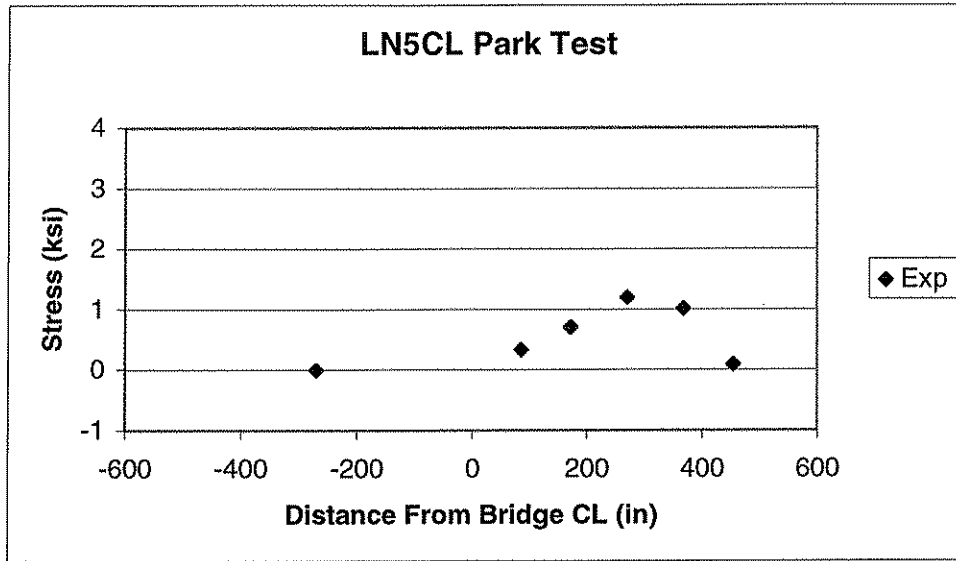
Figure 3.20. Experimental – Stringer bottom flange and upper chord bottom web results presented for a park test in Lane 5 with the centerline of the truck's back axles centered over the center of span between U16 and U18.

48
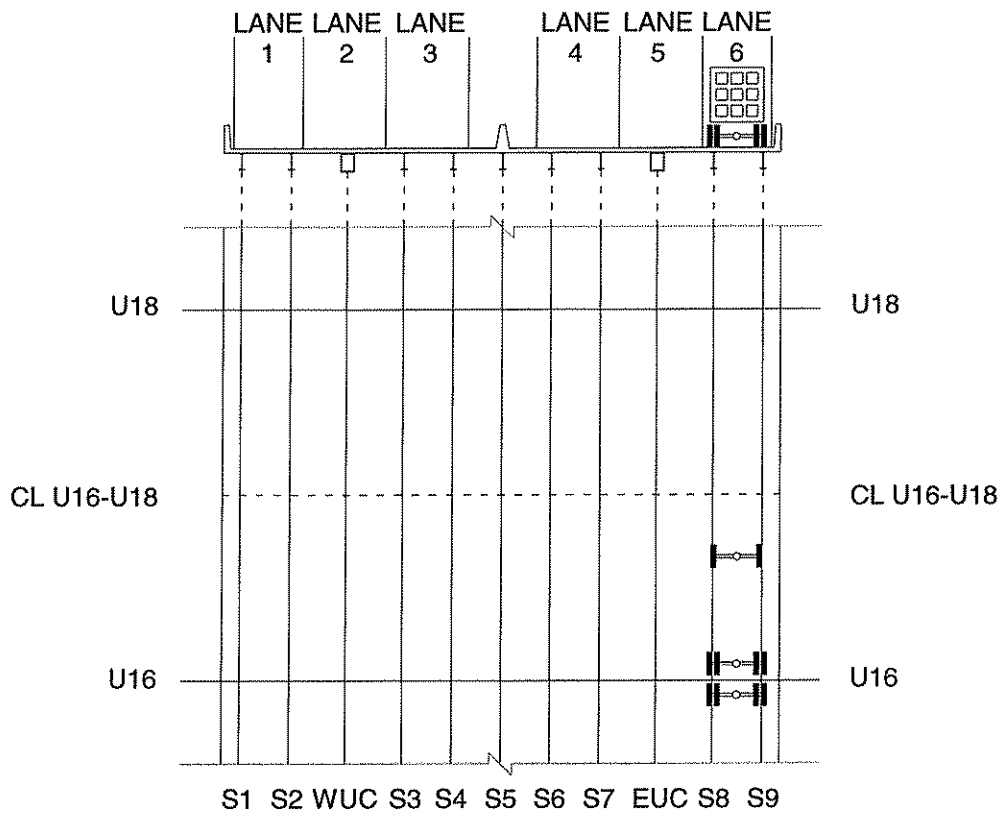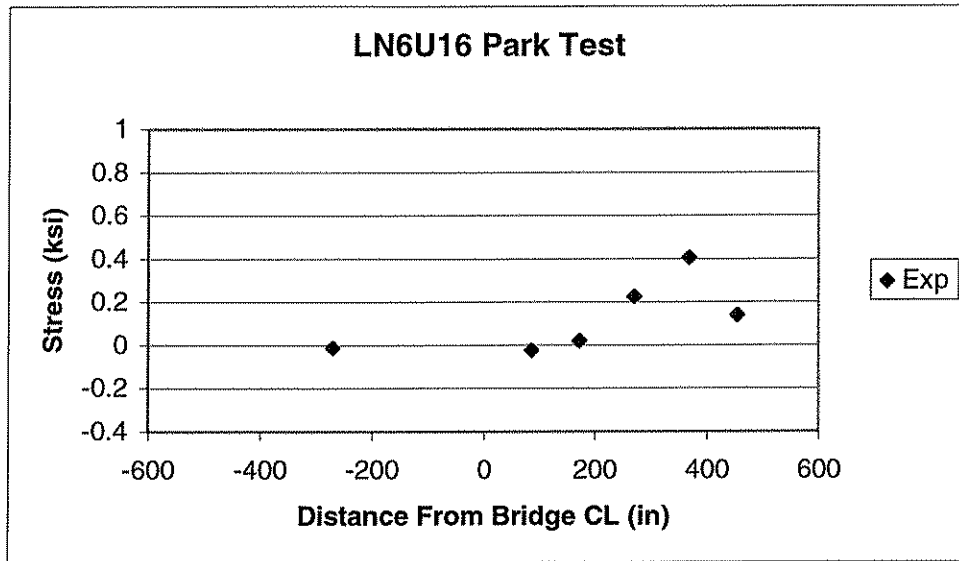
Figure 3.21. Experimental – Stringer bottom flange and upper chord bottom web results presented for a park test in Lane 6 with the centerline of the truck's back axles centered 18 in. north of U16.

49
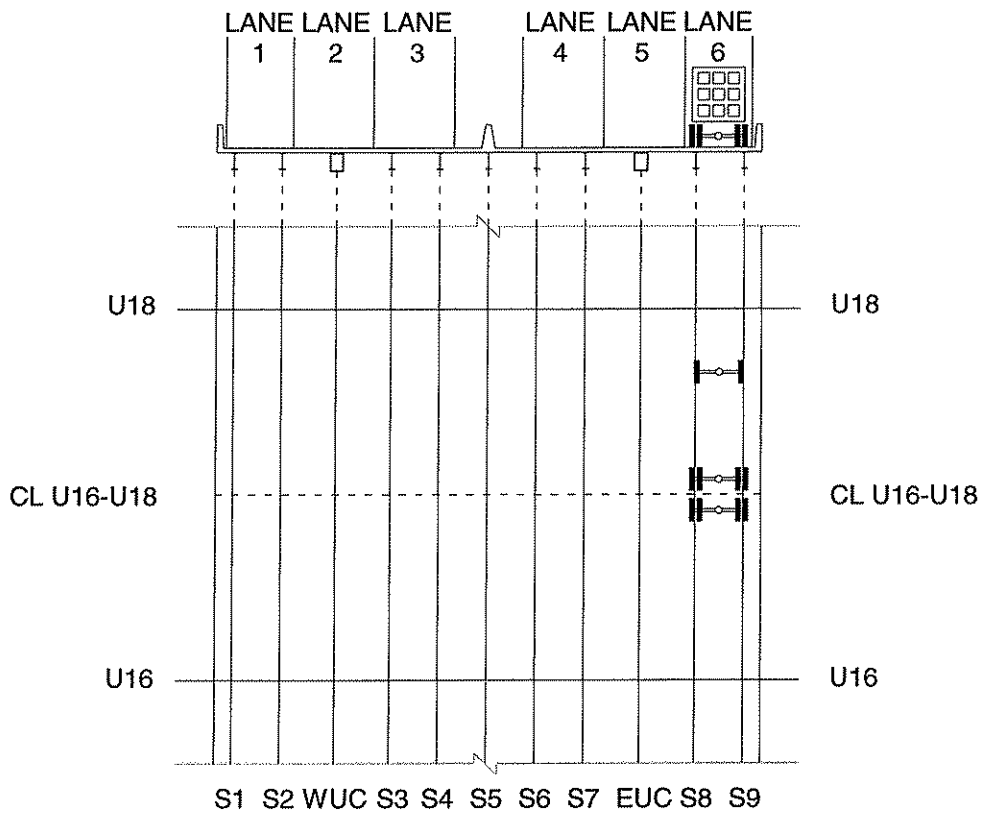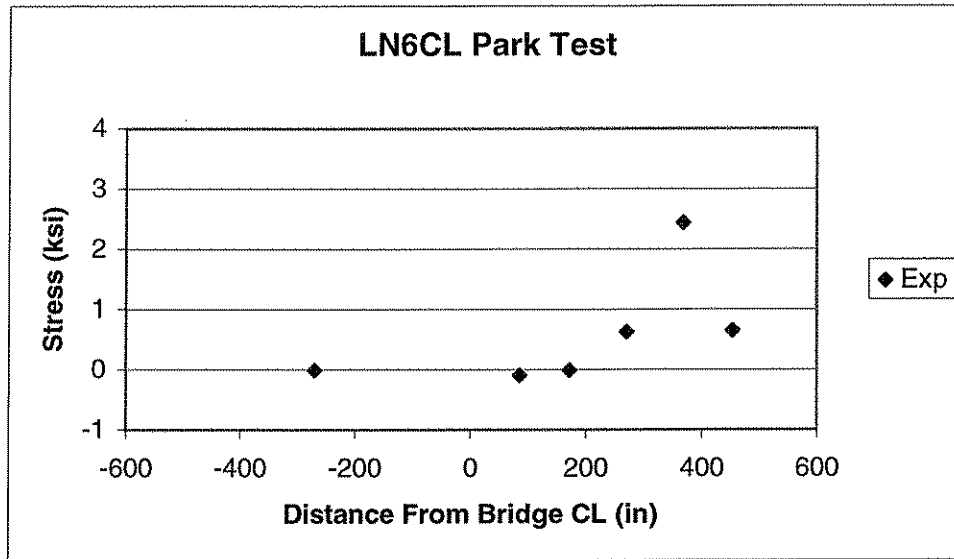
Figure 3.22. Experimental – Stringer bottom flange and upper chord bottom web results presented for a park test in Lane 6 with the centerline of the truck's back axles centered over the center of span between U16 and U18.
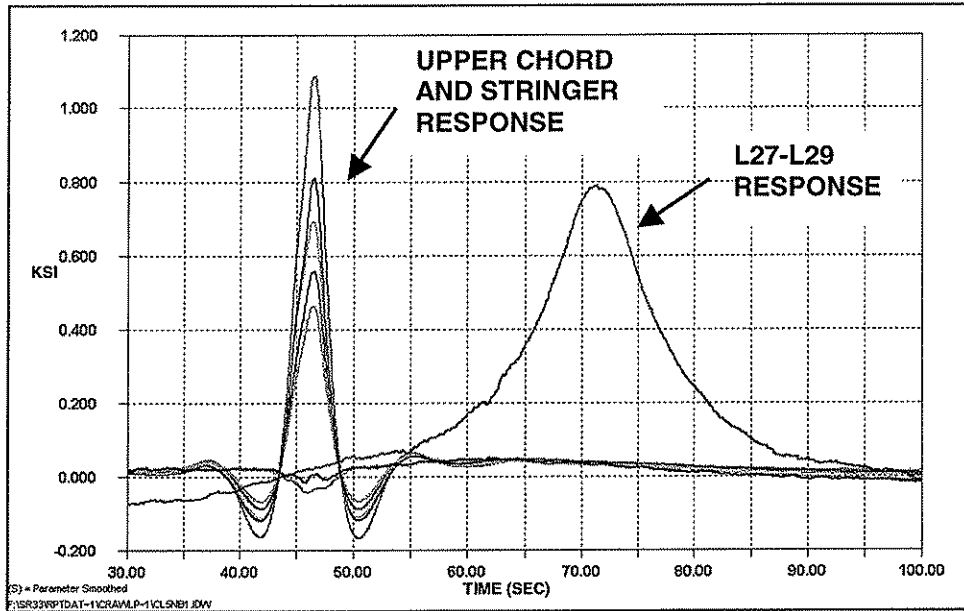
Figure 3.23. Upper chord and stringer response to a crawl test in Lane 5 (Truck #80 in Lane 5 headed north).
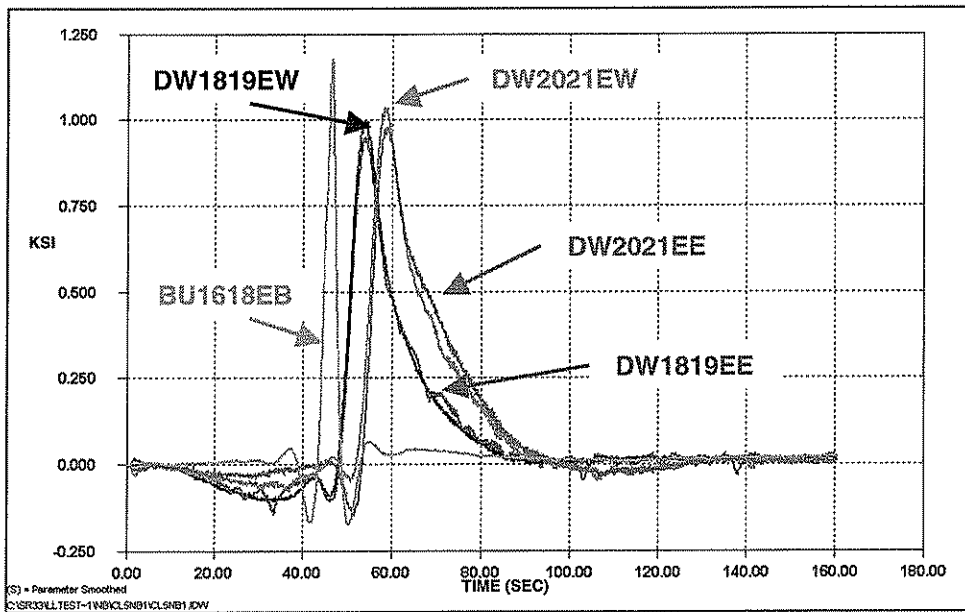
Figure 3.24. Response of east upper chord and diagonals during a crawl test in Lane 5 (Truck #80 in Lane 5 headed north).
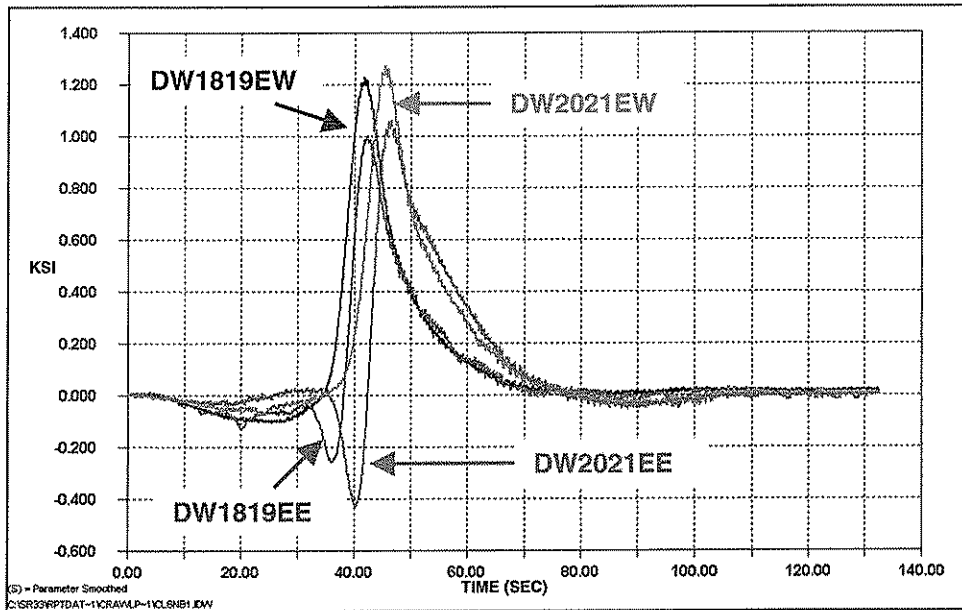
Figure 3.25. Typical east diagonal response to a crawl test in Lane 6 (Truck #80 in Lane 6 headed north).
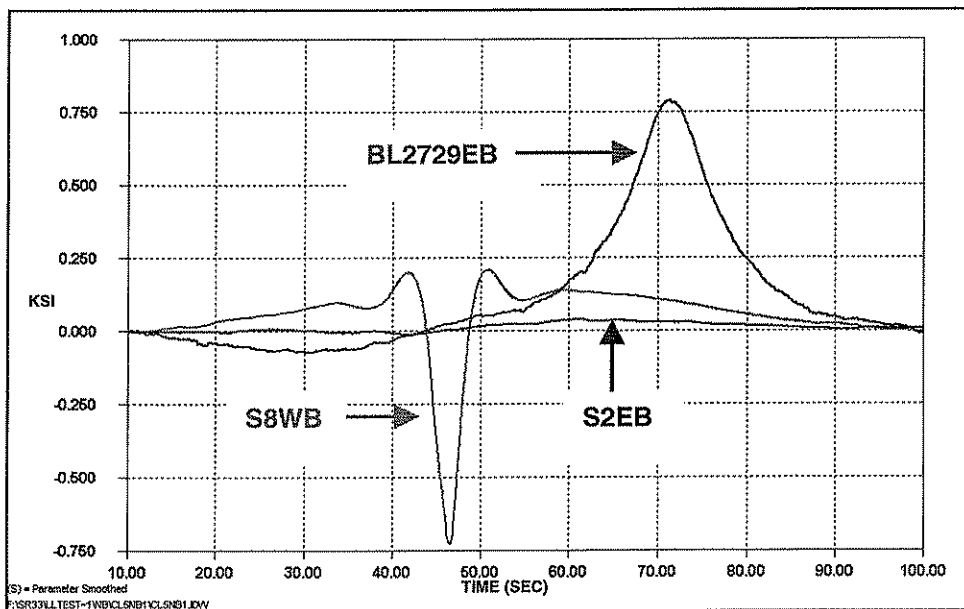
Figure 3.26. Typical embedded gage response to a crawl test in Lane 5 (Truck #80 in Lane 5 headed north).

CHAPTER 4
LATERAL WHEEL LOAD DISTRIBUTION

4.1   INTRODUCTION

This chapter describes the lateral load distribution model. Section 4.2 is an overview of the method of analysis used to obtain analytical results for lateral load distribution. Section 4.3 describes the lateral load distribution model and how it was created. First, a mesh refinement study is discussed. Next, an overview of some basic connections is addressed. Following this, the boundary conditions of the model are discussed before it is finalized. Lastly, more complex connections are addressed. Section 4.4 contains the results of the lateral load distribution model obtained from the park test loadings discussed in Chapter 3. The comparison of the lateral load distribution results with the experimental results is discussed in Section 4.5. Finally, Section 4.6 discusses the effect of the lateral load distribution analysis on the full bridge model, which is addressed in Chapter 5. This chapter provides analytical results that are compared to the lateral load distribution bridge design assumption selected for study. This comparison is presented in Chapter 6.

4.2   DESCRIPTION OF THE MODEL

A finite element model was constructed in order to verify design assumptions related to the lateral load distribution of the bridge. The area of interest of the bridge lies between panel points U16 and U18 on the bridge structure. Therefore, the lateral load distribution model only encompassed the structural elements from U14 to U20. Specialized boundary conditions were used to simulate the existence of the rest of the bridge. This section discusses this material further.

4.2.1 Shell Element Mesh Refinement Study

Shell elements were chosen to represent all of the structural elements associated with the bridge deck in the defined area of interest for the lateral load distribution analysis. This defined area can be seen in Figure 4.1. Shell elements were chosen because they combine both *membrane and plate-bending behavior... The membrane behavior... includes translational in-plane stiffness components and a rotational stiffness component in the direction normal to the plane of the element... The plate bending behavior includes two-way, out-of-plane, plate rotational stiffness components and a translational stiffness component in the direction normal to the plane of the element* (CSI, Inc., 2000). These properties and the availability of the full range of degrees of freedom were important in the modeling process to ensure an accurate result.

The first task was to determine how refined the mesh of shell elements through the depth and width of a given structural member had to be in order to produce an accurate result. Figure 4.2 shows isometric drawings of the models created to accomplish this task. Table 4.1 summarizes the mesh refinement features of these models. All models simulate a W30X124 (one of the sections

used as longitudinal stringers supporting the bridge deck) steel section with shell elements or frame elements. A point load of 25 kips was applied at the longitudinal third point of each model. In all models the length of the elements along the member was 10 inches and simple supports were used. The results of the models built of shell elements (Beam1w, Beam2w, Beam4w, and Beam8w) were compared to those of the model built with frame elements (Frame) to determine which of the shell element models represented reality most accurately. The web shell aspect ratio used in this model, defined as the larger shell width divided by the smaller shell width, was then used as a guide for similar construction in this research.

The first shell model, Beam1w, consisted of two shell elements through the width of each flange and one shell element through the depth of the web in each cross section. Subsequent models retained the selection of two elements through the width of the flange of the members but increased the number of elements through the depth of the web of the member. Additional analyses were run with two (Beam2w), four (Beam4w), and eight (Beam8w) elements through the depth of the web. In each subsequent model the aspect ratio of the web shells changed while that of the flange shells was static.

Figure 4.3 presents the results of the analyses run on these models. The results for the model with only one element (Beam1w) through the web were not accurate. The results for the models with two (Beam2w), four (Beam4w), and eight (Beam8w) elements through the web were very similar to those obtained using the frame element. It was determined from the plot presented in Figure 4.2 that it was best to use four elements through the depth of the members. This provided acceptable accuracy without requiring excessive computational time to run the models. Based on these results, all stringers were modeled using four shell elements through the depth of the web and two shell elements through the width of each flange cross-section.

A similar configuration was utilized to construct the cross section of the box members of the bridge's upper chord. These members are roughly 34 in. tall and 28 in. wide. This height is comparable to the 30 in. height of the steel stringer section already discussed. To keep as uniform an aspect ration as possible, four elements were used through the depth of each side flange, and three elements were used across the width of each top and bottom web. Figure 4.4 shows the final mesh configurations for the box and stringer sections.

The floorbeams, gusset plates, reinforced concrete deck elements, and various others also in this research used a similar aspect ratio where this was possible. Some changes in geometry required deviation from this standard, but these instances were few.

4.2.2 Shear Studs

In the lateral load distribution model, the connectivity provided by the shear studs was simulated with short links having a high stiffness. Figure 4.5 shows an example view of these shear links. O'Connell and Dexter (2001), Mourad and Tabsh (1999), and Cao and Shing (1999) also used this method

when simulating the composite action of a deck truss bridge when evaluating fatigue truck loading of steel trusses. Section 2.4 of this report reviews the models used in these previous works.

These shear link elements were given enough stiffness to hold the reinforced concrete deck in composite action with the truss, but were flexible enough to eliminate the possibility of an ill-conditioned stiffness matrix. The section used had the properties of steel with a moment of inertia in each direction of 25,000 in.[4]. These shear links connected the deck to the supporting structural steel every 9 in. along the length of the model.

4.2.3 Stringer to Floorbeam Connections

The longitudinal stringers supporting the deck in the field were connected to the transverse floorbeams in two ways. Stringers S1 and S9 were continuous exterior beams with full moment splices in designated locations along the length of the bridge. Figure 4.6 presents this connection as it was erected in the field. They were connected to the tapered end of the floorbeams with steel angles that bolted into the webs of both members. Shear studs were installed on the floorbeam top flange and the stringer top flange, allowing the reinforced concrete deck to complete the connection.

In the lateral load distribution model, flange and web shell connections were provided continuously along the entire length to discretize these continuous beams. The connection between the floorbeams and Stringers S1 and S9 was modeled by connecting the web shell elements of the members in four locations. Figure 4.7(a) presents this connection as it was created in the lateral load distribution model.

Stringers S2 through S8 were connected to the webs of the floorbeams in the field with bolts and angles. The top flange of each stringer was coped where it framed into the floorbeam. This connection was reproduced in the lateral load distribution model as shown in Figure 4.7(b). Both the top and bottom flanges were coped to allow for flange discontinuity at the floorbeam locations. The webs of the floorbeams and the stringers were attached in three locations, mimicking the bolted angle connection that was installed in the field. These interior stringers were also made composite with the concrete deck through the use of shear links (not shown in Figure 4.7).

4.2.4 Upper Chord Box Girder to Floorbeam Connections

The connection between the upper chord box girders and the floorbeams is quite complicated. It is one of the few connections made at the panel points, all of which are discussed within the next sections. Photographs of this connection are shown in Figure 4.8. At a panel point in the field, the upper chord box members are butted up against each other and connected with large gusset plates. The floorbeams are of constant depth between the trusses. A plate welded to the end of the members allowed them to be set perpendicular to the truss lines and bolted to the gusset connection. On the outside of the trusses, the floorbeam tapers in depth as the cantilever extends away from the truss line.

55

The free end of these cantilevers was discussed in Section 4.2.3. The fixed end of these cantilevers also had a welded plate attached to it that allowed them to be set perpendicular to the truss line and bolted to the gusset connection. A diaphragm was added to the inside of the box section in plane with the web of the floorbeam. A continuity plate was added underneath this diaphragm (outside the box section and also in plane with the web of the floorbeam) between the gusset plates and a tie plate was strapped across the box section and bolted to the top flanges of the adjoining floorbeam sections to complete the connection.

In the lateral load distribution model, the upper chord box girders were assumed to be continuous through the gusset plates due to the large number of bolts specified for the field connection and the size of the gusset plates. Therefore the web and flange members were continuously connected through nodes along the length of the lateral load distribution model. A view of this connection is shown in Figure 4.9. Only slight changes in geometry occurred at the connection to account for changing box member sizes. The stresses at this connection were not a focus of this report, so this approximation was appropriate. The floorbeams were modeled as continuous through the gusset plates. This assumption stemmed from the field addition of the diaphragms and the tension tie plate for continuity. The upper chord box members passing through these continuous floorbeams were attached at coincident nodes.

4.2.5 Gusset Plates

The gusset plates used to hold the panel points together were constructed of plate stock drilled in the appropriate locations to receive all of the structural steel that framed into them. A photograph of one of these plates is shown in Figure 4.10(a). This is just one example, as each set of plates was sized and shaped according to its demands. In order to model these plates efficiently, two important simplifications were made. The large number of bolts used to attach the gusset plates to the upper chord and diagonal members did not allow any slip on these surfaces. Therefore the gusset plates and these members were for the most part modeled in the same plane. (As mentioned in Section 4.2.4, small changes in geometry were necessary to account for changing upper chord width.) At any location where the upper chord or diagonal members were coincident with the gusset plates the thickness of the shell elements was increased to reflect this coincidence. A view of extruded finite elements is shown in Figure 4.10(b) for visual clarification.

The other simplification stemmed from the presence of members in the field that did not significantly contribute to the stiffness of the model in the direction in which it was loaded. For instance, the horizontal cross bracing between the trusses had little to no bearing on the stress results in the area of interest marked in Figure 4.1. Falling into the same category were the two upper diagonal members of the sway bracing attached to the upper chord at U16 and U18. These members were omitted in the lateral load distribution model and had little to no bearing on the gathered results.

4.2.6 Diagonal to Gusset Connections

The diagonal members of the truss were another set of members that framed into the panel points. Figure 4.10(a) is a photograph of the connection in the field that was constructed by slipping the diagonal sections, whether they were box sections or H sections, between the gusset plates that extended down from the sides of the upper chord members and bolting them into place. In the lateral load distribution model, this connection was constructed in much the same fashion. Figure 4.10(b) is a view of what it looks like in the lateral load distribution model. As was done for the upper chord sections, the diagonal members were modeled with a positive moment connection due to the number of bolts used in this connection.

4.2.7 Parapets

Figure 4.11 shows the concrete median parapet as it exists on the bridge and in the lateral load distribution model. The parapets on either side of the bridge are very similar in nature. In the lateral load distribution model, they are connected to the concrete deck through coincident nodes at every nine inches longitudinally along the length of the bridge.

4.2.8 Boundary Refinement Study

In order to manage the lateral load distribution model, a study was conducted to limit the size of the refined shell mesh region. The whole bridge could not be modeled using shell elements because the model would be too large. In addition, a model using shell elements to represent every member was not required to produce good results in the area of interest for this research. Therefore, the boundary refinement study's purpose is to obtain the required number of spans between panel points (54 ft. sections) needed to produce reasonable results in the area of interest. Once this property is known, the refined mesh area needed to produce desirable stress results in the area of interest can be modeled with shell elements, and the rest of the structure can be modeled using the appropriate boundary conditions to reduce computation time.

This study was conducted during the process of model refinement. The specific boundary conditions explained in this section were used for the purpose of determining the number of 54 ft. sections required to produce good stress results in the area of interest and are not the final boundary conditions of the lateral load distribution model.

The loading conditions used to test the boundary conditions were the loading conditions used to represent the park tests discussed in Chapter 3. This choice allowed the iterations of results to be compared against the previously collected experimental data.

In order to determine how many panel points of the bridge needed to be modeled to capture precise stress results in the region between U16 and U18, the deck and supporting steel stringers, floorbeams, and upper chord members were modeled without the diagonals or the lower chord of the truss. Three boundary refinement models were constructed: one with three spans (U14 to

57

U20), one with five spans (U12 to U22), and one with seven spans (U10 to U24). Figure 4.12 presents views of these models. The 54 ft. sections between panel points are defined as a *span* throughout this chapter. In each case, the far ends of the model were given a pinned boundary condition on each side of the bottom flange of each of the stringers and upper chord box sections. This boundary condition was chosen because the floorbeam at this bridge cross-section was omitted from the model. The purpose of the pin was to allow rotation but to constrain longitudinal movement of the floorbeam location. This simulated the presence of the rest of the bridge deck structure. At the interior floorbeam locations, the upper chord box sections were pinned on either side of the bottom flange. The purpose of this boundary condition was to limit longitudinal movement while allowing rotation in the plane of the bridge cross-section. It also somewhat restrained rotation out of plane, as the diagonal members would do in the lateral load distribution model.

Figures 4.13 to 4.22 show the results of the three boundary refinement models and experimental results due to the park test load cases. In each figure, the data points represent the stress in the bottom flange of the stringer or bottom web of the upper chord box member at the center of the span between U16 and U18. This deck cross-section had the most amount of instrumentation on it during the experimental testing, and therefore it was the source of comparison to the experimental results.

The data is plotted over two domains. The tests conducted with the back axles of the truck 18 in. north of U16 are plotted over a domain of –0.4 ksi to 1.0 ksi. The tests conducted with the back axles of the truck 27 ft. north of U16 are plotted over a domain of –1.0 ksi to 4.0 ksi.

As shown in the figures, the results were very similar for all the models. The seven-span model was a good choice as it gave results closest to the experimental results in most cases. The computational time required to produce these results, however, was prohibitive. The five-span and three-span models produced very good and extremely similar results. Therefore, the three-span model was chosen for further development into the lateral load distribution model.

4.2.9 Transitions from Shell Elements to Frame Elements

In order to reduce the number of shell elements in the lateral load distribution model and hence reduce the computing run-time, the diagonal members were transitioned from shell elements to frame elements at a distance away from the gusset plates along the member of at least twice the depth of the diagonal member. This connection is shown in Figure 4.23. In order to preserve rotational and translational continuity along the member, a diaphragm of stiff shell elements was added at the end of the built-up shell cross-section. The frame element was then connected rigidly to the node on this diaphragm at the center of gravity of the member. The lower sway bracing diagonals and the mid-height horizontal strut were connected to the diagonal frame sections where appropriate.

58

4.2.10 Lateral Load Distribution Model Boundary Conditions

The lateral load distribution model consisted of three 54 ft. spans. Figure 4.24 shows views of this model. The boundary conditions applied to it were similar to those explained in Section 4.2.7 during the discussion of the boundary refinement study. The members at the far ends of the model were pinned at the each side of the bottom flanges. This boundary condition was chosen to restrain longitudinal movement of the model ends, but allow rotation in the plane of the trusses. Pier 2 was represented by a pin boundary condition at its location.

4.3 LATERAL LOAD DISTRIBUTION MODEL LOAD CASES

The ten load cases applied to the lateral load distribution model were formulated in a fashion that most closely represented the truck loading during the ten park tests selected for comparison. In each load case the load was placed in one of Lanes 2 through 6. In five of the load cases, an equivalent load pattern representing Truck #80 was applied with the centerline of the back axles centered 18 in. north of U16. In the other five load cases, the same load pattern was applied with the centerline of the back axles centered 27 ft. north of U16. In each load case the load was applied to simulate the truck facing north, as was done for the actual load test in the field.

4.4 LATERAL LOAD DISTRIBUTION MODEL RESULTS

Figures 4.25 through 4.34 contain the experimental and analytical results for the stress in the bottom flange of each stringer and the bottom web of each upper chord box section at a cross-section of the bridge deck centered between U16 and U18.

The data is plotted over two domains. The tests conducted with the back axles of the truck 18 in. north of U16 are plotted over a domain of −0.4 ksi to 1.0 ksi. The tests conducted with the back axles of the truck 27 ft. north of U16 are plotted over a domain of −1.0 ksi to 4.0 ksi.

The most important feature of these results was that they were effectively able to produce the same shape distribution as the experimental data on the bridge cross-section. Another feature of the results was that they were not sensitive to small changes in concrete strength or deck thickness. The stress results for the same locations were improved once this lateral load distribution model was incorporated into the full bridge model. These results are presented in Chapter 5.

4.5 COMPARISON WITH EXPERIMENTAL RESULTS

Table 4.2 shows the ratio of the analytical results of the lateral load distribution model to the experimental results where this calculation was appropriate (i.e. if the calculation would have contained at least one of the results as a zero value, or if experimental data was not available, the ratio was omitted). All stress values are rounded to the nearest 0.1 ksi. This estimation was appropriate for an error calculation because stresses measured experimentally in the field are usually not trusted beyond the tenths place.

In some cases the ratio was close to 1, meaning there was no difference between the analytical and experimental result. In other cases it should be noted that although the ratio deviation from 1 is large, the realistic difference in the reported values is small. For instance, for S6 subjected to the LN5U16 park test, the ratio is reported as 0.5. This difference seems quite large, but the values reported for the experimental data and the analytical data are 0.2 ksi and 0.1 ksi respectively.

4.6   INCLUSION OF LLDM IN FULL BRIDGE MODEL

The finely meshed lateral load distribution model of the deck truss was utilized as the building block upon which to assemble the rest of the bridge structure. As the distance from the gaged area of interest (see Figure 4.1) increased in the model, the shell mesh was transitioned to a more coarsely meshed frame model that was finally transitioned to a frame element representing each side of the twin truss structure. More details of this model are presented in Chapter 5.

Trial Section	Length Per Section (in)	Number of Elements Per Flange Width	Flange Element Aspect Ratio	Number of Elements Per Web Depth	Web Element Aspect Ratio	Support Type	Point Load Applied @ 1/3 L[3] (kips)
Beam1w[1]	10	2	1.90	1	2.92	Simple	25
Beam2w[1]	10	2	1.90	2	1.46	Simple	25
Beam4w[1]	10	2	1.90	4	1.37	Simple	25
Beam8w[1]	10	2	1.90	8	2.74	Simple	25
Frame[2]	10	-	-	-	-	Simple	25

Notes
1. Section comprised only of shell elements.
2. Section comprised only of frame elements.
3. L is the longitudinal length of the model.

Table 4.1. Properties of finite element models used during the shell mesh refinement study.

61

Test	LN2U16			Test	LN2CL		
Data	EXP (ksi)	LLDM (ksi)	LLDM/EXP	Data	EXP (ksi)	LLDM (ksi)	LLDM/EXP
S1	-	0.1	-	S1	-	0.3	-
S2	-	0.3	-	S2	-	1.2	-
WUC	0.3	0.4	1.3	WUC	1.2	1.5	1.3
S3	-	0.2	-	S3	-	1.0	-
S4	-	0.1	-	S4	-	0.3	-
S5	-	0.0	-	S5	-	0.1	-
S6	0.0	0.0	-	S6	0.0	0.0	-
S7	0.0	0.0	-	S7	0.0	0.0	-
EUC	0.0	0.0	-	EUC	0.0	0.0	-
S8	0.0	0.0	-	S8	0.0	0.0	-
S9	-	0.0	-	S9	-	0.0	-
Test	LN3U16			Test	LN3CL		
Data	EXP (ksi)	LLDM (ksi)	LLDM/EXP	Data	EXP (ksi)	LLDM (ksi)	LLDM/EXP
S1	-	0.0	-	S1	-	-0.1	-
S2	-	0.0	-	S2	-	0.1	-
WUC	0.2	0.2	1.0	WUC	0.8	0.6	0.8
S3	-	0.4	-	S3	-	2.8	-
S4	-	0.5	-	S4	-	3.1	-
S5	-	0.3	-	S5	-	1.1	-
S6	0.2	0.1	0.5	S6	0.6	0.3	0.5
S7	0.1	0.0	-	S7	0.2	0.0	-
EUC	0.0	0.0	-	EUC	0.1	0.0	-
S8	0.0	0.0	-	S8	0.0	0.0	-
S9	-	0.0	-	S9	-	0.0	-

Table 4.2. Experimental and analytical result comparison for the lateral load distribution model subjected to park tests.

Test Data	LN4U16			Test Data	LN4CL		
	EXP (ksi)	LLDM (ksi)	LLDM EXP		EXP (ksi)	LLDM (ksi)	LLDM EXP
S1	-	0.0	-	S1	-	0.0	-
S2	-	0.0	-	S2	-	0.0	-
WUC	0.0	0.0	-	WUC	0.0	0.0	-
S3	-	0.0	-	S3	-	0.0	-
S4	-	0.1	-	S4	-	0.3	-
S5	-	0.4	-	S5	-	1.1	-
S6	0.4	0.5	1.3	S6	2.7	3.1	1.1
S7	0.4	0.4	1.0	S7	2.4	2.8	1.2
EUC	0.2	0.2	1.0	EUC	0.6	0.6	1.0
S8	0.0	0.0	-	S8	0.0	0.1	-
S9	-	0.0	-	S9	-	-0.1	-
Test Data	LN5U16			Test Data	LN5CL		
	EXP (ksi)	LLDM (ksi)	LLDM EXP		EXP (ksi)	LLDM (ksi)	LLDM EXP
S1	-	0.0	-	S1	-	0.0	-
S2	-	0.0	-	S2	-	0.0	-
WUC	0.0	0.0	-	WUC	0.0	0.0	-
S3	-	0.0	-	S3	-	0.0	-
S4	-	0.0	-	S4	-	0.0	-
S5	-	0.0	-	S5	-	0.1	-
S6	0.2	0.1	0.5	S6	0.3	0.3	1.0
S7	0.2	0.2	1.0	S7	0.7	1.0	1.4
EUC	0.3	0.4	1.3	EUC	1.2	1.5	1.3
S8	0.2	0.3	1.5	S8	1.0	1.2	1.2
S9	-	0.1	-	S9	-	0.3	-
Test Data	LN6U16			Test Data	LN6CL		
	EXP (ksi)	LLDM (ksi)	LLDM EXP		EXP (ksi)	LLDM (ksi)	LLDM EXP
S1	-	0.0	-	S1	-	0.0	-
S2	-	0.0	-	S2	-	0.0	-
WUC	0.0	0.0	-	WUC	0.0	0.0	-
S3	-	0.0	-	S3	-	0.0	-
S4	-	0.0	-	S4	-	-0.1	-
S5	-	-0.1	-	S5	-	-0.1	-
S6	0.0	-0.1	-	S6	-0.1	-0.1	1.0
S7	0.2	0.0	-	S7	0.0	0.1	-
EUC	0.2	0.2	1.0	EUC	0.6	0.6	1.0
S8	0.4	0.5	1.3	S8	2.4	2.7	1.1
S9	-	0.8	-	S9	-	3.1	-

Table 4.2(Cont.). Experimental and analytical result comparison for the lateral load distribution model subjected to park tests.
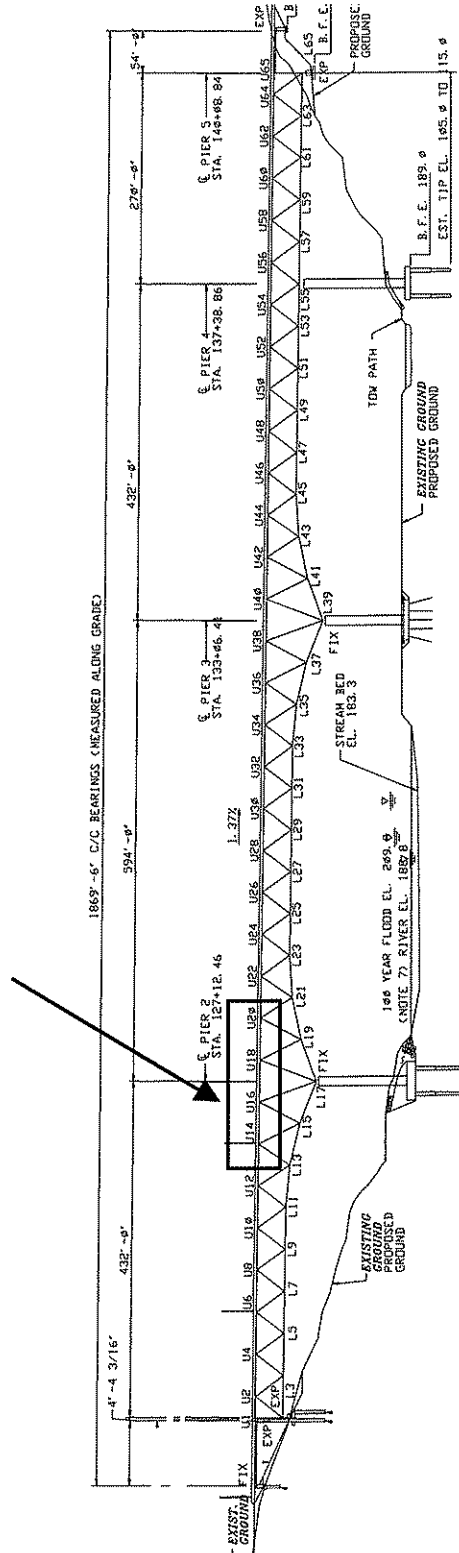
Figure 4.1. Bridge elevation showing the area modeled using shell elements in the lateral load distribution model.
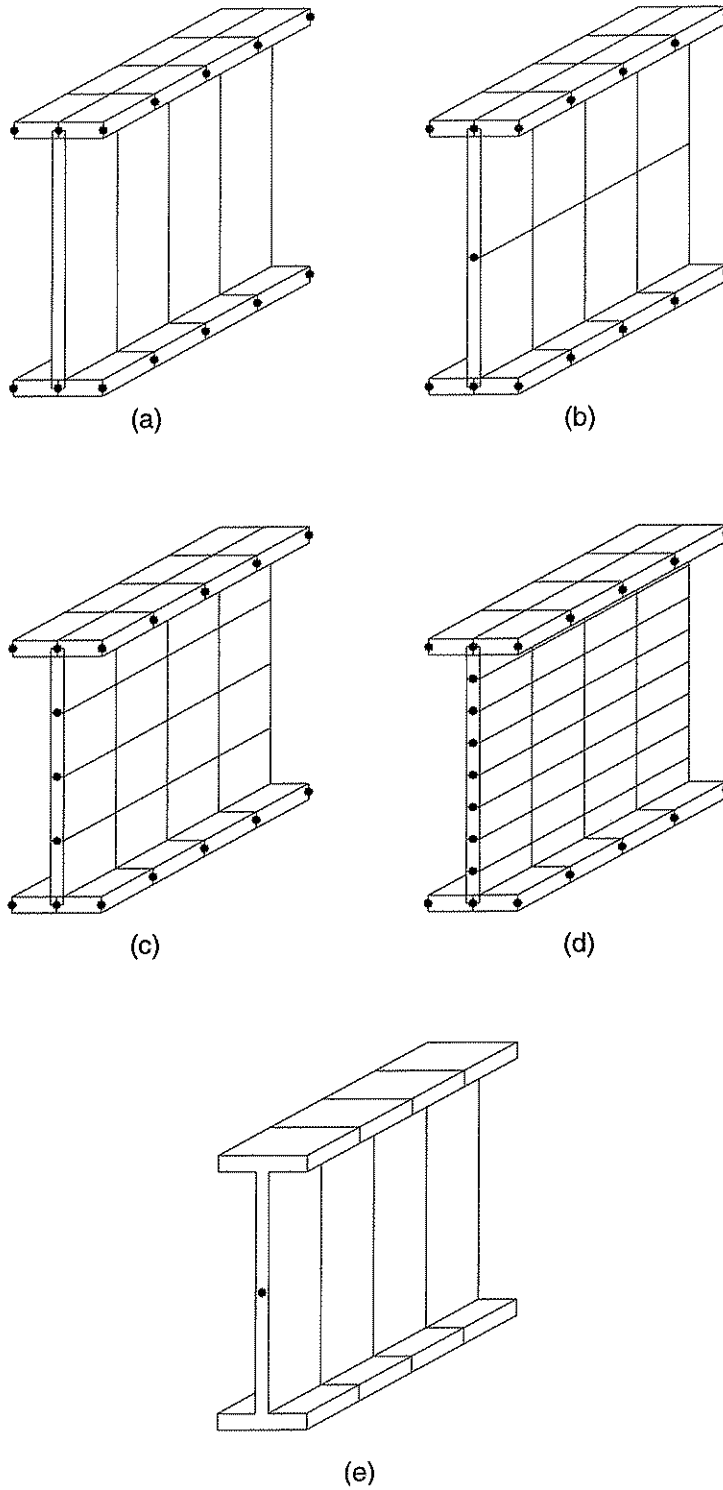
Figure 4.2. Finite element arrangements used during the shell element mesh refinement study: (a) Beam1w; (b) Beam2w; (c) Beam4w; (d) Beam8w; (e) Frame.
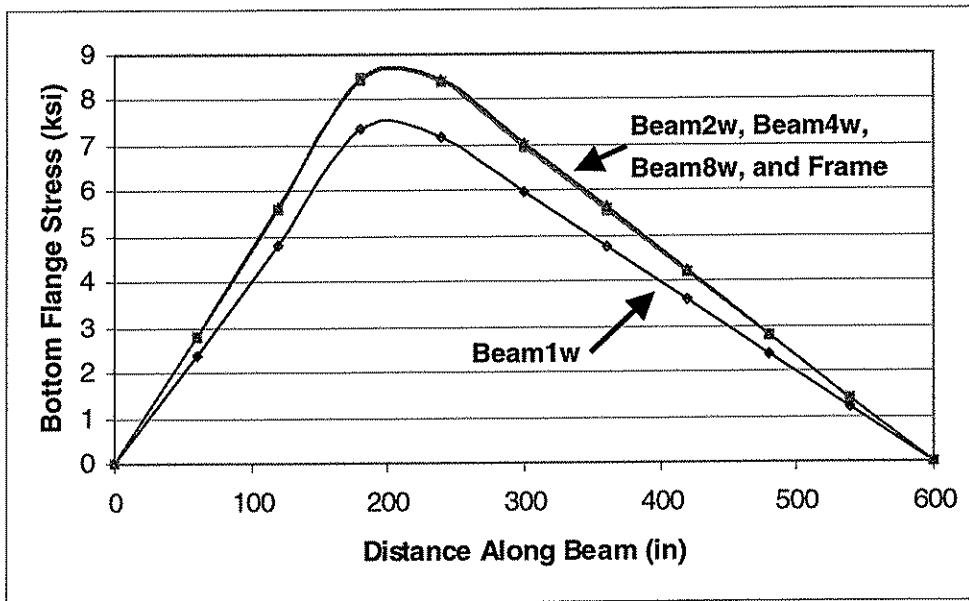
Figure 4.3. Shell mesh refinement results.

BOX
CROSS-SECTION
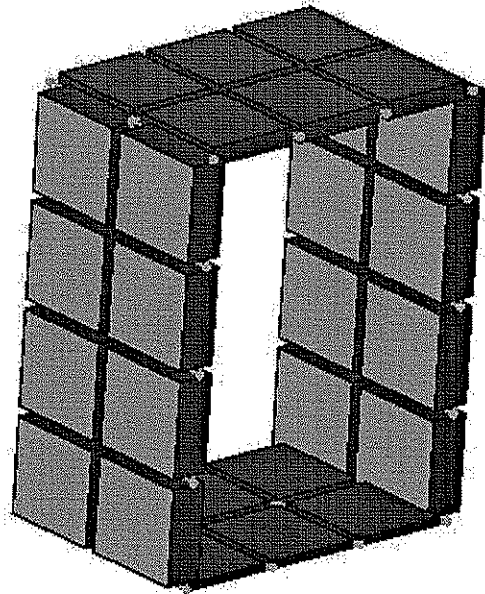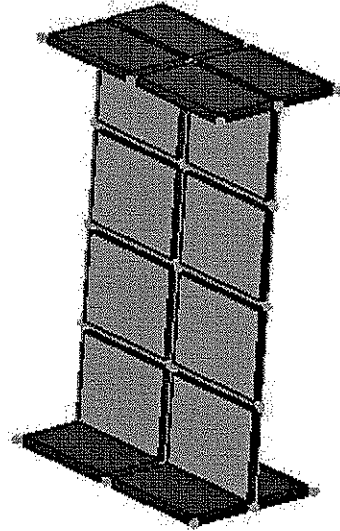
STRINGER
CROSS-SECTION

(a)

(b)

Figure 4.4. Final mesh configurations used in the lateral load distribution model:
(a) Box section; (b) Stringer section.
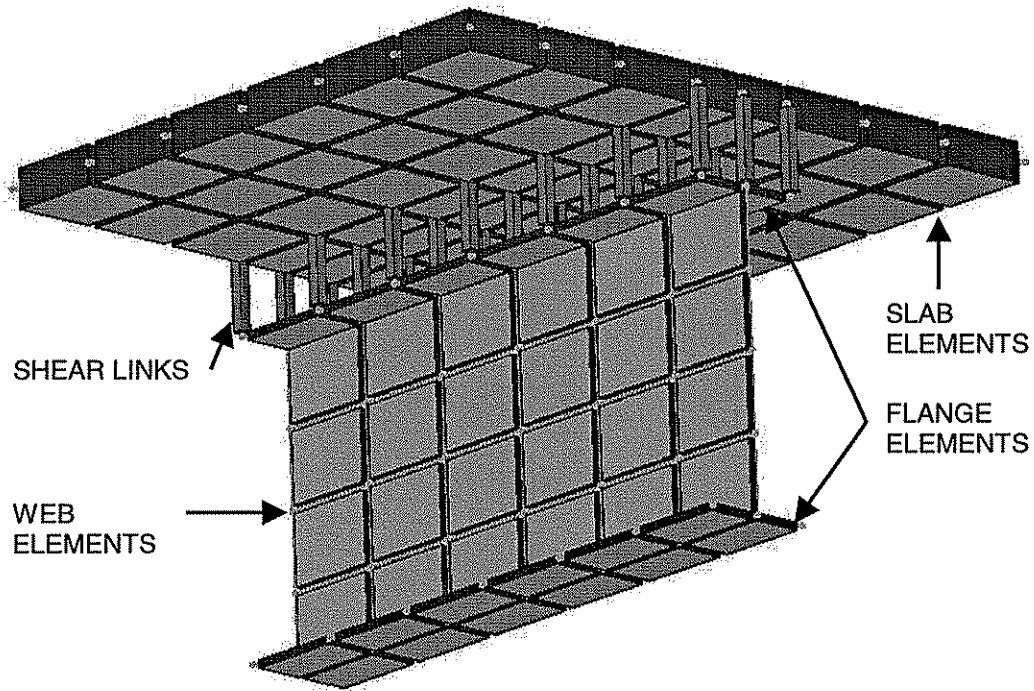
Figure 4.5. View of shear link elements attaching flange elements to slab elements.

FLOORBEAM END PRIOR TO
STRINGER INSTALLATION

FLOORBEAM TO OUTSIDE
STRINGER CONNECTION

(a)

(b)
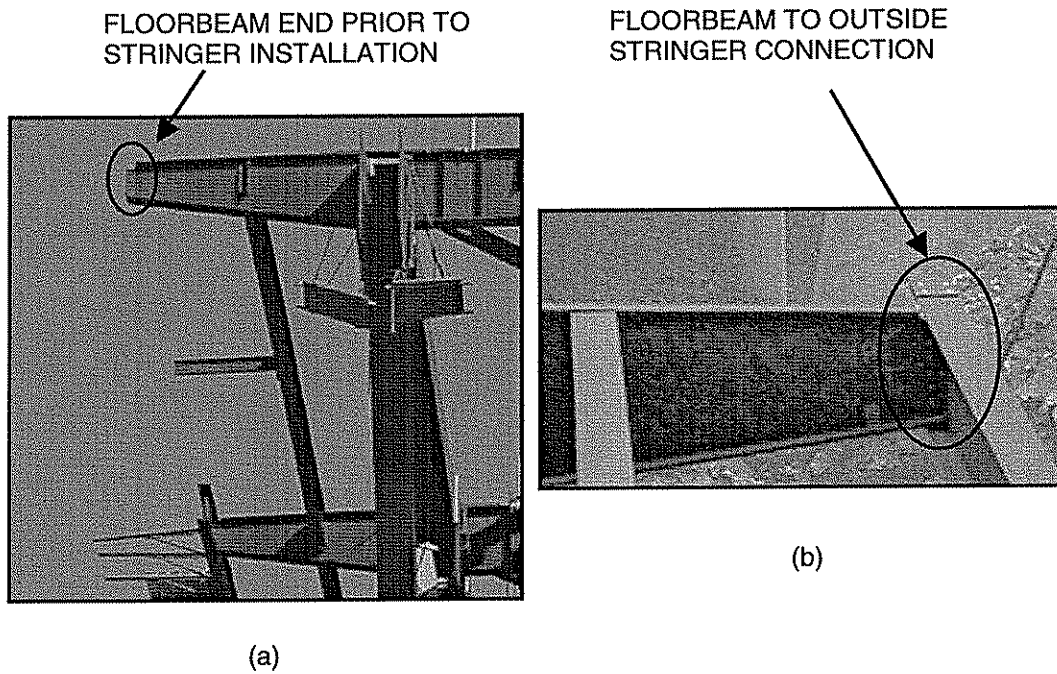
Figure 4.6. Photographs of the connection between the outside stringers and the floorbeams: (a) Exposed end of the floorbeam with a coped top flange; (b) Connected stringer and floorbeam members.
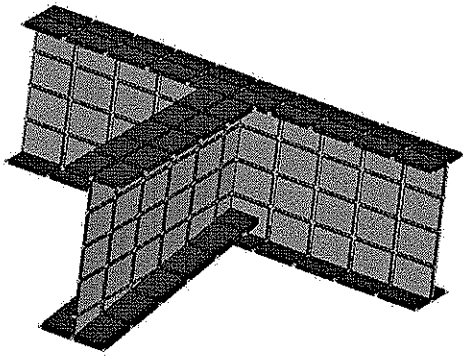
EXTERIOR STRINGER TO
FLOORBEAM CONNECTION
(a)
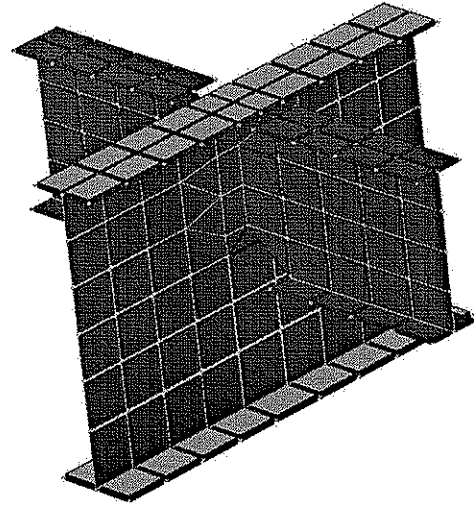
INTERIOR STRINGER TO
FLOORBEAM CONNECTION
(b)

Figure 4.7. Lateral load distribution model stringer to floorbeam connections: (a)
Exterior stringer connections; (b) Interior stringer connections.

MIDDLE SECTION OF FLOORBEAM

TAPERED END OF FLOORBEAM

MIDDLE SECTION OF FLOORBEAM

GUSSET PLATE

TIE PLATE
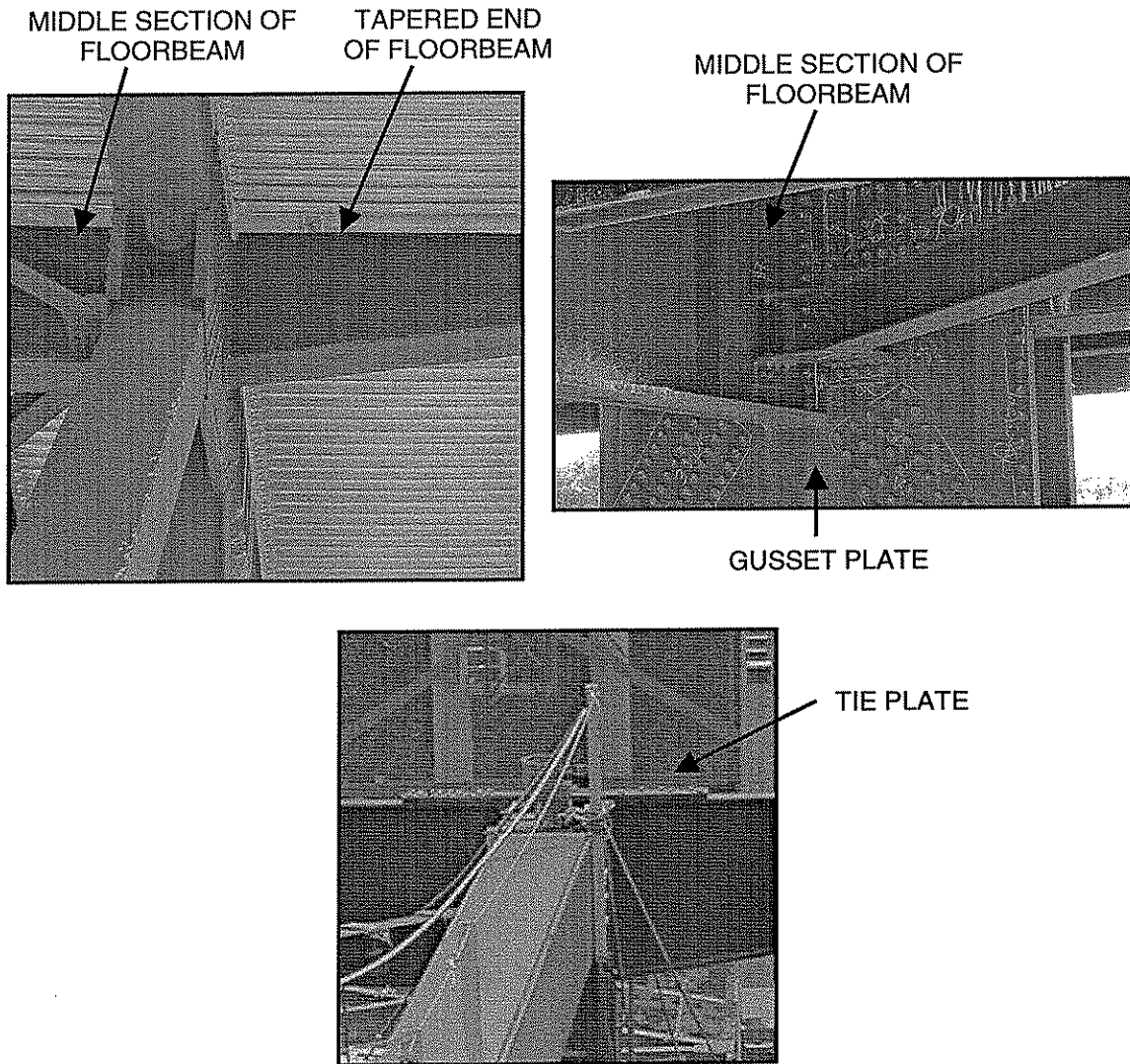
Figure 4.8. Photographs of the floorbeam as it passes through the upper chord box sections.

MIDDLE SECTION
OF FLOORBEAM

TAPERED SECTION
OF FLOORBEAM

CONTINUITY
PLATE
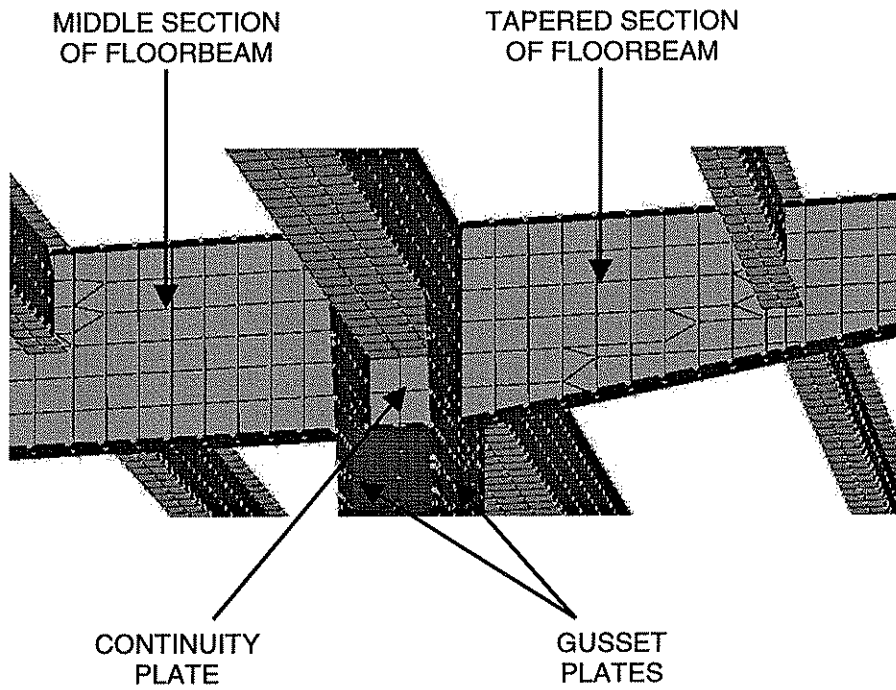
GUSSET
PLATES

Figure 4.9. Floorbeam connection through the upper chord box sections and the gusset plates in the lateral load distribution model.
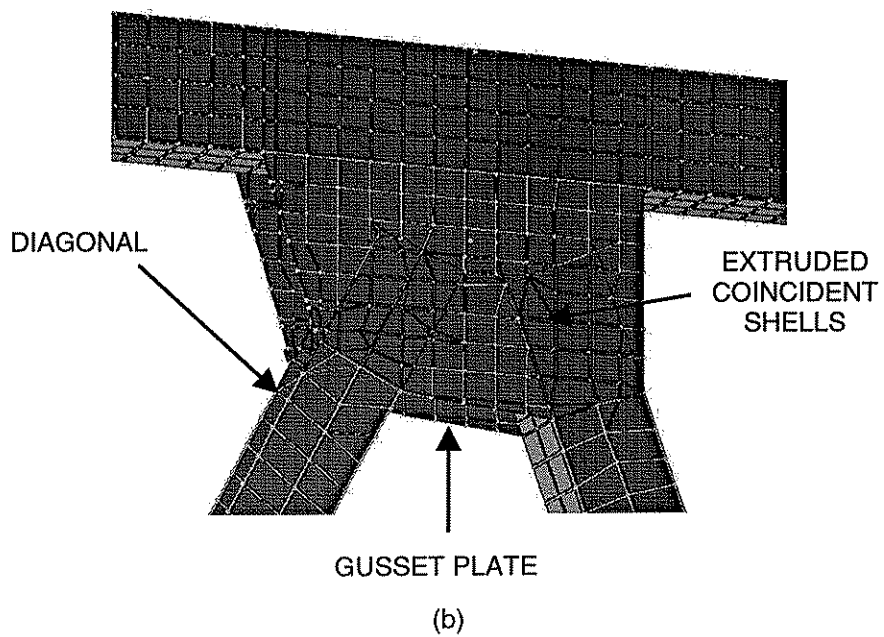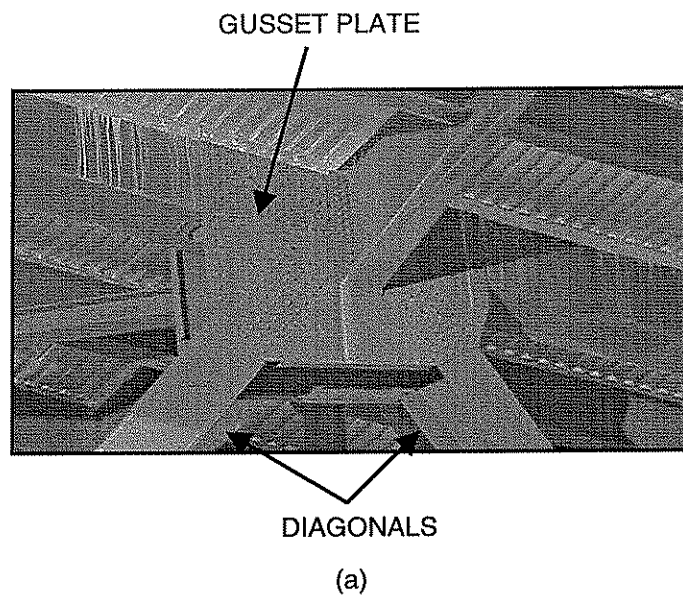
Figure 4.10. Diagonal member connection with gusset plate: (a) Photograph of actual installation; (b) Corresponding finite element mesh.
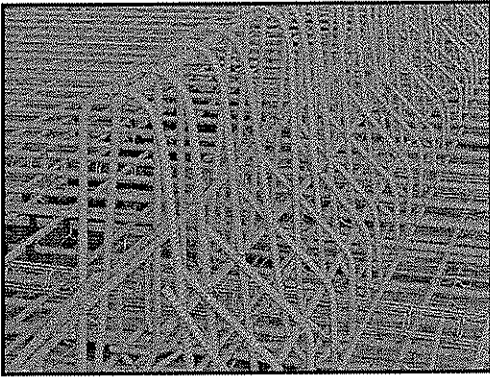
(a)

(b)
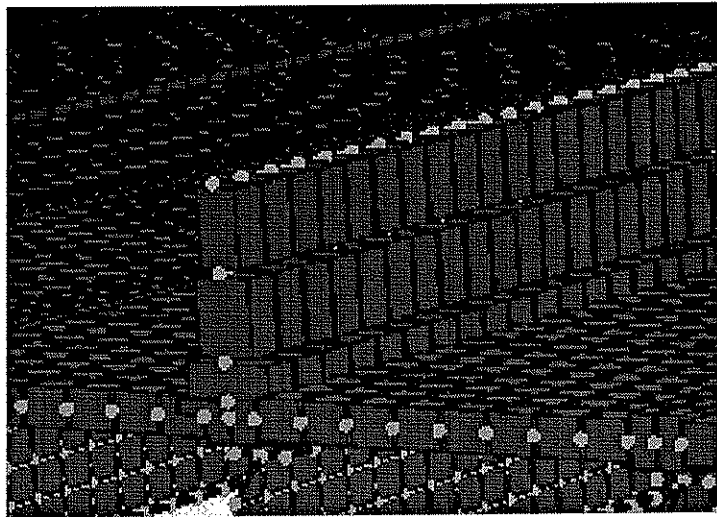
(c)

Figure 4.11. Photographs and finite element mesh of concrete median parapet: (a) Reinforcement shaped for median parapet; (b) Median parapet in service; (c) Median parapet in lateral load distribution model.
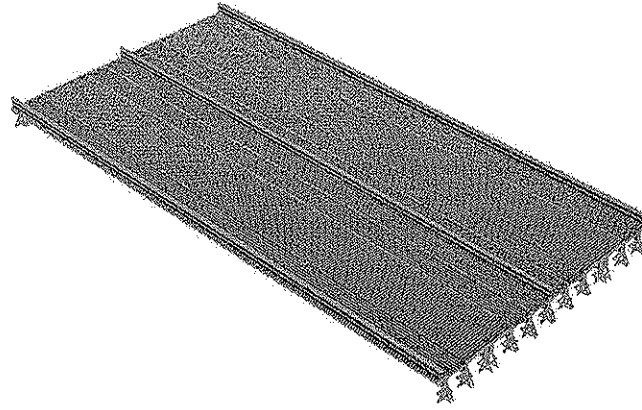
(a)
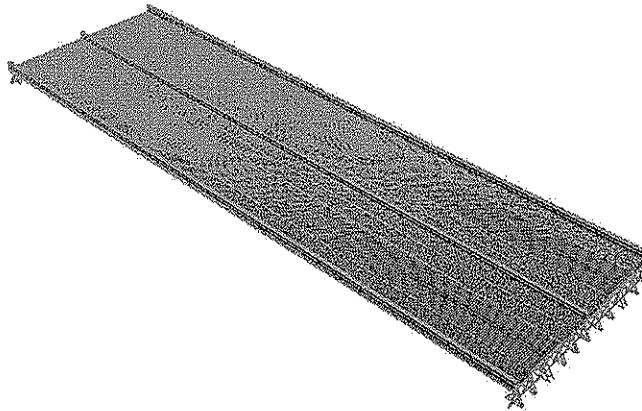
(b)
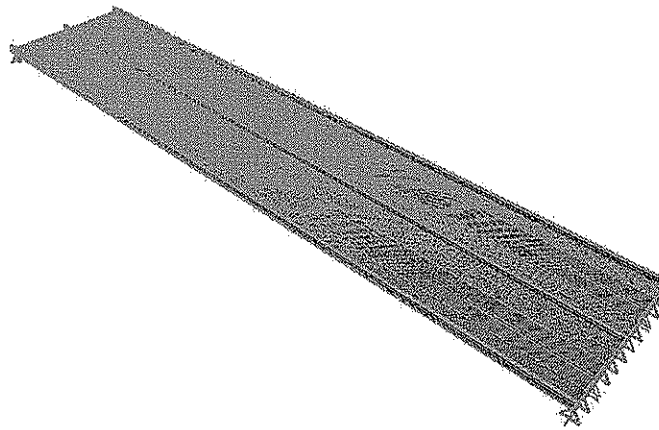
(c)

Figure 4.12. Finite element meshes used to during the boundary refinement
study: (a) three span model (U14 to U20); (b) five span model (U12 to U22);
(c) seven span model (U10 to U24).
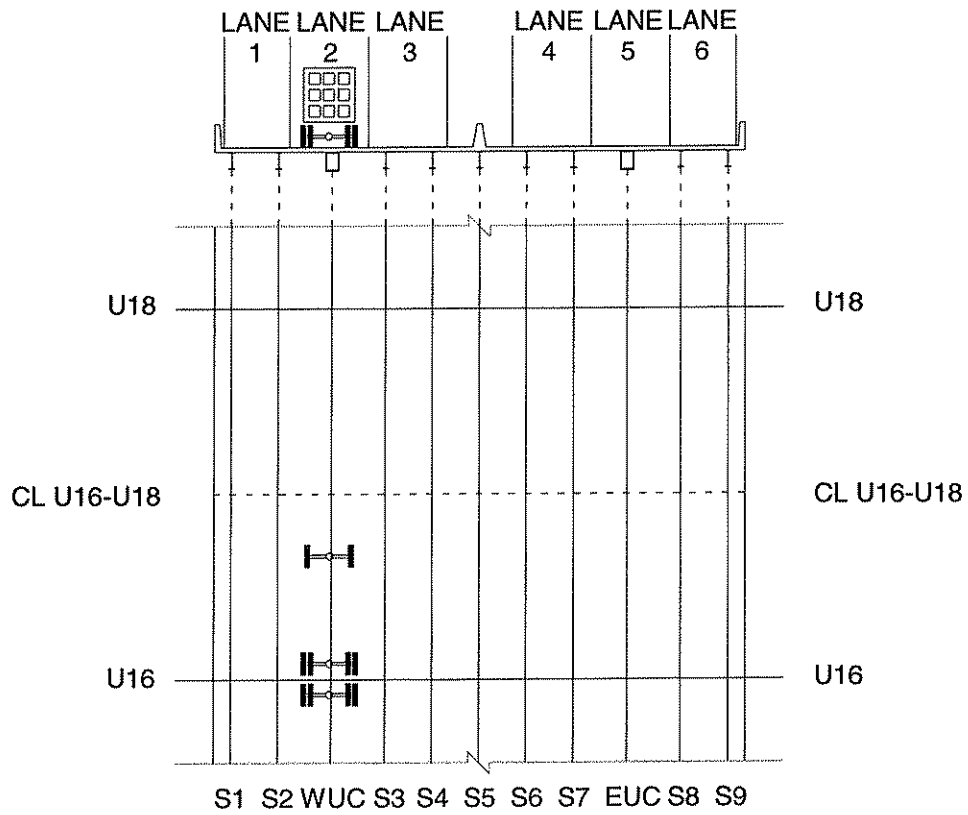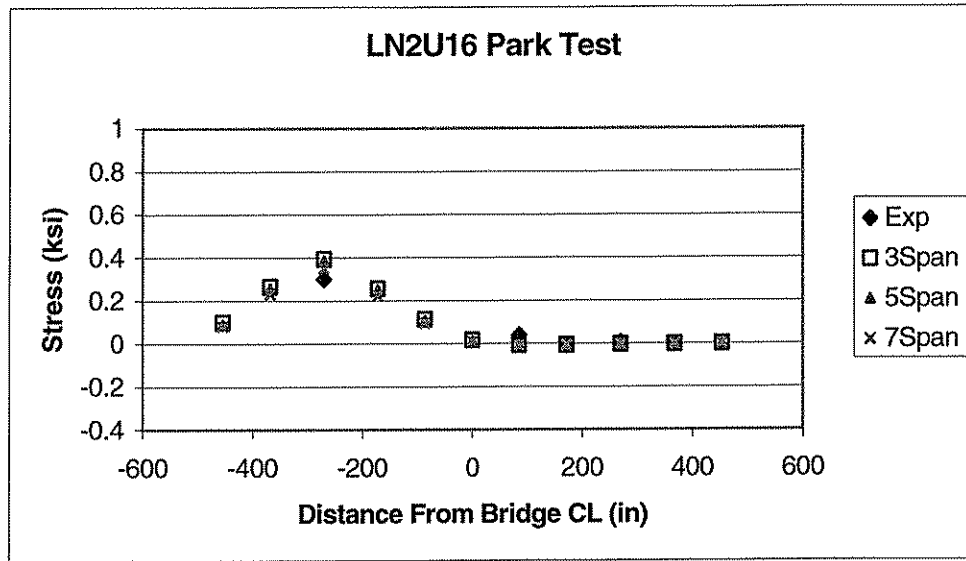
Figure 4.13. Boundary Refinement Study – Stringer bottom flange and upper chord bottom web stresses at the center of span between U16 and U18 for a park test in Lane 2 with the centerline of the truck's back axles centered 18 in. north of U16.
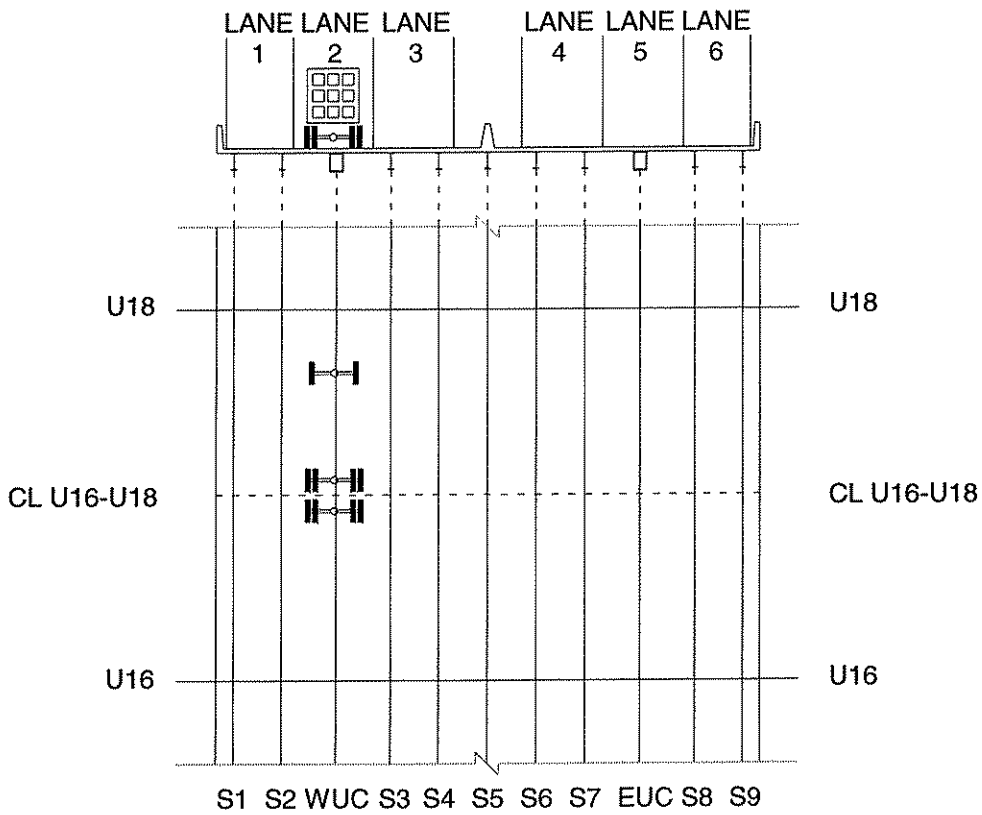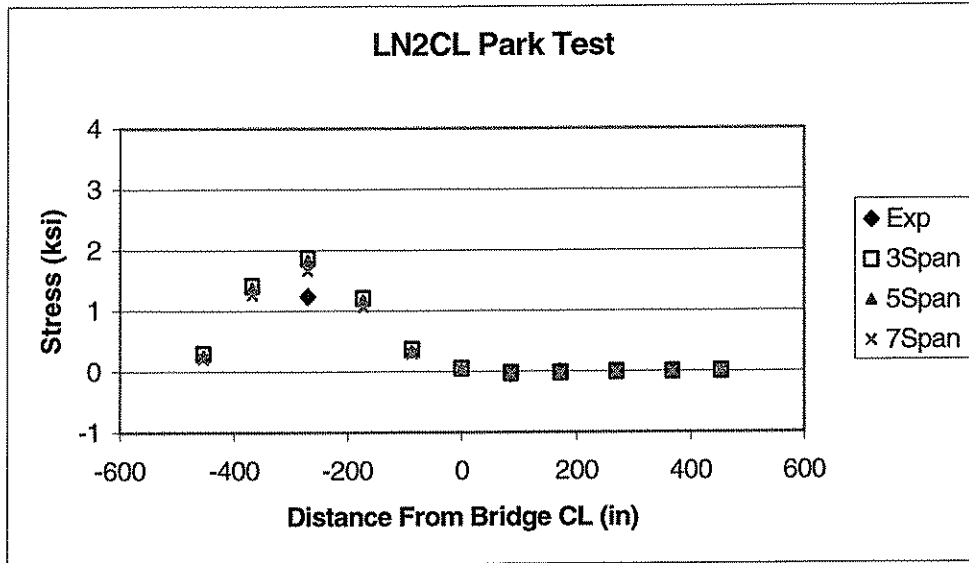
Figure 4.14. Boundary Refinement Study – Stringer bottom flange and upper chord bottom web stresses at the center of span between U16 and U18 for a park test in Lane 2 with the centerline of the truck's back axles centered over the center of span between U16 and U18.
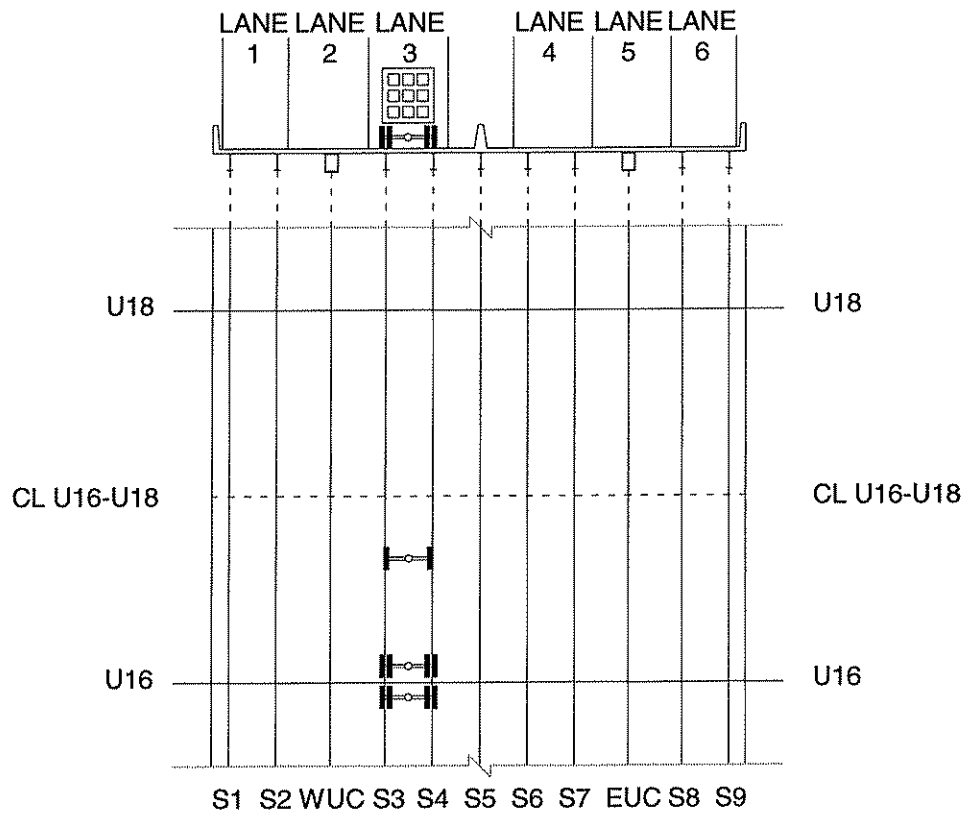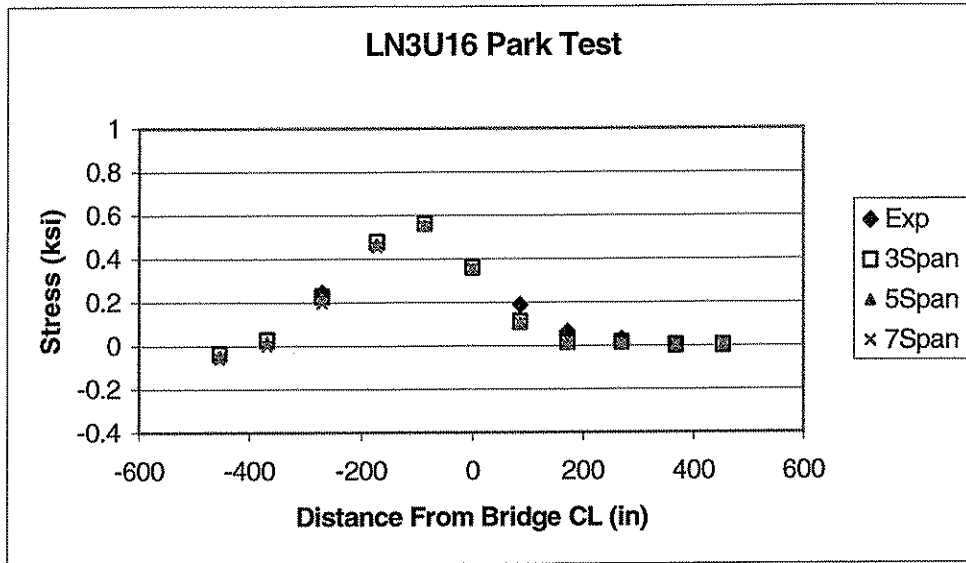
Figure 4.15. Boundary Refinement Study – Stringer bottom flange and upper chord bottom web stresses at the center of span between U16 and U18 for a park test in Lane 3 with the centerline of the truck's back axles centered 18 in. north of U16.

78
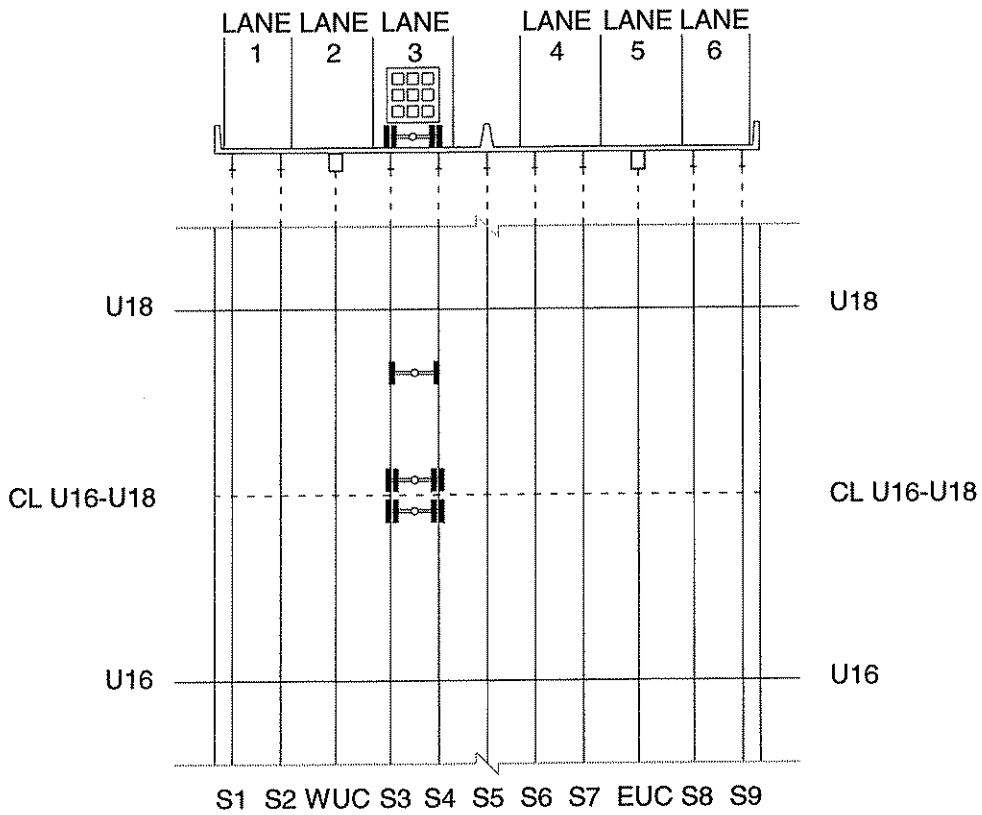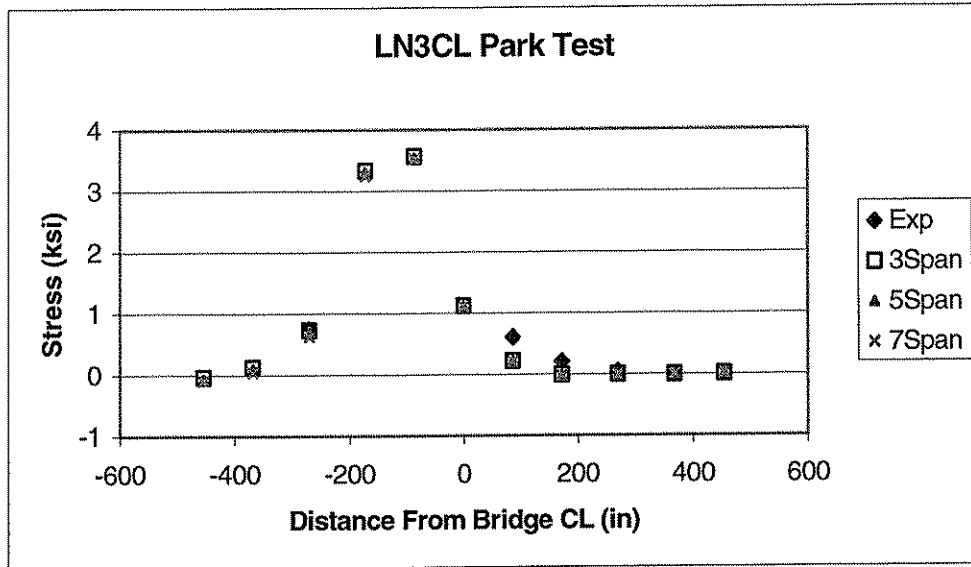
Figure 4.16. Boundary Refinement Study – Stringer bottom flange and upper chord bottom web stresses at the center of span between U16 and U18 for a park test in Lane 3 with the centerline of the truck's back axles centered over the center of span between U16 and U18.

79
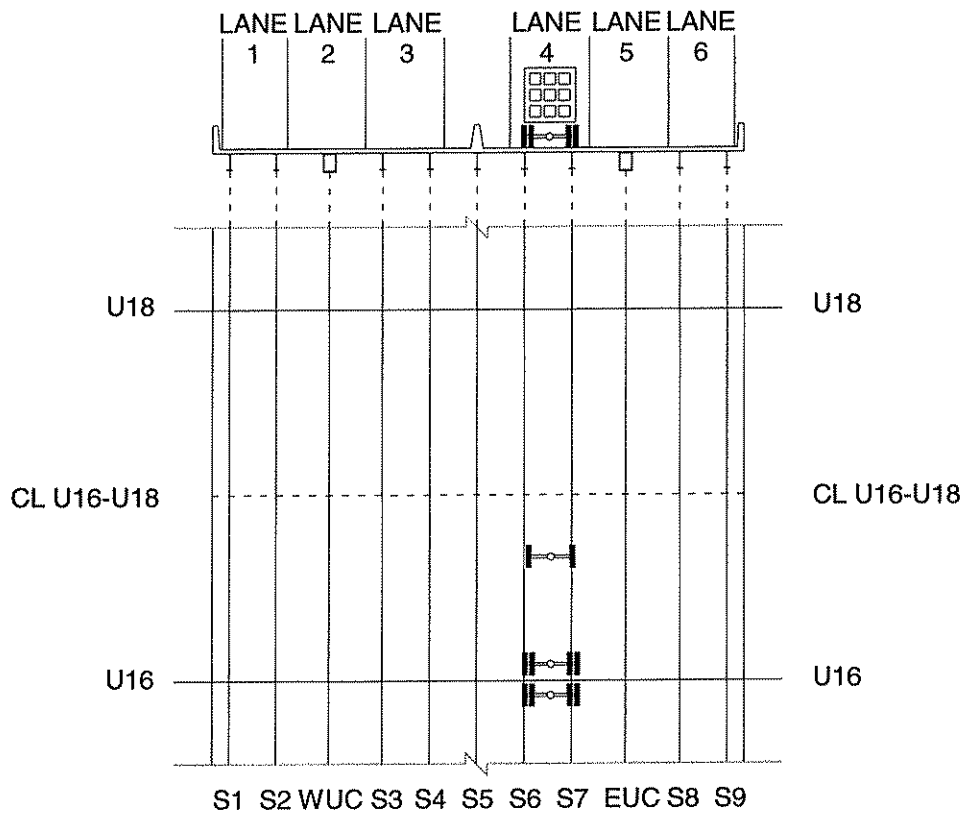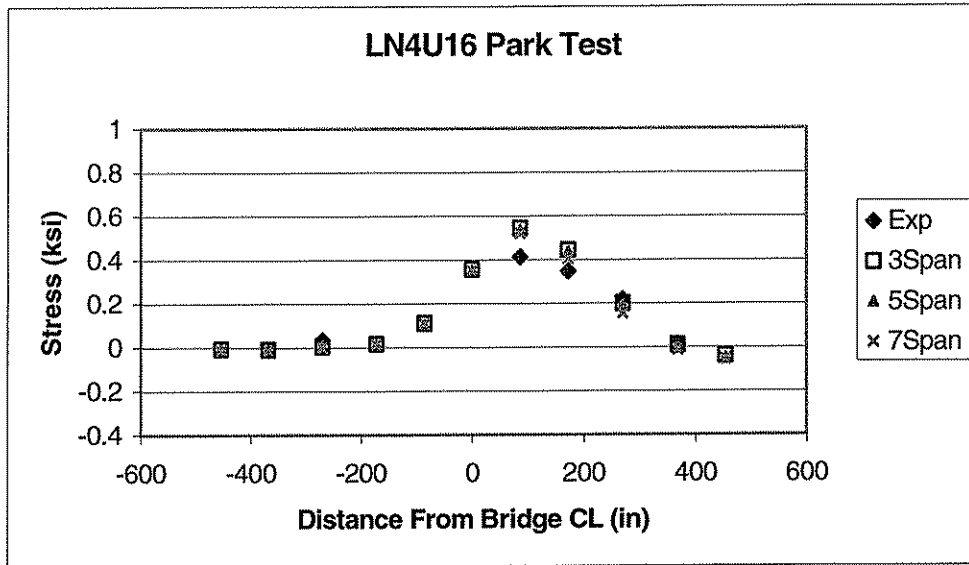
Figure 4.17. Boundary Refinement Study – Stringer bottom flange and upper chord bottom web stresses at the center of span between U16 and U18 for a park test in Lane 4 with the centerline of the truck's back axles centered 18 in. north of U16.
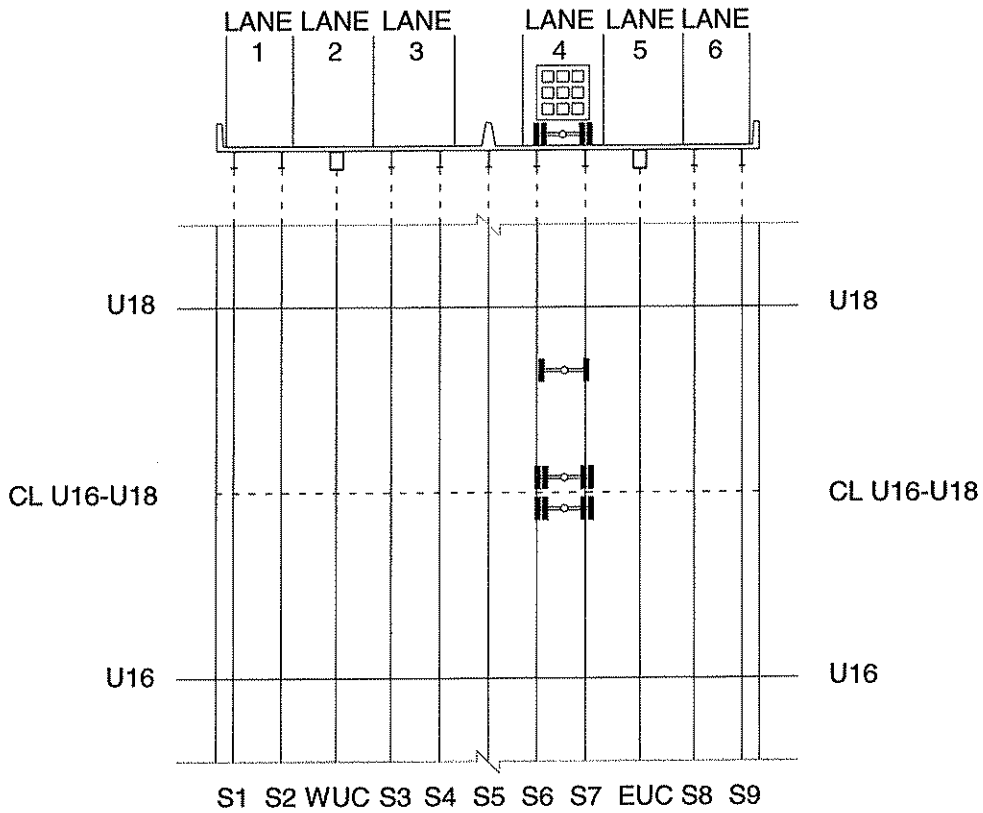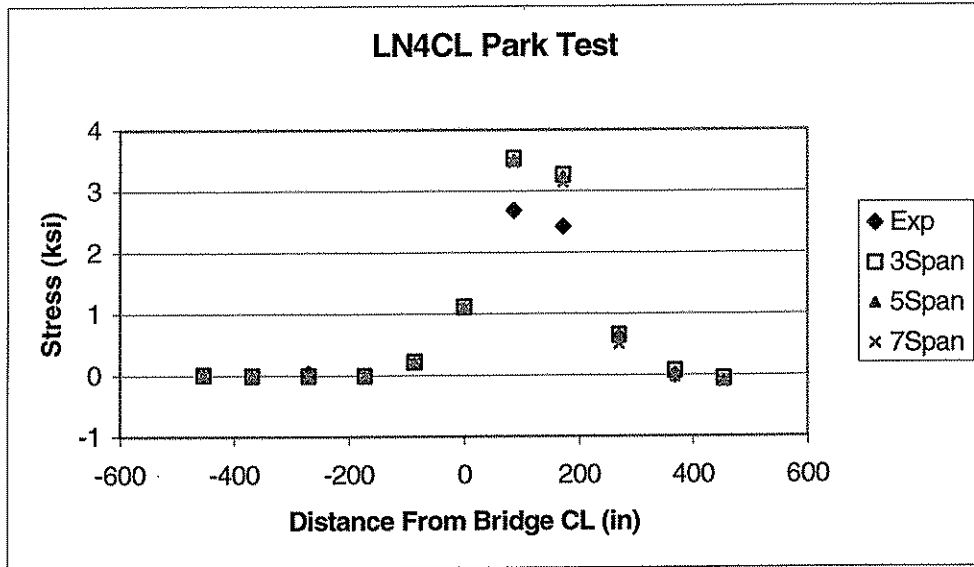
Figure 4.18. Boundary Refinement Study – Stringer bottom flange and upper chord bottom web stresses at the center of span between U16 and U18 for a park test in Lane 4 with the centerline of the truck's back axles centered over the center of span between U16 and U18.

81
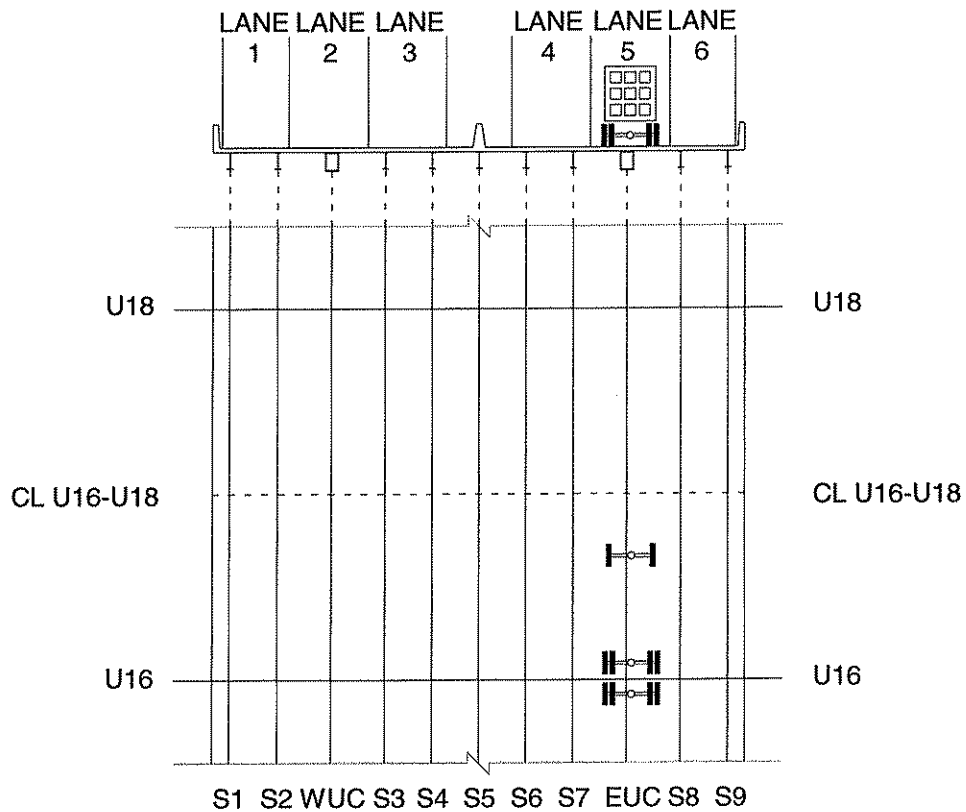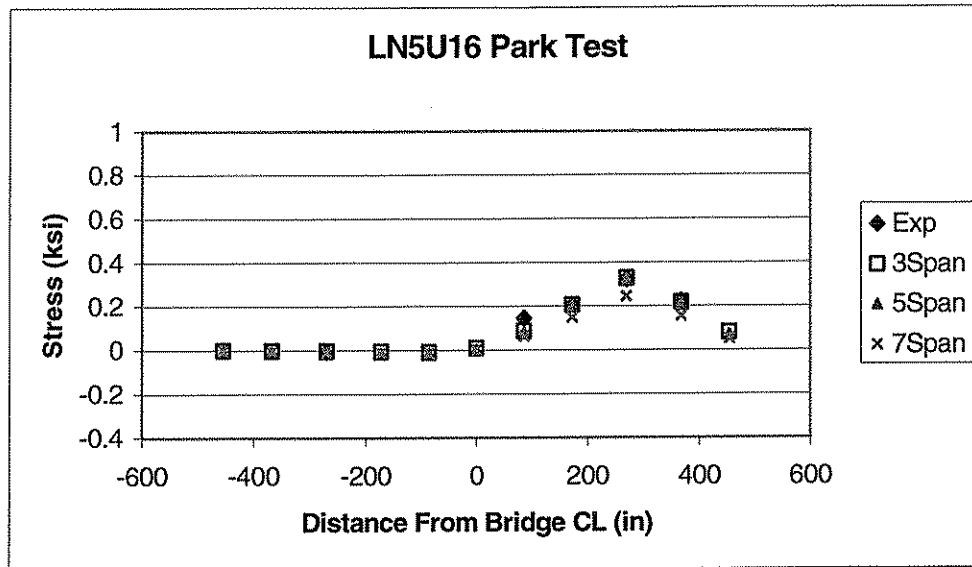
Figure 4.19. Boundary Refinement Study – Stringer bottom flange and upper chord bottom web stresses at the center of span between U16 and U18 for a park test in Lane 5 with the centerline of the truck's back axles centered 18 in. north of U16.

82
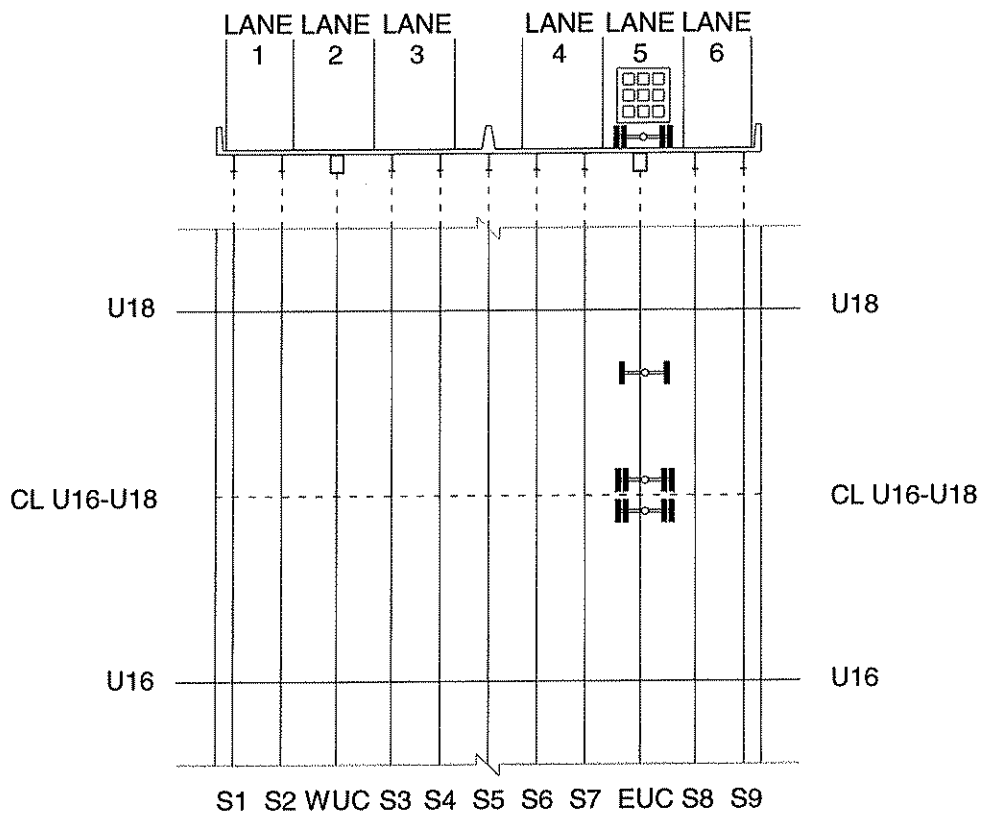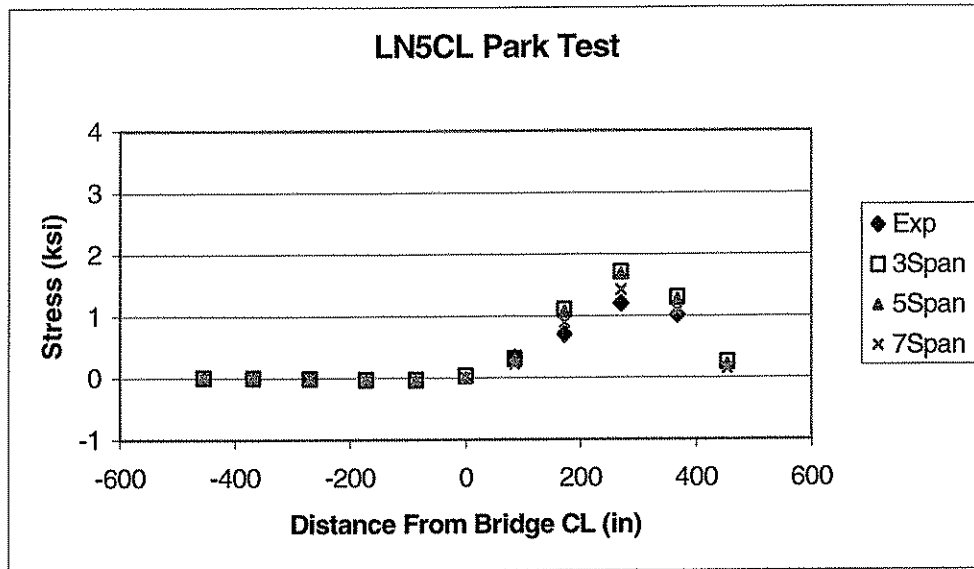
Figure 4.20. Boundary Refinement Study – Stringer bottom flange and upper chord bottom web stresses at the center of span between U16 and U18 for a park test in Lane 5 with the centerline of the truck's back axles centered over the center of span between U16 and U18.

83

LN6U16 Park Test
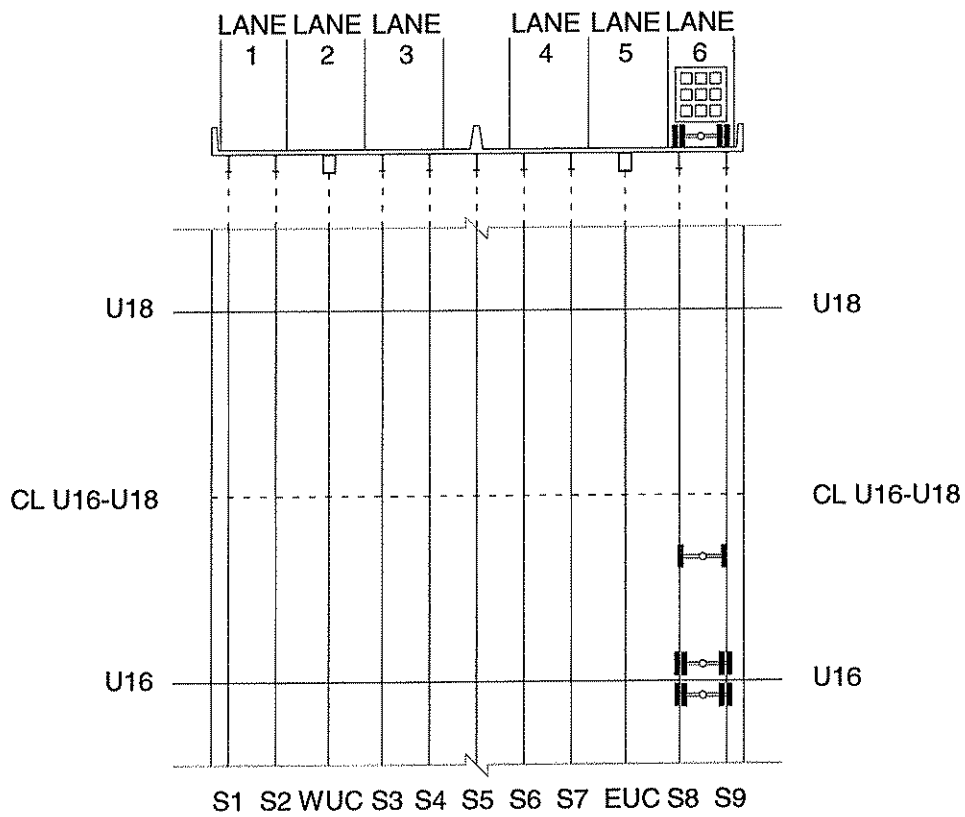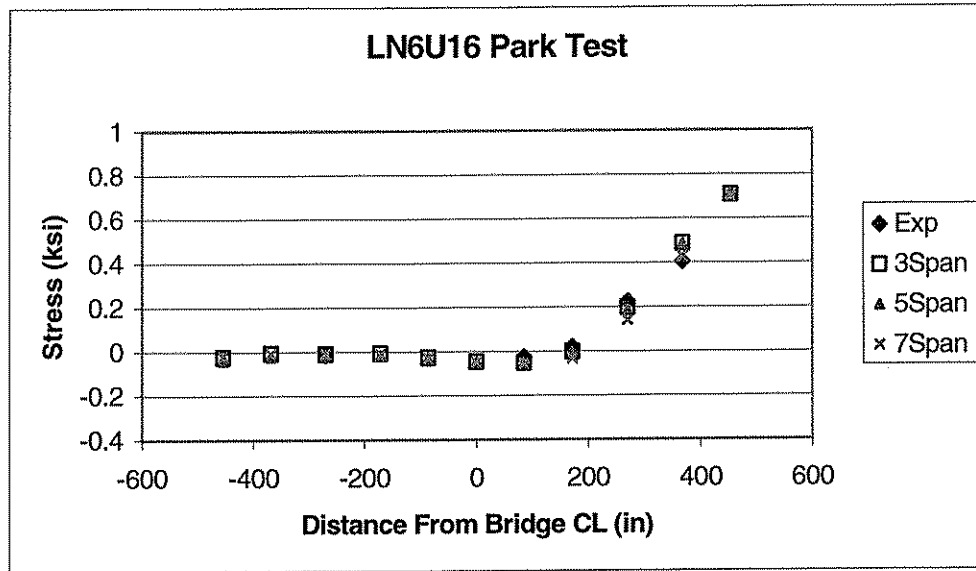
Figure 4.21. Boundary Refinement Study – Stringer bottom flange and upper chord bottom web stresses at the center of span between U16 and U18 for a park test in Lane 6 with the centerline of the truck's back axles centered 18 in. north of U16.
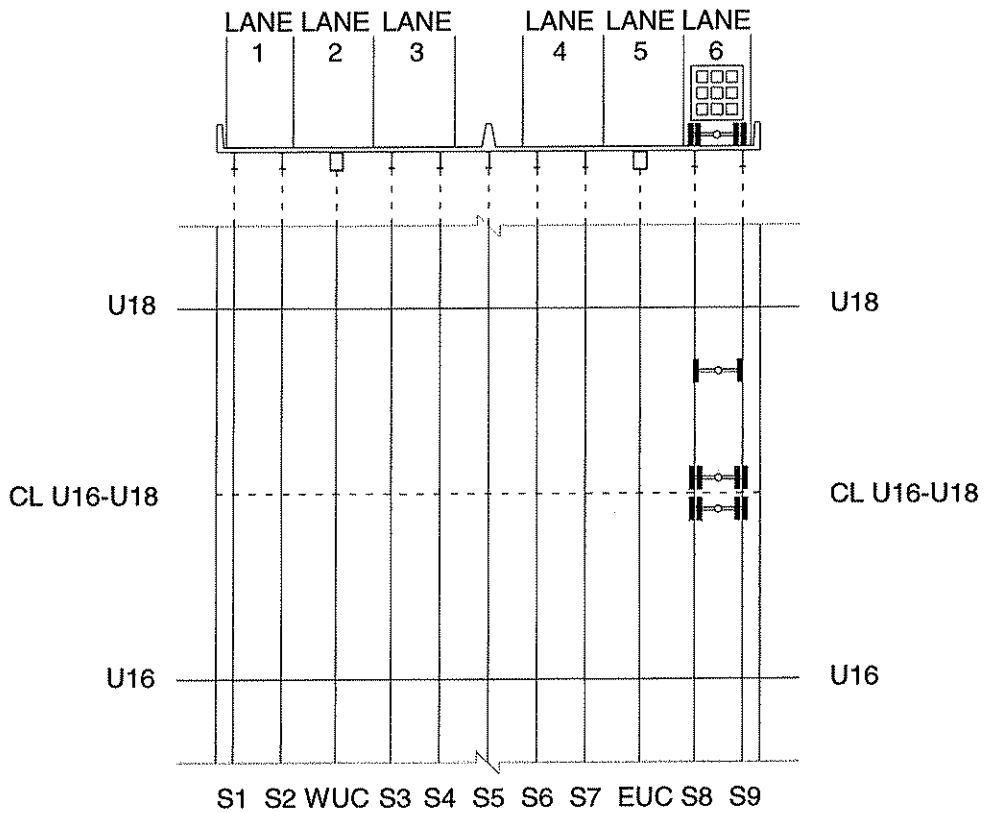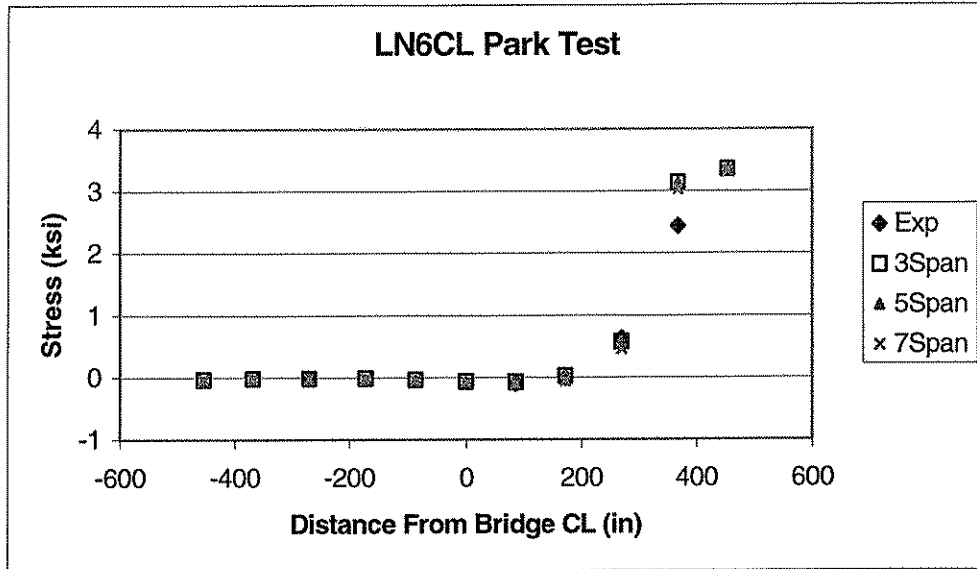
Figure 4.22. Boundary Refinement Study – Stringer bottom flange and upper chord bottom web stresses at the center of span between U16 and U18 for a park test in Lane 6 with the centerline of the truck's back axles centered over the center of span between U16 and U18.
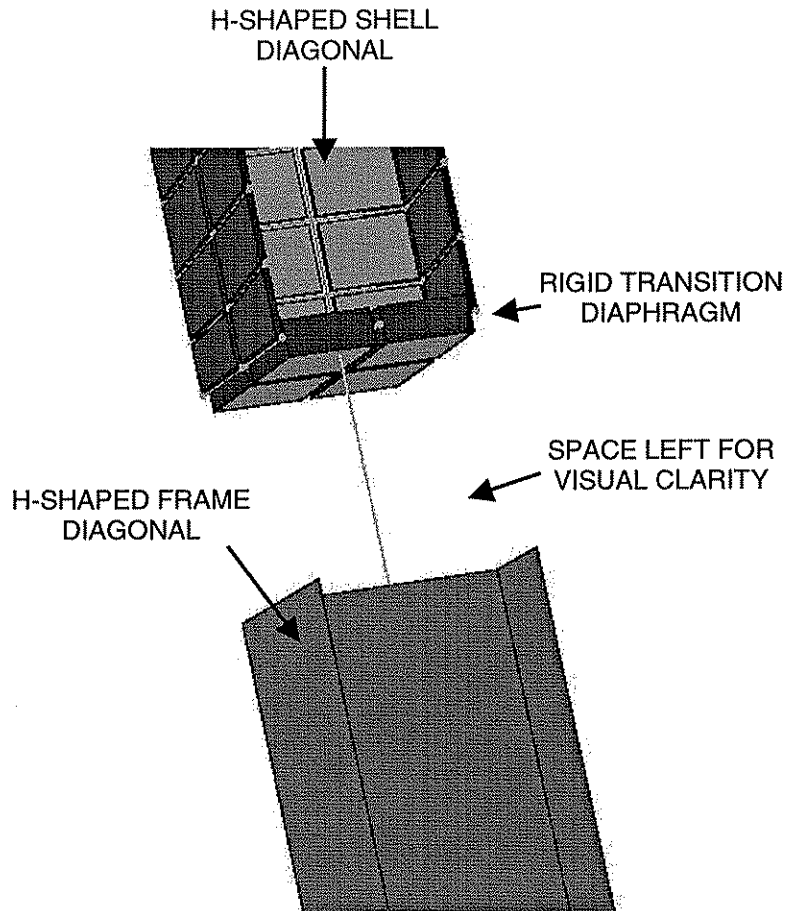
Figure 4.23. Finite element mesh of the transition from shell elements to frame elements on a diagonal truss member.
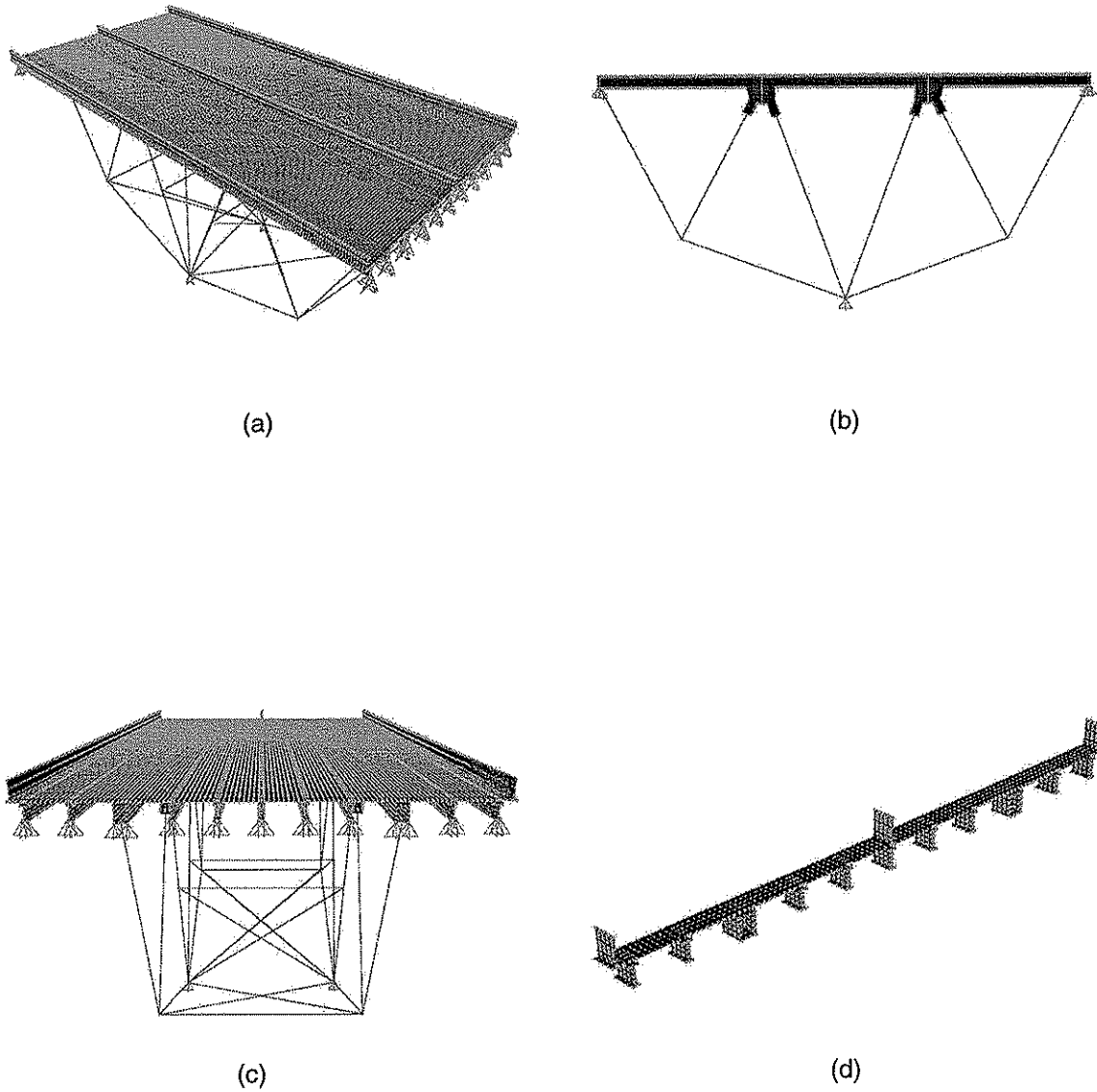
Figure 4.24. Views of the lateral load distribution model: (a) Three-dimensional view looking north and east; (b) Elevation view looking west; (c) Three-dimensional view looking north; (d) Three-dimensional section view.

87
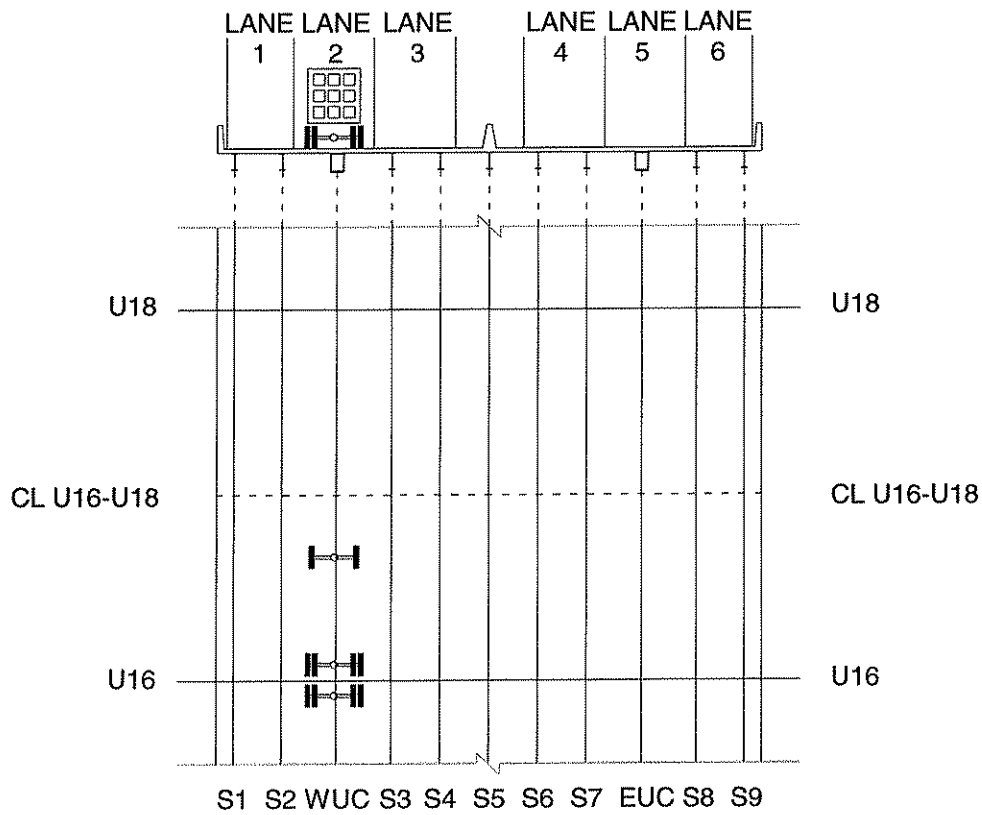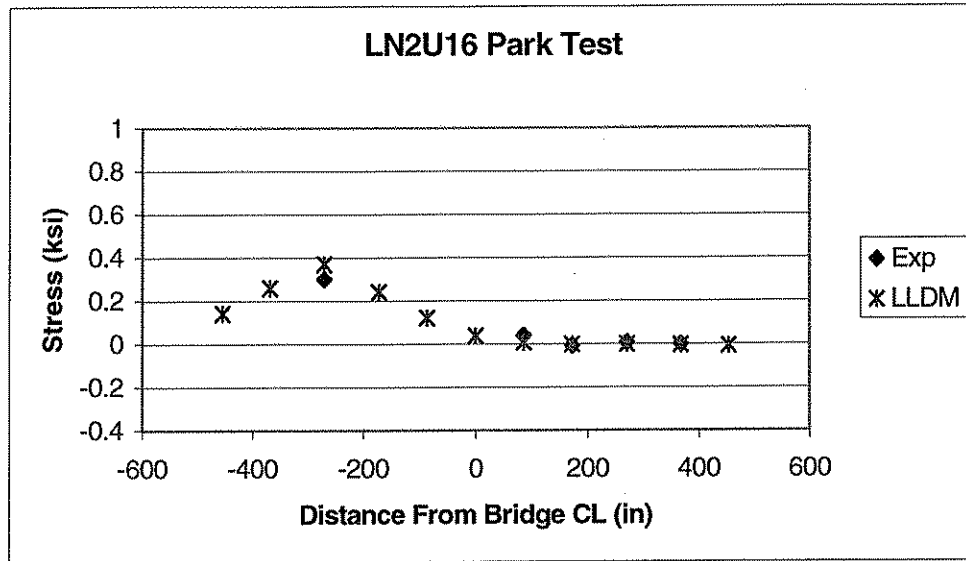
Figure 4.25. LLDM – Stringer bottom flange and upper chord bottom web stresses at the center of span between U16 and U18 for a park test in Lane 2 with the centerline of the truck's back axles centered 18 in. north of U16.

LN2CL Park Test
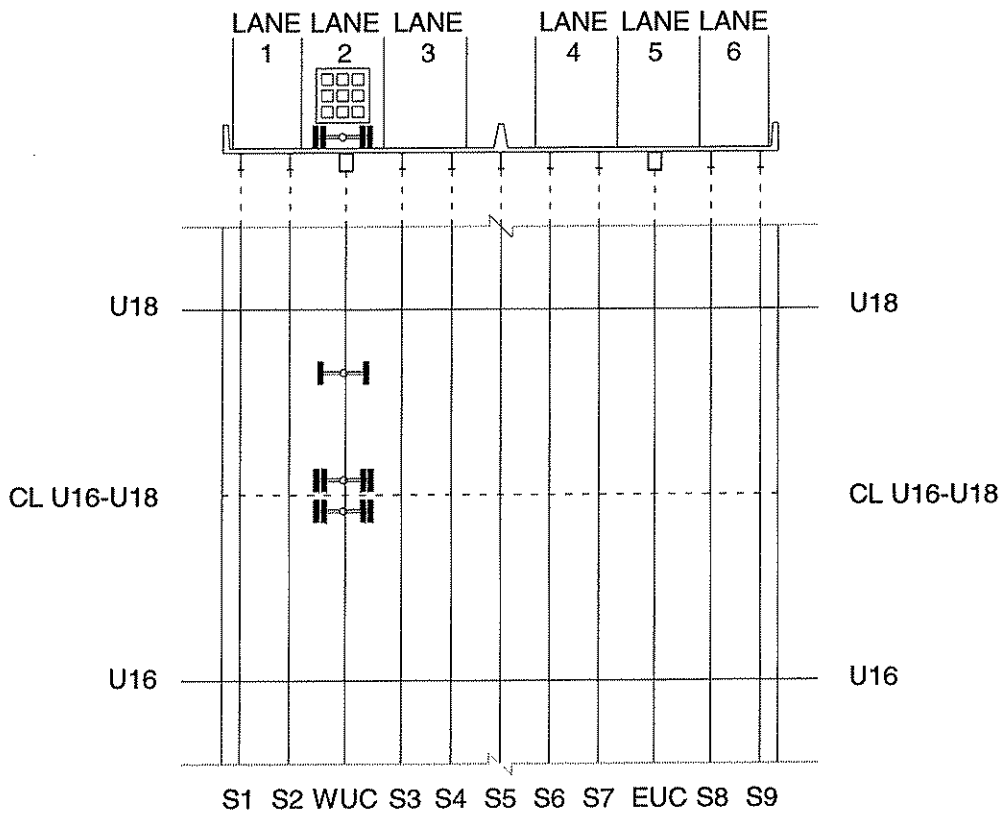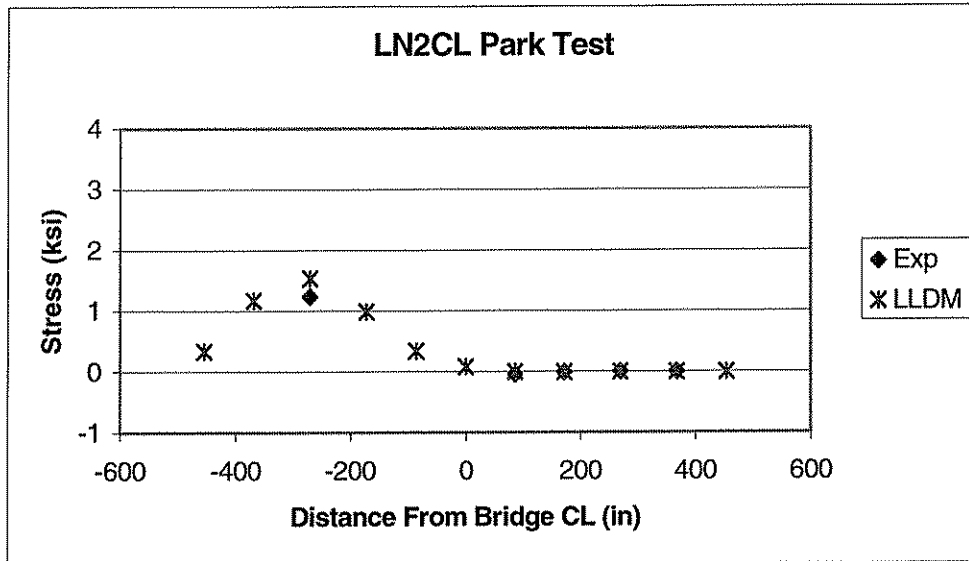
Figure 4.26. LLDM – Stringer bottom flange and upper chord bottom web stresses at the center of span between U16 and U18 for a park test in Lane 2 with the centerline of the truck's back axles centered over the center of span between U16 and U18.
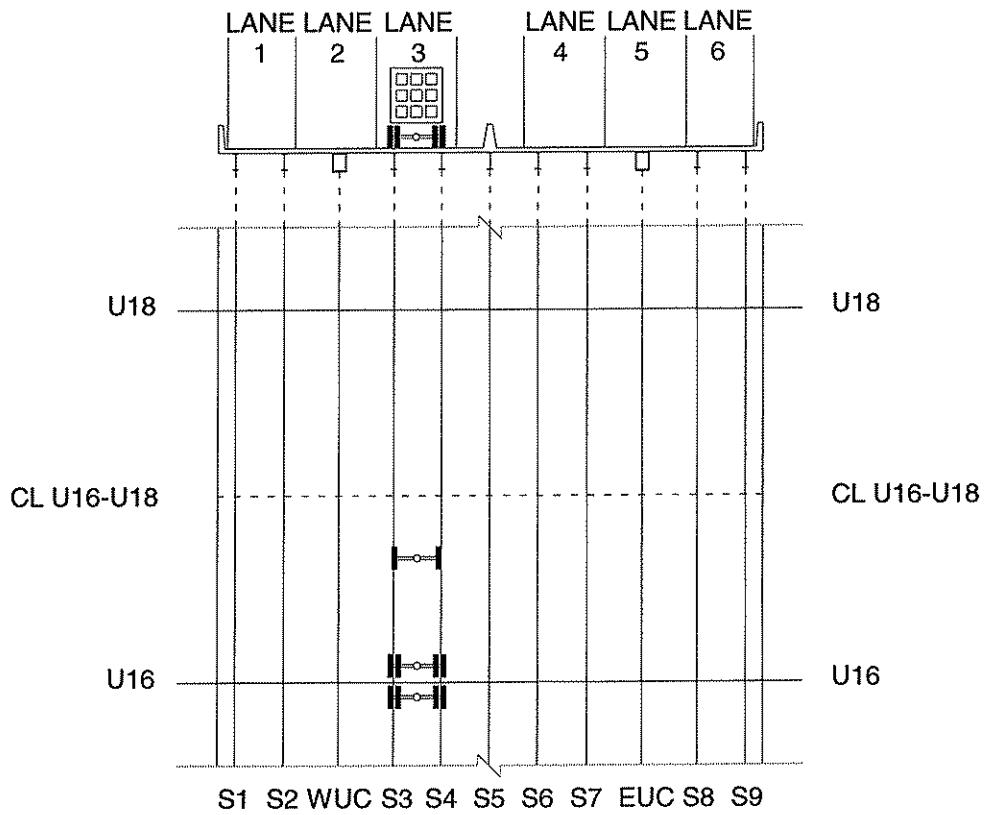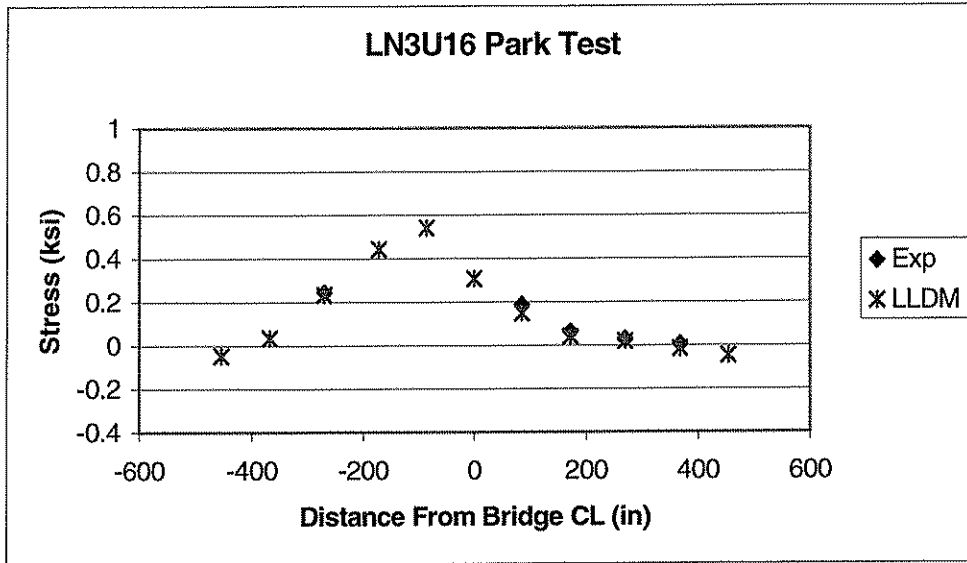
Figure 4.27. LLDM – Stringer bottom flange and upper chord bottom web stresses at the center of span between U16 and U18 for a park test in Lane 3 with the centerline of the truck's back axles centered 18 in. north of U16.
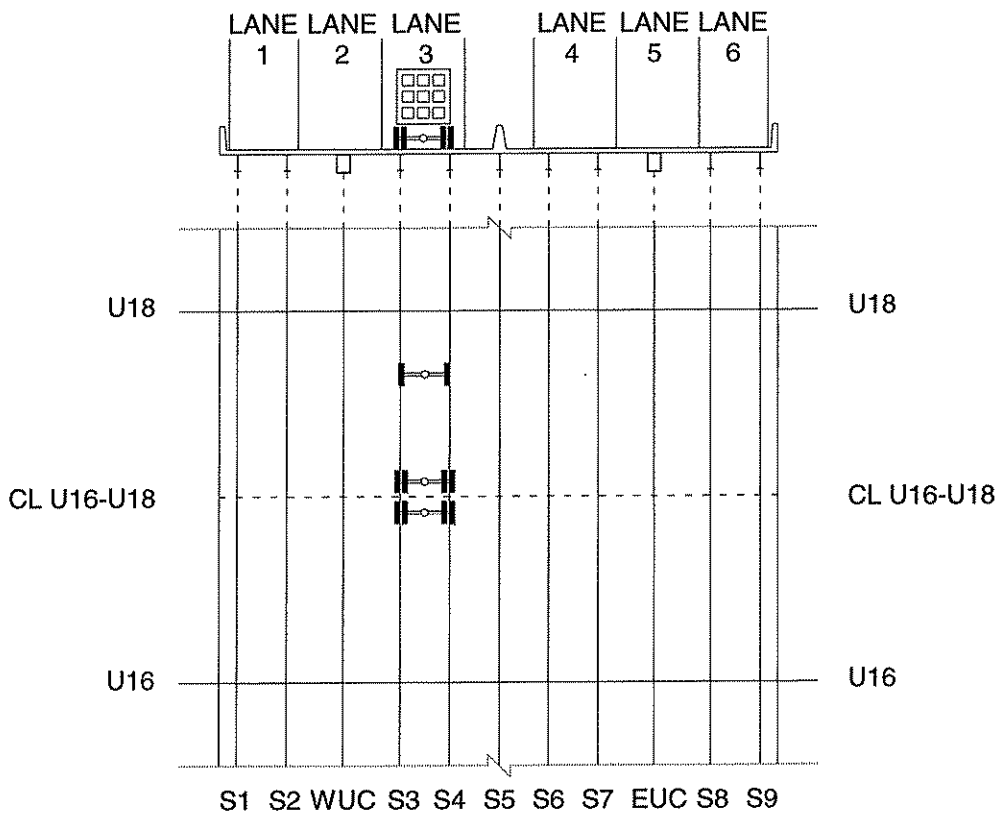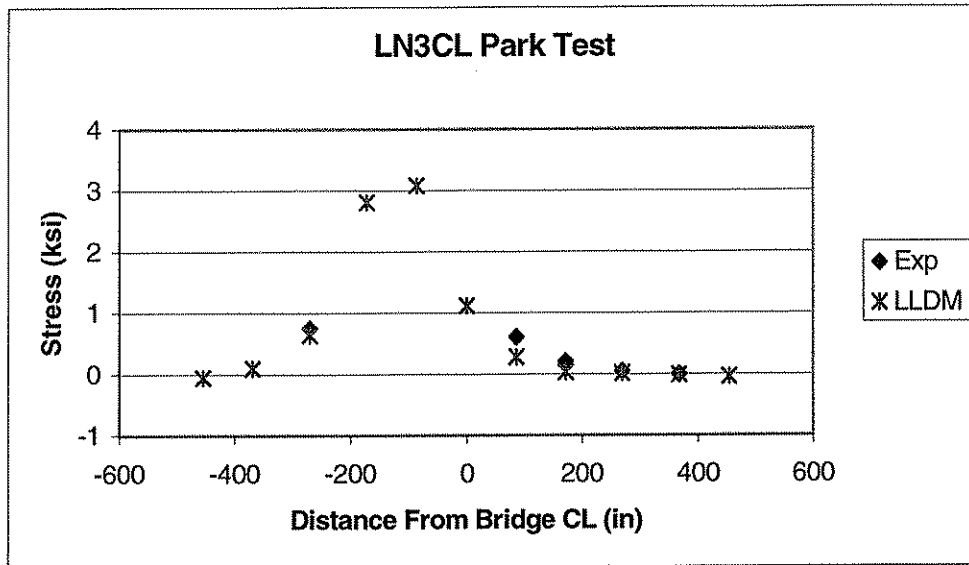
Figure 4.28. LLDM – Stringer bottom flange and upper chord bottom web stresses at the center of span between U16 and U18 for a park test in Lane 3 with the centerline of the truck's back axles centered over the center of span between U16 and U18.
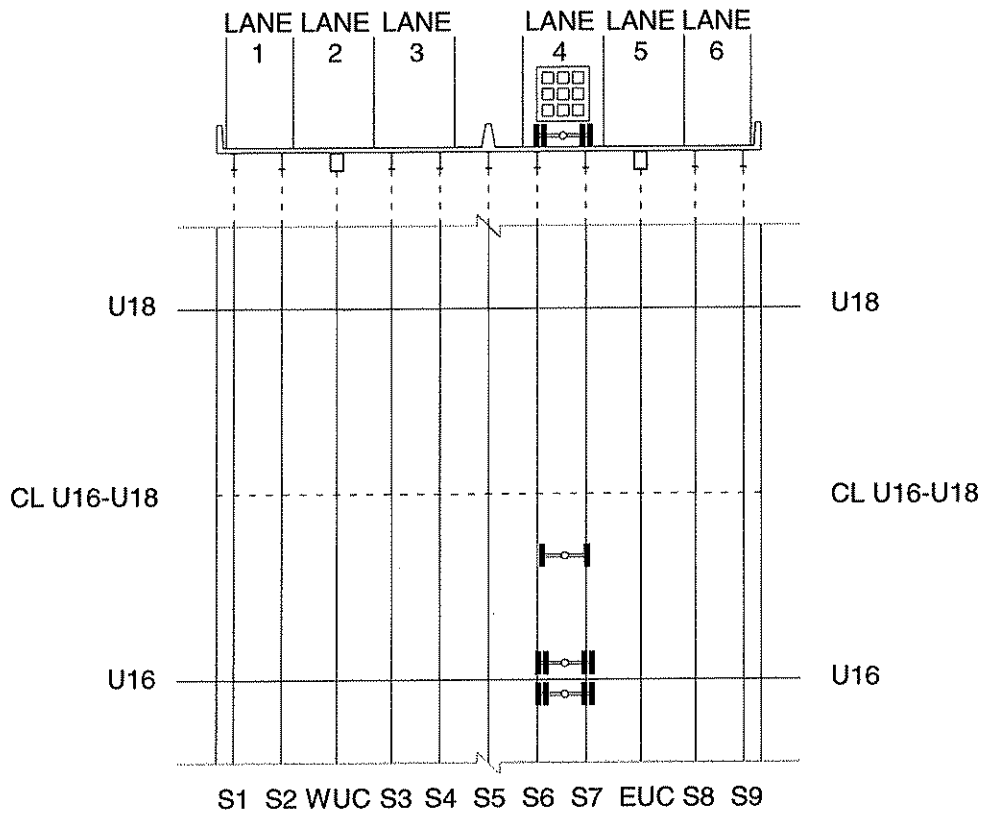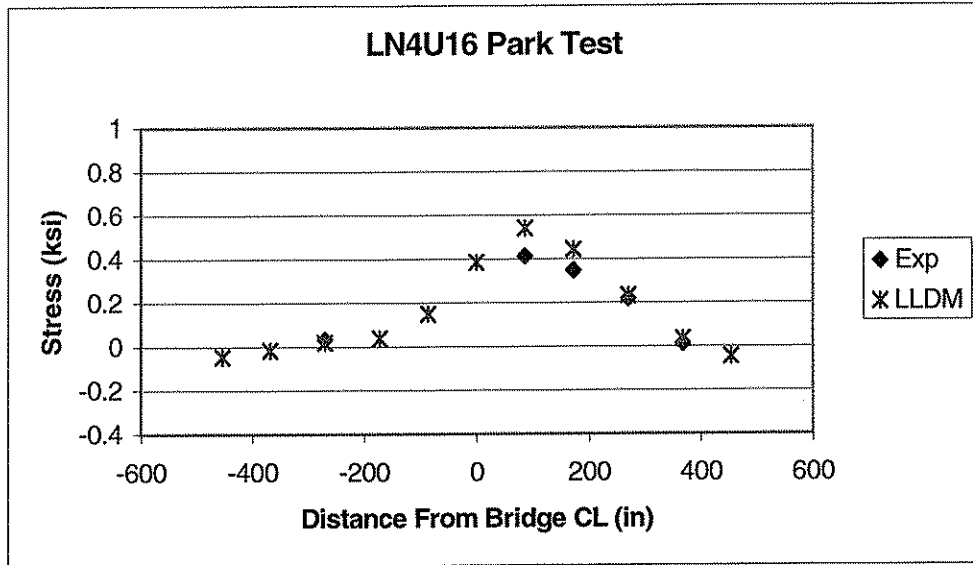
Figure 4.29. LLDM – Stringer bottom flange and upper chord bottom web stresses at the center of span between U16 and U18 for a park test in Lane 4 with the centerline of the truck's back axles centered 18 in. north of U16.
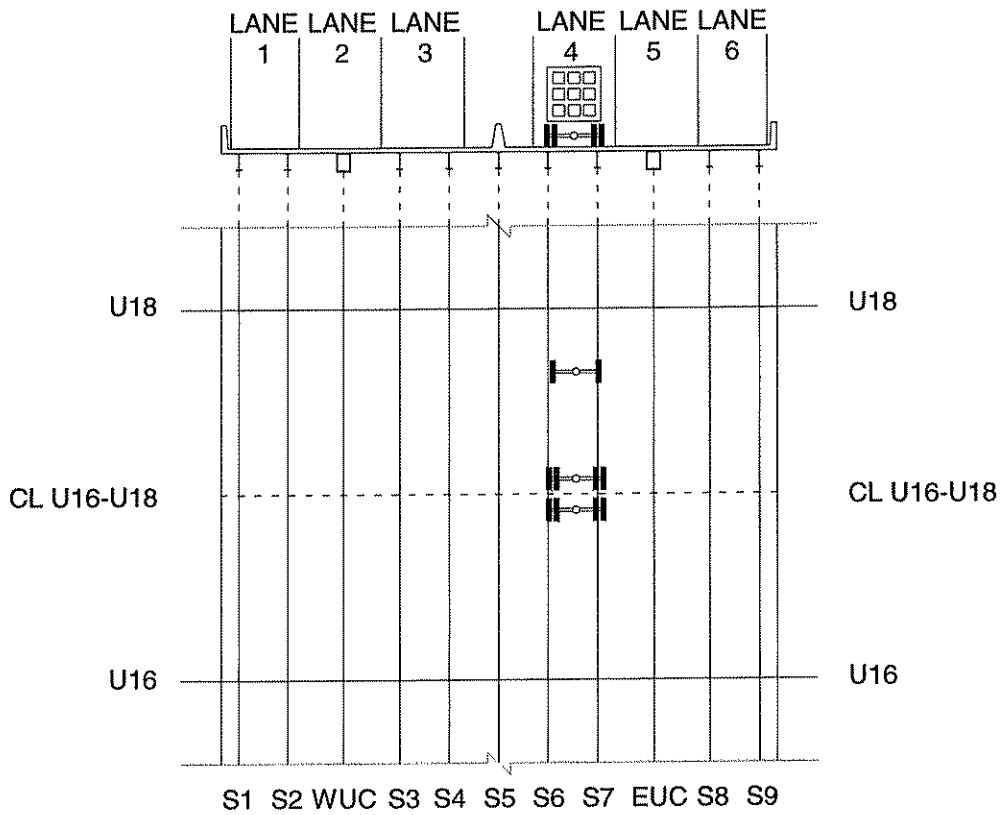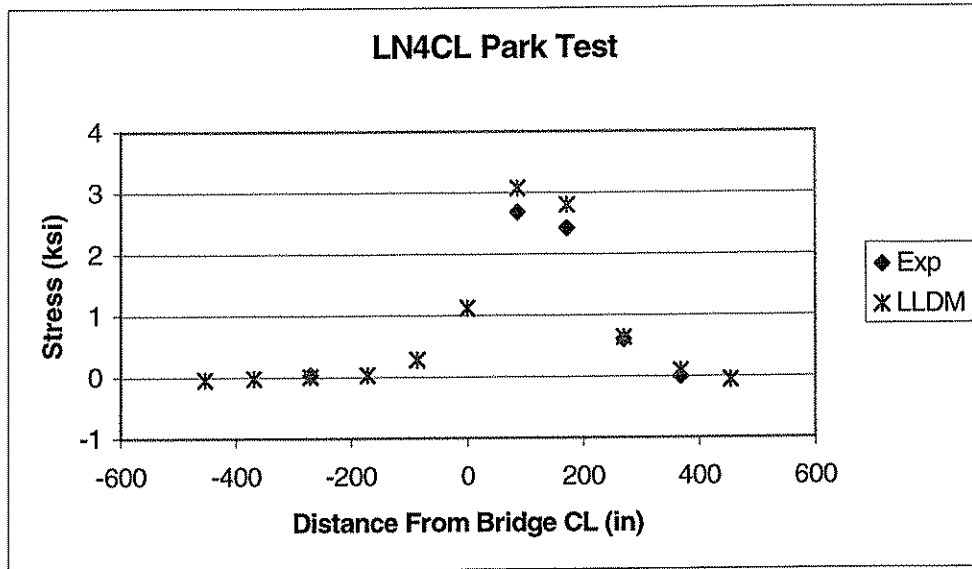
Figure 4.30. LLDM – Stringer bottom flange and upper chord bottom web stresses at the center of span between U16 and U18 for a park test in Lane 4 with the centerline of the truck's back axles centered over the center of span between U16 and U18.

93
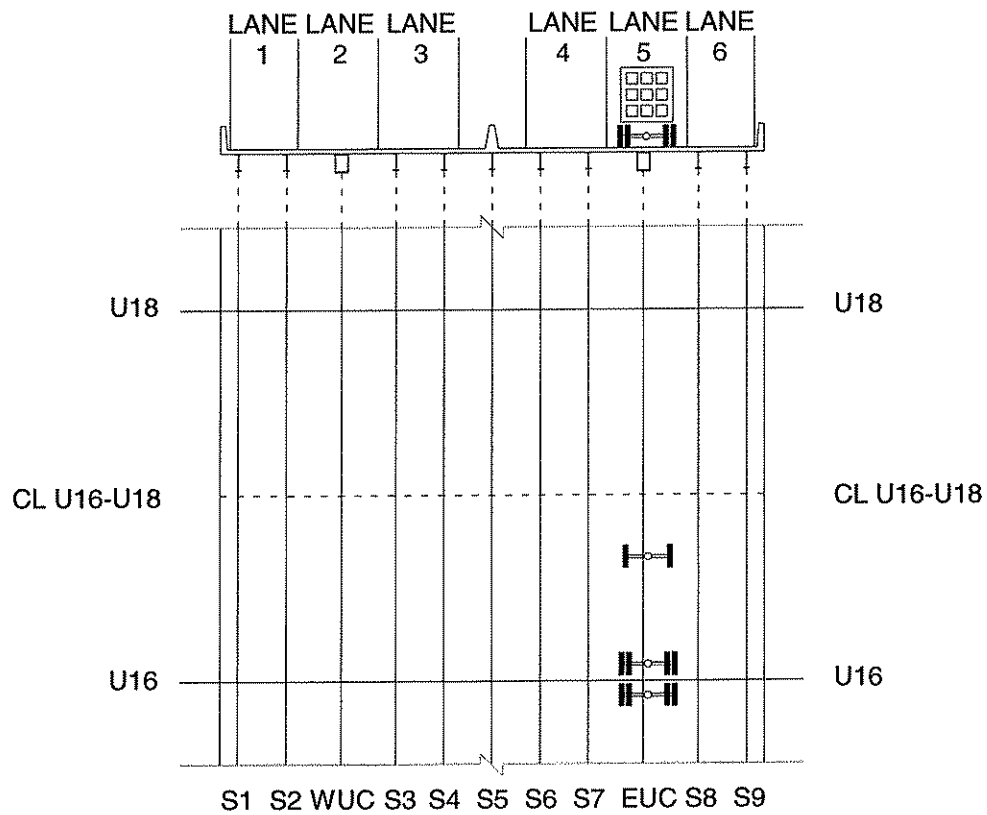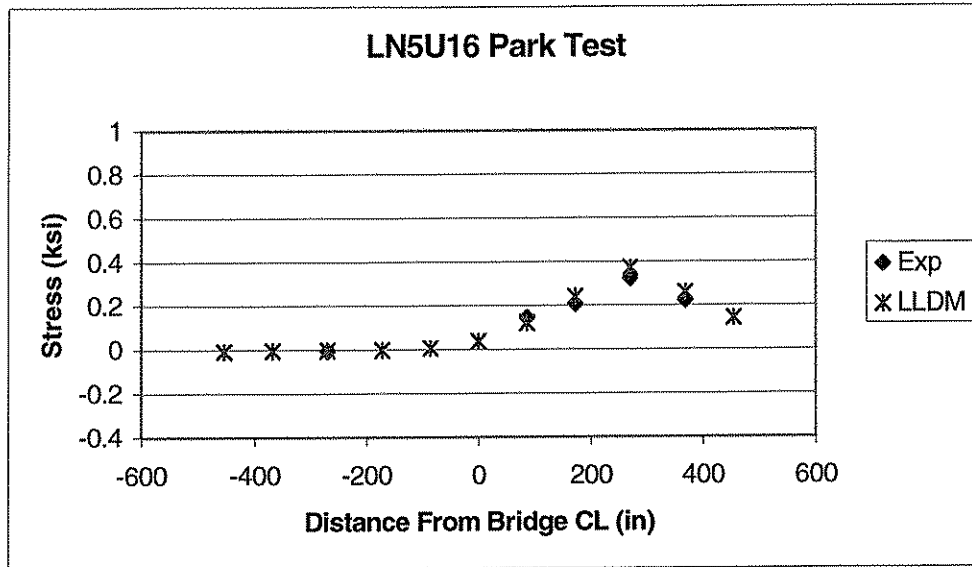
Figure 4.31. LLDM – Stringer bottom flange and upper chord bottom web stresses at the center of span between U16 and U18 for a park test in Lane 5 with the centerline of the truck's back axles centered 18 in. north of U16.
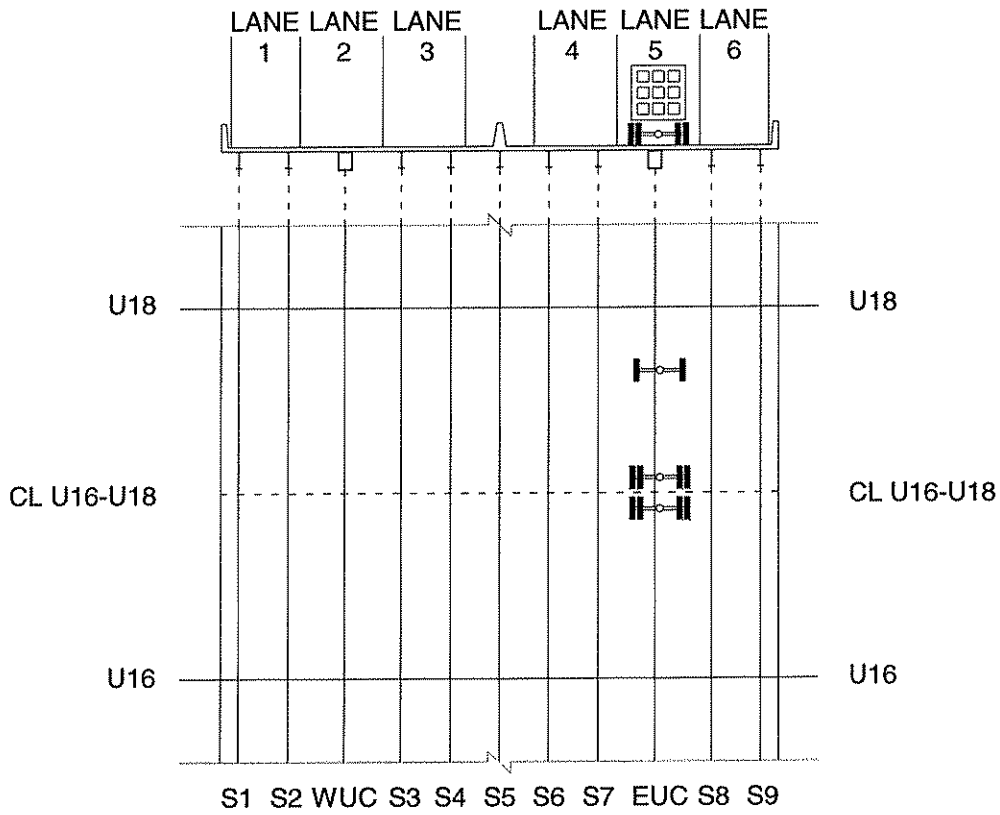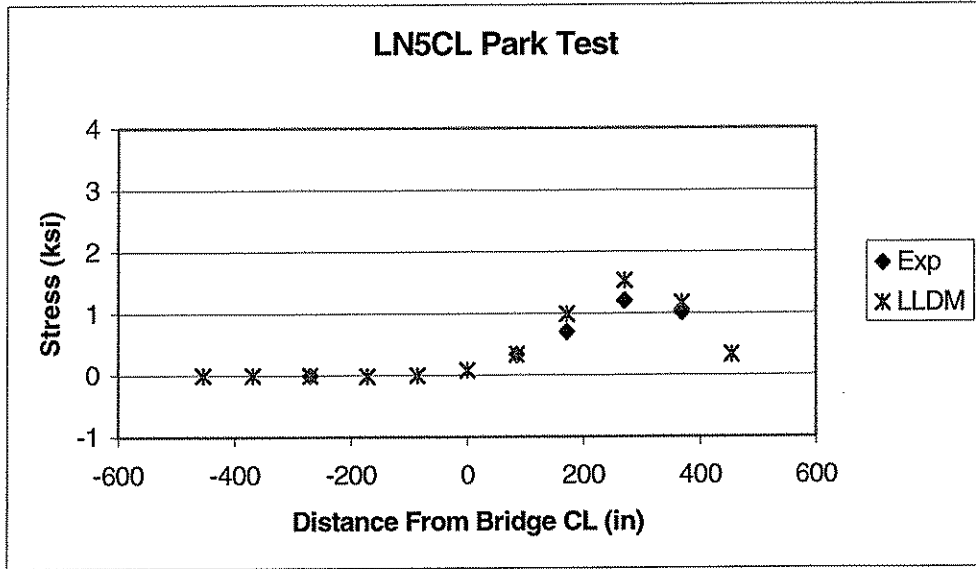
Figure 4.32. LLDM – Stringer bottom flange and upper chord bottom web stresses at the center of span between U16 and U18 for a park test in Lane 5 with the centerline of the truck's back axles centered over the center of span between U16 and U18.

95
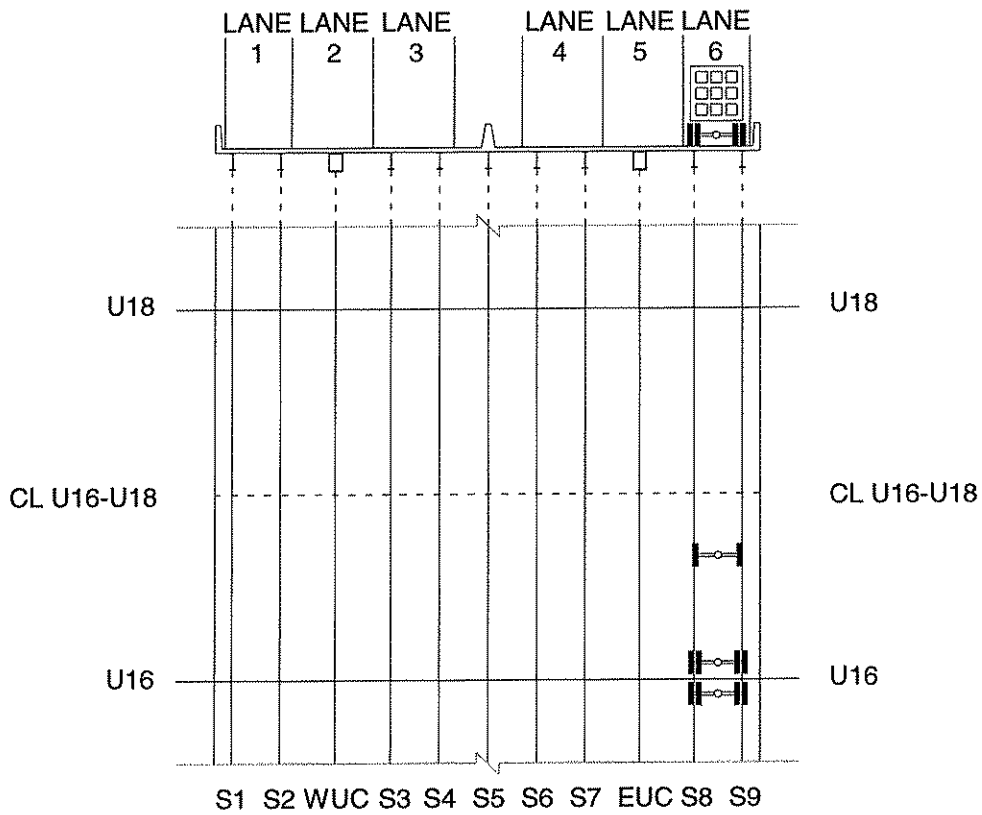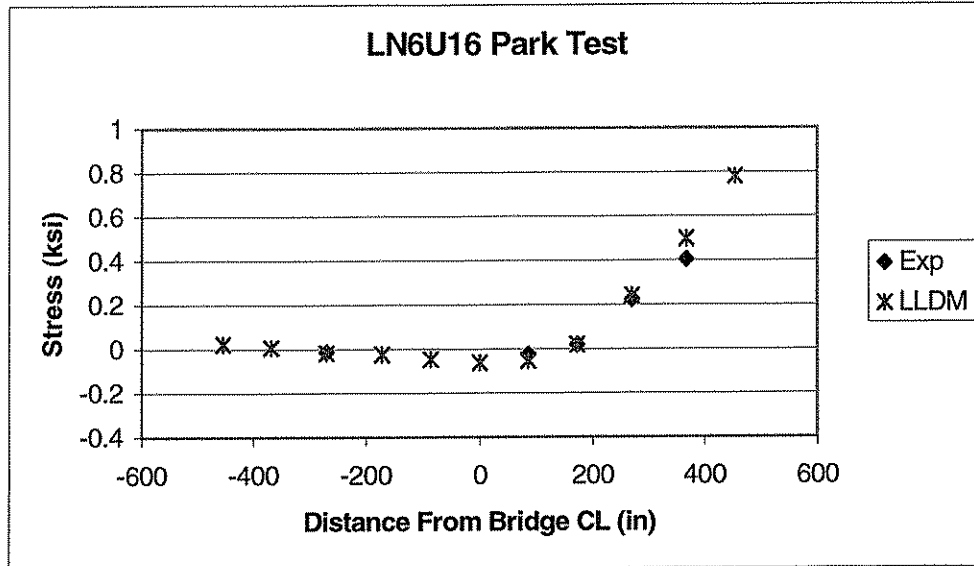
Figure 4.33. LLDM – Stringer bottom flange and upper chord bottom web stresses at the center of span between U16 and U18 for a park test in Lane 6 with the centerline of the truck's back axles centered 18 in. north of U16.

96
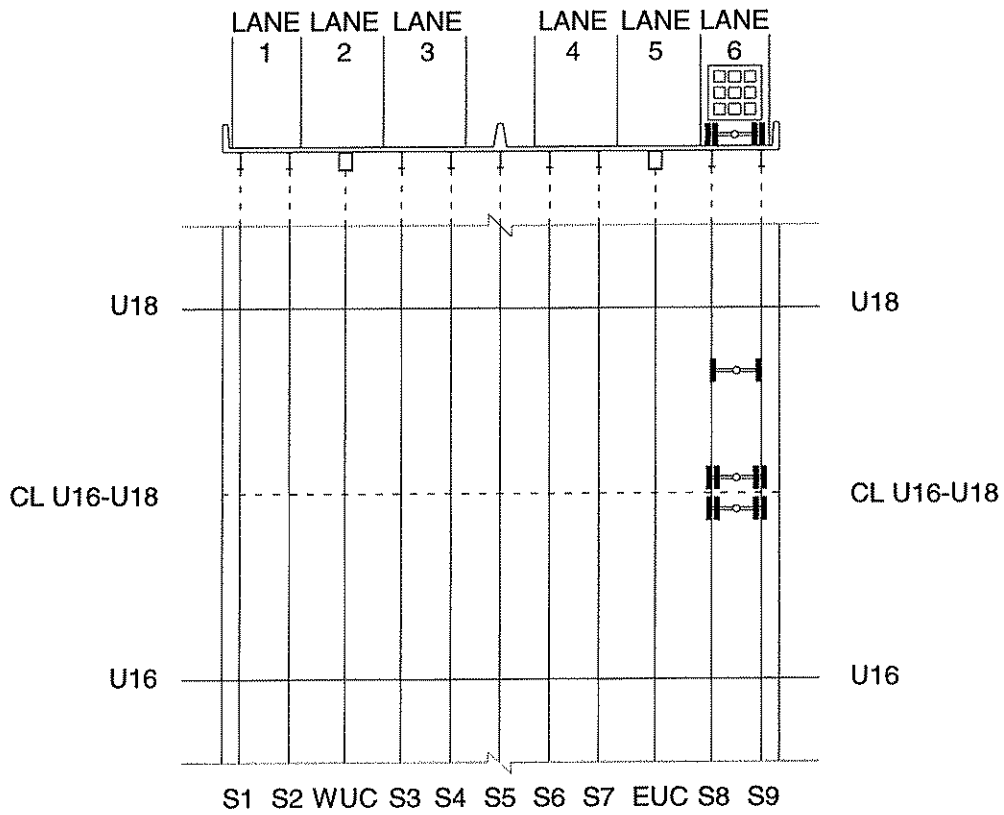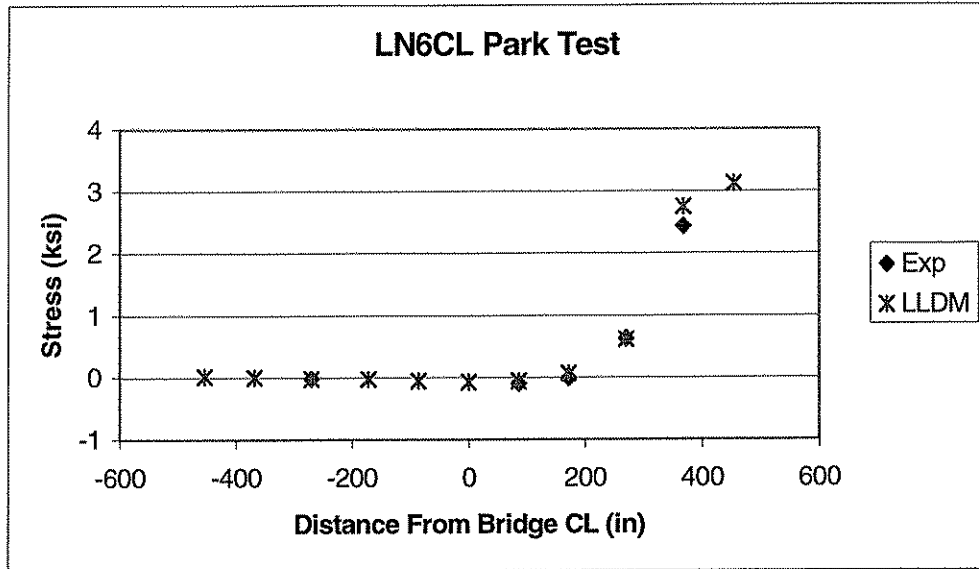
Figure 4.34. LLDM – Stringer bottom flange and upper chord bottom web stresses at the center of span between U16 and U18 for a park test in Lane 6 with the centerline of the truck's back axles centered over the center of span between U16 and U18.

97

CHAPTER 5
FULL BRIDGE ANALYSIS

5.1 INTRODUCTION

This chapter presents the analysis of the bridge using the full bridge model. Section 5.2 describes the full bridge model and how it was created. This section includes a description of how the lateral load distribution model was incorporated into the full bridge model. Section 5.3 describes the load cases applied to the full bridge model. Section 5.4 treats the local behavior results for the stringers and upper chord members. Section 5.5 presents results from the diagonal members. Lastly, Section 5.6 presents results related to global composite deck behavior. In this chapter, these last three sections compare the analytical and experimental results. The analytical and experimental results are compared with the design assumptions in Chapter 6.

5.2 DESCRIPTION OF THE MODEL

The full bridge model, a finite element model representing the full bridge structure, was constructed in SAP 2000. The area of interest for this model extends from U16 to U30, because it is intended to provide information relative to the local and global action of the stringers and upper chord members between U16 and U18, and the behavior of the diagonals as a result of specialized load cases.

The lateral load distribution model was the building block upon which the full bridge model was constructed. The boundary conditions applied to the lateral load distribution model were removed and replaced with elements that represented the remaining structural components of the bridge. For instance, the pin restraint formerly at the position of Pier 2 in the lateral load distribution model was removed and replaced with a member representing the actual pier. This method of replacement was employed at the pin restraints formerly at the ends of each of the stringers and upper chord members as well. The remainder of the lateral load distribution model remained unchanged as it was incorporated into the full bridge model.

The entire full bridge model is shown in elevation view in Figure 5.1. The model is comprised of two main regions. Region 1 includes all members between U1 and L41. In this region, the bridge is modeled with either shells (by the incorporation of the lateral load distribution model) or by frame elements. Region 2 includes the remainder of the bridge.

5.2.1 Region 1

The upper chords and stringers from U1 through U14 and U20 through L41 were entered into the model as general frame sections with the properties of a composite steel section and reinforced concrete deck. The effective width of the deck above the steel section was chosen as the addition of half the distance from the centerline of the member to the centerline of the next adjacent member on each side.

The diagonals, lower chords, sway bracing, cross bracing, and piers were also modeled using frame elements for the members between U1 and L41. Each section was entered with its respective properties as noted on the structural drawings. Figure 5.2 is a photograph of a typical steel bridge connection among these members and a view of how they were entered into the full bridge model.

5.2.2 Region 2

Region 2 of the full bridge model includes the structural components from L41 to U65. In this region of the bridge structure, the entire cross-section of the bridge was represented in the model using two frame sections. Each frame section had the properties of both the upper and lower chord of one longitudinal truss line and half of the composite concrete deck. The centroid of each frame section was added to the model at the centroid of the section comprised of the top and bottom chords and deck.

5.2.3 Use of Shell Elements

Shell elements were used in the full bridge model to join Region 1 and Region 2 at L41. Figure 5.3 is a three-dimensional view of the full bridge model at L41. Shell elements were entered into the full bridge model at this cross-section forming a large rectangular plate to which both Regions 1 and 2 were attached. This plate was intended to remain as a plane section, so it was assigned properties to make it stiff enough to transfer shear, axial force, and moment between Regions 1 and 2.

5.2.4 Boundary Conditions

The boundary conditions of the full bridge model were provided to represent the support conditions on the bridge. Included in Figure 5.1 are representations of the boundary conditions that were used in the full bridge model.

The full bridge model was pinned at Pier 1B, the top of which sits at the grade elevation in the field. This boundary condition represents the spherical bearing at this location in the field. Figure 5.4 is a photograph containing one of the spherical bearings.

The full bridge model was given pin supports at the tops of Piers 2, 3, and 4. This choice came directly from the existence of spherical bearings on the pier caps that join the bridge structure to the piers in the field. The bottoms of these piers in the full bridge model were provided with fixed supports. This choice arose from the large number of driven micropiles under the concrete pier foundations in the field.

Lastly, the full bridge model was given a roller boundary condition at Pier 5. The top of this pier, like Pier 1B, also sits at grade elevation in the field. Sliding pot bearings were provided at this location. Therefore the chosen boundary condition models the support situation in the field.

5.3 FULL BRIDGE MODEL LOAD CASES

The many load cases applied to the full bridge model are grouped into three main categories. The first category contains park tests. These tests were previously described in Chapter 4, and are briefly summarized again here. In each of the ten park test load cases the equivalent of Truck #80 was placed in one of Lanes 2 through 6. In five of the tests, the truck load was applied with the centerline of the back axles centered 18 in. north of U16. In the other five cases, the same load was applied with the centerline of the back axles centered 27 ft. north of U16. In each case the truck was facing north, and this was replicated in the model loading. The results of these load cases are directly compared to the design assumption regarding lateral load distribution in Chapter 6.

The second category of loading applied to the full bridge model contains static loadings intended to represent a heavy vehicle inside or outside of the two longitudinal truss lines. These load cases were intended to examine out-of-plane bending in the diagonal truss members and consisted of two 42.5 kip point loads to simulate the weight of Truck #80. There were two load cases positioned inside the two longitudinal truss lines. One was applied at the intersection of Stringers S6 and S7 with the Floorbeam at U20. The other was applied at the intersection of Stringers S6 and S7 with the Floorbeam at U24. These two load cases were named ID20 and ID24 respectively. There were also two load cases positioned outside the two longitudinal truss lines. One was applied at the intersection of Stringers S8 and S9 with the Floorbeam at U20. The other was applied at the intersection of Stringers S8 and S9 with the Floorbeam at U24. These two load cases were named OD20 and OD24 respectively.

The third category of loading applied to the full bridge model contains a static loading at the center of Span 2 at the upper chord node (U28). A point load of 150 kips was placed at truss node U28 on both truss lines. This static loading pattern was applied at a far distance away from the area of interest chosen for study in this research in order to assess the effect of a distant load on the composite deck and stringers in the area of interest. It was used to determine the global participation of the reinforced concrete deck and stringers positioned over Pier 2 in the negative moment region for this load case.

5.4 FULL BRIDGE MODEL PARK TEST RESULTS

Figures 5.5 through 5.14 contain the experimental and analytical results for the stress in the bottom flange of each stringer and the bottom web of each upper chord box section at a cross-section of the bridge deck centered between U16 and U18 (27 ft. north of U16) for the pertinent load cases discussed in Section 5.2.3. The figures contain the experimentally measured stresses, the stresses gathered from the lateral load distribution model, and the stresses gathered from the full bridge model. All of this data is presented on the same figures for clarity and comparison. The results from this cross-section are presented because they represent the most heavily experimentally instrumented cross-section.

The data is plotted over two domains. The tests conducted with the back axles of the truck 18 in. north of U16 are plotted over a domain of −0.4 ksi to 1.0 ksi. The tests conducted with the back axles of the truck 27 ft. north of U16 are plotted over a domain of −1.0 ksi to 4.0 ksi.

The most important feature of these results was that they were effectively able to produce the same shape distribution as the experimental data on the bridge cross-section. The lateral load distribution model and the full bridge model results are used to determine the lateral load distribution factors affecting each steel member in the deck cross-section at 27 ft. north of U16. This is presented in Chapter 6.

5.5 COMPARISON OF EXPERIMENTAL AND ANALYTICAL RESULTS

Table 5.1 shows the ratio of the analytical results of the lateral load distribution model to the experimental results where this calculation was appropriate (i.e. if the calculation would have contained at least one of the results as a zero value, or if experimental data was not available, the ratio was omitted.) Similar to Chapter 4, the table contains stress values rounded to the nearest 0.1 ksi. In some cases the ratio was close to 1, meaning there was no difference between the analytical and experimental result. In other cases it should be noted that although the ratio deviation from 1 is large, the realistic difference in the reported values is small. For instance (as in Table 4.2), for stringer S6 subjected to the LN5U16 park test, the ratio is reported as 0.5. This difference seems quite large, but the values reported for the experimental data and the analytical data are 0.2 ksi and 0.1 ksi respectively.

5.6 FULL BRIDGE MODEL DIAGONAL MEMBER RESULTS

Table 5.2 contains analytical results obtained from diagonal truss members L19-U20, U20-L21, L23-U24, and U24-L25 for the pertinent load cases discussed in Section 5.2.3.

Several important characteristics are prevalent in the data. The first is that the axial stress for each member in each case is rather low (between −0.9 ksi and 1.0 ksi). This result was expected due to the applied load cases and is an important base to which the bending stresses can be compared.

The second important characteristic is that the absolute value of the maximum in-plane moment for each member in each case is small (between 0 and 82 kip-in). This, in turn, means that the in-plane bending stresses developed by these in-plane moments are close to zero, and that the truss members are behaving similarly to a pinned truss in-plane.

Another important characteristic is that the out out-of-plane moment values are significant relative to the in-plane moment values for members locally affected by each specific load case. Hence, the out-of-plane stress values are significant relative to the in-plane stress values in these members. For instance, load case ID20 produced a maximum out-of-plane bending stress of 0.1 ksi in members L19-U20 and U20-L21. ID20 produced no noticeable in-plane bending stresses in these members. It is also important to note that ID20 produced no

noticeable in-plane or out-of-plane bending stresses in members L23-U24 and U24-L25. This information demonstrates that the out-of-plane bending stresses induced in the diagonal members of the truss lines are significant relative to the in-plane bending stresses and are the result of a local loading. When a load is placed just a few panel points away from a specific diagonal member, no out-of-plane stresses are observed.

The last important characteristic is the value of the out-of-plane bending stress relative to the value of the axial stress in the diagonal members. The out-of-plane bending stresses, as discussed above, are the result of a local load case. Hence, it is only appropriate to compare the axial stresses with out-of-plane bending stresses when both types of stress exist in a particular member. The values in Table 5.2 lead to the determination that the out-of-plane bending stresses can be as little as 11% (see load case BD20 for member L19-U20) and as much as 50% (see load case ID24 or BD24 for member U24-L25) of the axial stress in a given diagonal member. Therefore the out-of-plane bending stress values are significant relative to the axial stresses in the diagonal members. These results are compared to the appropriate design assumption in Chapter 6.

5.7 FULL BRIDGE MODEL GLOBAL DECK RESULTS

Table 5.3 contains the analytical results gathered from the full bridge model at a cross-section located between U16 and U18 on the upper chord of the truss due to a load applied at midspan of Span 2 (at U28). These data are reported in terms of steel stress and were calculated as the average from a linear strain distribution across the cross-section. This allowed any local bending influence to be subtracted from the results.

The most important characteristic of this data is that all of the stringers and upper chord members in the deck cross-section at 27 ft. north of U16 are shown to participate in carrying global tension when a load is placed out in a span far away from it. The stress reported is low (less than 0.1 ksi for all members), but the area for this section is significant. This means that the components of the cross-section are working together with a very even lateral strain distribution. These results are compared to the appropriate design assumption in Chapter 6.

102

Test	LN2U16			Test	LN2CL		
Data	EXP (ksi)	FBM (ksi)	FBM/EXP	Data	EXP (ksi)	FBM (ksi)	FBM/EXP
S1	-	0.1	-	S1	-	0.3	-
S2	-	0.2	-	S2	-	1.2	-
WUC	0.3	0.3	1.0	WUC	1.2	1.5	1.3
S3	-	0.2	-	S3	-	1.0	-
S4	-	0.1	-	S4	-	0.3	-
S5	-	0.0	-	S5	-	0.1	-
S6	0.0	0.0	-	S6	0.0	0.0	-
S7	0.0	0.0	-	S7	0.0	0.0	-
EUC	0.0	0.0	-	EUC	0.0	0.0	-
S8	0.0	0.0	-	S8	0.0	0.0	-
S9	-	0.0	-	S9	-	0.0	-
Test	LN3U16			Test	LN3CL		
Data	EXP (ksi)	FBM (ksi)	FBM/EXP	Data	EXP (ksi)	FBM (ksi)	FBM/EXP
S1	-	-0.1	-	S1	-	-0.1	-
S2	-	0.0	-	S2	-	-0.1	-
WUC	0.2	0.2	1.0	WUC	0.8	0.6	0.8
S3	-	0.4	-	S3	-	3.0	-
S4	-	0.5	-	S4	-	3.2	-
S5	-	0.3	-	S5	-	1.2	-
S6	0.2	0.1	0.5	S6	0.6	0.3	0.5
S7	0.1	0.0	-	S7	0.2	0.0	-
EUC	0.0	0.0	-	EUC	0.1	0.0	-
S8	0.0	0.0	-	S8	0.0	0.0	-
S9	-	0.0	-	S9	-	0.0	-

Table 5.1. Experimental and analytical result comparison for the full bridge model subjected to park tests.

Test Data	LN4U16			Test Data	LN4CL		
	EXP (ksi)	FBM (ksi)	FBM/EXP		EXP (ksi)	FBM (ksi)	FBM/EXP
S1	-	0.0	-	S1	-	0.0	-
S2	-	0.0	-	S2	-	0.0	-
WUC	0.0	0.0	-	WUC	0.0	0.0	-
S3	-	0.0	-	S3	-	0.0	-
S4	-	0.1	-	S4	-	0.3	-
S5	-	0.4	-	S5	-	1.2	-
S6	0.4	0.5	1.3	S6	2.7	3.2	1.2
S7	0.4	0.4	1.0	S7	2.4	3.0	1.3
EUC	0.2	0.2	1.0	EUC	0.6	0.6	1.0
S8	0.0	0.0	-	S8	0.0	0.1	-
S9	-	-0.1	-	S9	-	-0.1	-

Test Data	LN5U16			Test Data	LN5CL		
	EXP (ksi)	FBM (ksi)	FBM/EXP		EXP (ksi)	FBM (ksi)	FBM/EXP
S1	-	0.0	-	S1	-	0.0	-
S2	-	0.0	-	S2	-	0.0	-
WUC	0.0	0.0	-	WUC	0.0	0.0	-
S3	-	0.0	-	S3	-	0.0	-
S4	-	0.0	-	S4	-	0.0	-
S5	-	0.0	-	S5	-	0.1	-
S6	0.2	0.1	0.5	S6	0.3	0.3	1.0
S7	0.2	0.2	1.0	S7	0.7	1.0	1.4
EUC	0.3	0.3	1.0	EUC	1.2	1.5	1.3
S8	0.2	0.2	1.0	S8	1.0	1.2	1.2
S9	-	0.1	-	S9	-	0.3	-

Test Data	LN6U16			Test Data	LN6CL		
	EXP (ksi)	FBM (ksi)	FBM/EXP		EXP (ksi)	FBM (ksi)	FBM/EXP
S1	-	0.0	-	S1	-	0.0	-
S2	-	0.0	-	S2	-	0.0	-
WUC	0.0	0.0	-	WUC	0.0	0.0	-
S3	-	0.0	-	S3	-	0.0	-
S4	-	0.0	-	S4	-	-0.1	-
S5	-	-0.1	-	S5	-	-0.1	-
S6	0.0	-0.1	-	S6	-0.1	-0.1	1.0
S7	0.2	0.0	-	S7	0.0	0.1	-
EUC	0.2	0.2	1.0	EUC	0.6	0.6	1.0
S8	0.4	0.5	1.3	S8	2.4	2.8	1.2
S9	-	0.7	-	S9	-	3.1	-

Table 5.1 (Cont.). Experimental and analytical result comparison for the full bridge model subjected to park tests.

Load Case	Member	Axial Force (kip)	Axial Stress (ksi)	In Plane		Out of Plane	
				|Max| Moment (kip-in)	Max Stress (ksi)	|Max| Moment (kip-in)	Max Stress (ksi)
ID20	L19-U20	-70	-0.7	51	0.0	874	0.1
ID20	U20-L21	1	0.0	4	0.0	607	0.1
ID20	L23-U24	6	0.1	9	0.0	40	0.0
ID20	U24-L25	-4	-0.1	1	0.0	20	0.0
BD20	L19-U20	-101	-0.9	82	0.0	1900	0.1
BD20	U20-L21	0	0.0	7	0.0	1336	0.1
BD20	L23-U24	10	0.1	11	0.0	89	0.0
BD20	U24-L25	-6	-0.1	0	0.0	11	0.0
ID24	L19-U20	-38	-0.4	37	0.0	17	0.0
ID24	U20-L21	44	0.7	13	0.0	66	0.0
ID24	L23-U24	-56	-0.6	35	0.0	1182	0.1
ID24	U24-L25	-14	-0.2	8	0.0	876	0.1
BD24	L19-U20	-56	-0.5	56	0.0	55	0.0
BD24	U20-L21	66	1.0	20	0.0	84	0.0
BD24	L23-U24	-84	-0.9	27	0.0	2199	0.2
BD24	U24-L25	-22	-0.4	16	0.0	1557	0.2

Table 5.2. Diagonal member analytical results from the full bridge model due to loadings inside and outside of the two longitudinal truss lines.

Member	Global Tension Stress (ksi)
S1	0.09
S2	0.09
WUC	0.08
S3	0.09
S4	0.09
S5	0.09
S6	0.09
S7	0.09
EUC	0.08
S8	0.09
S9	0.09

Table 5.3. Stress results from the composite deck cross-section at the centerline of U16-U18 due to a load pattern placed at the center of Span 2.
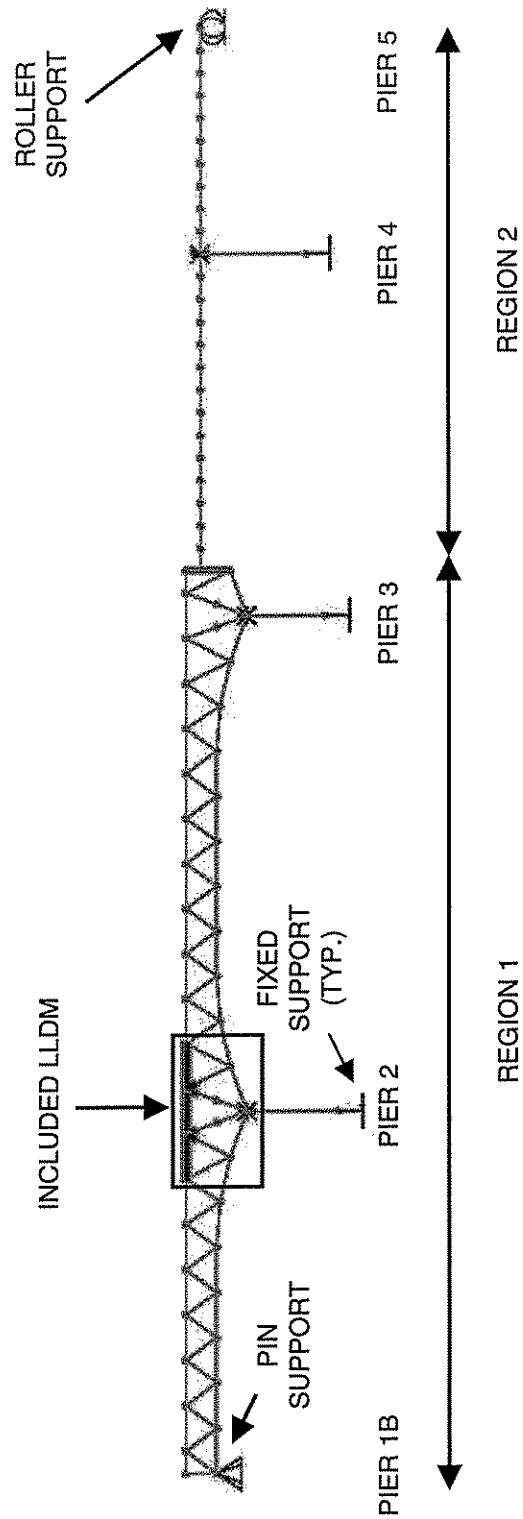
Figure 5.1. Elevation view of the full bridge model, looking west.
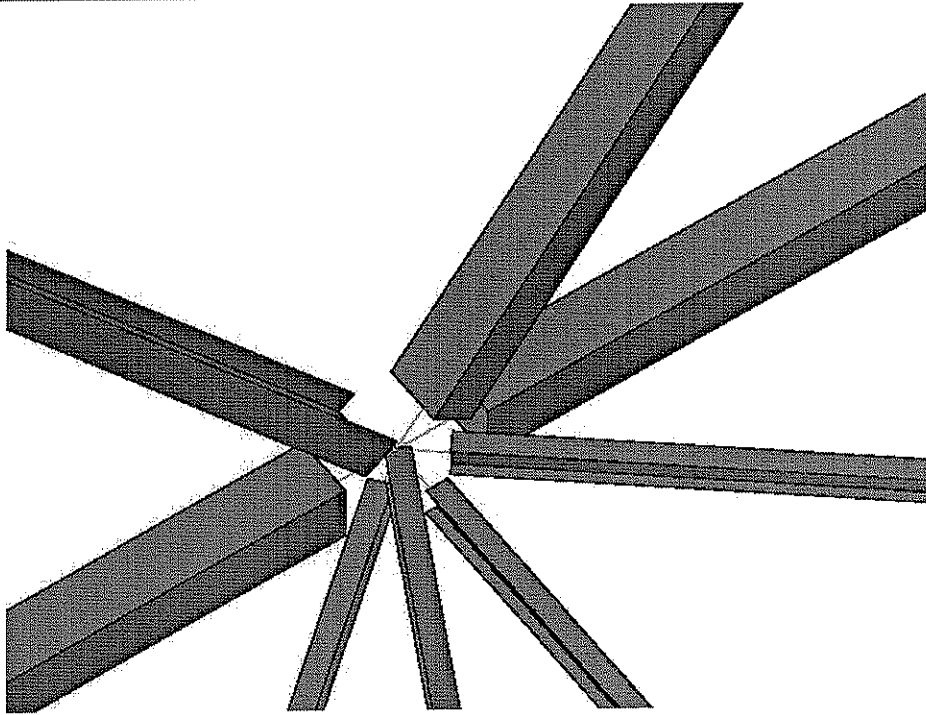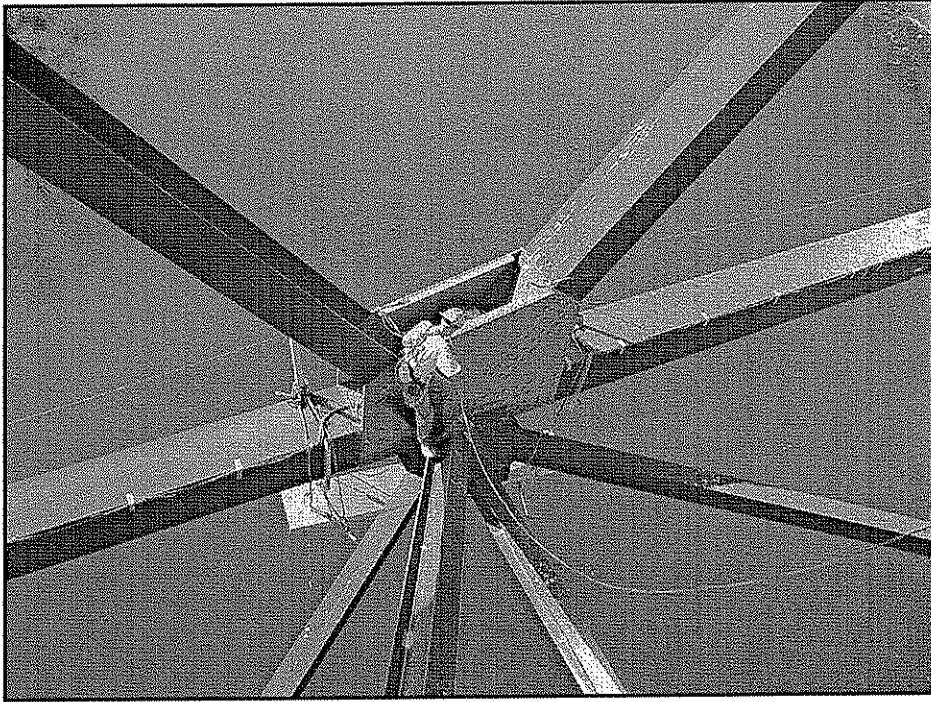
Figure 5.2. Photograph and full bridge model representation of a typical connection in Region 1.
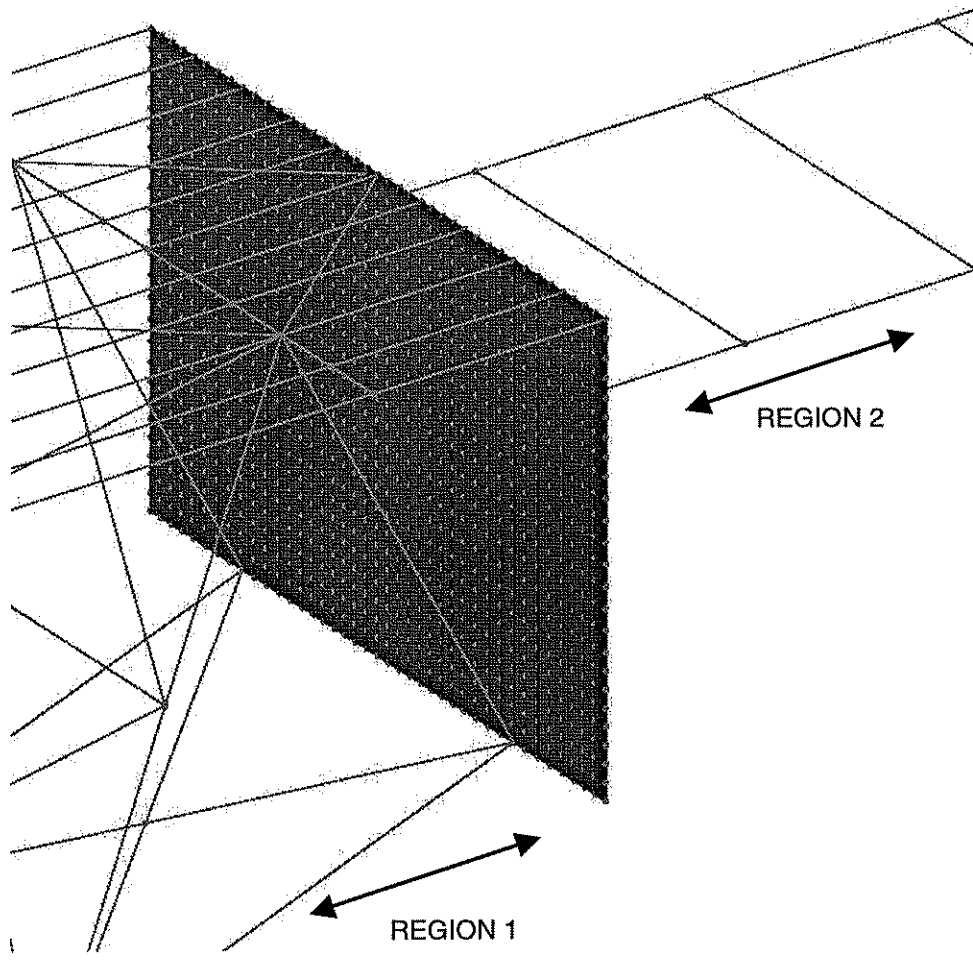
Figure 5.3. Three-dimensional view of full bridge model at L41.
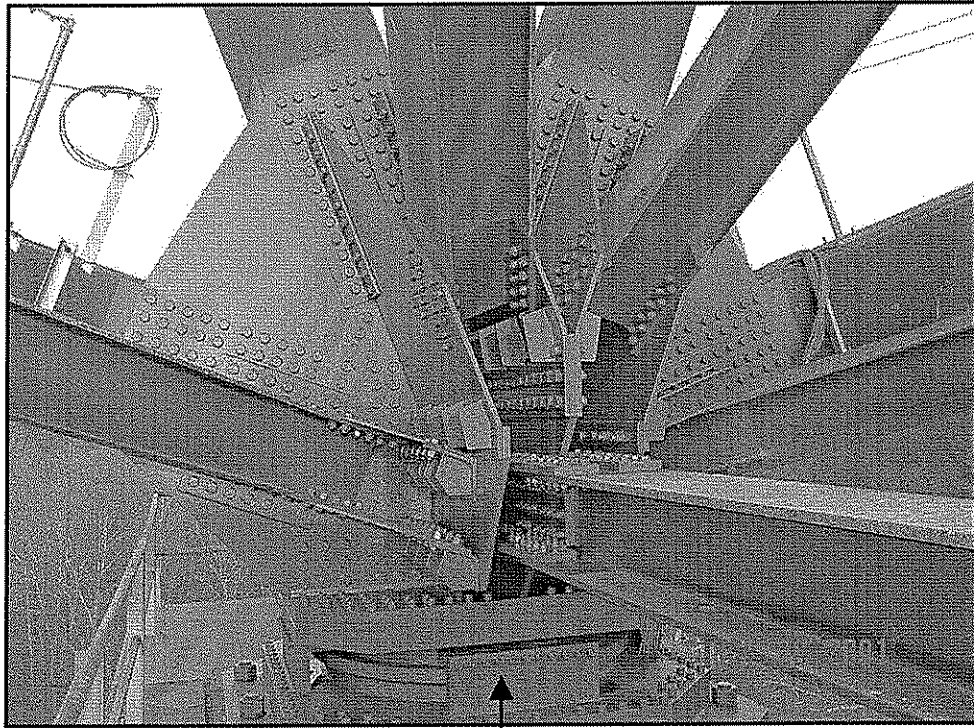
SPHERICAL BEARING
MOUNTED ON PIER 2

Figure 5.4. Photograph of panel point L17 looking east.

110
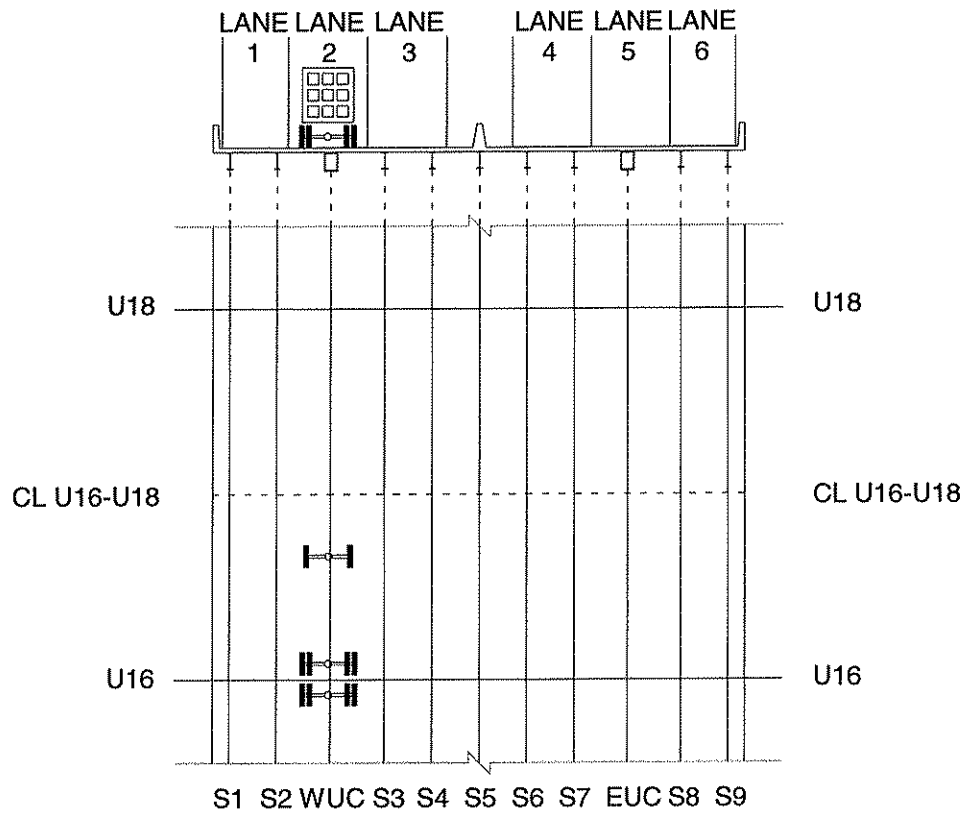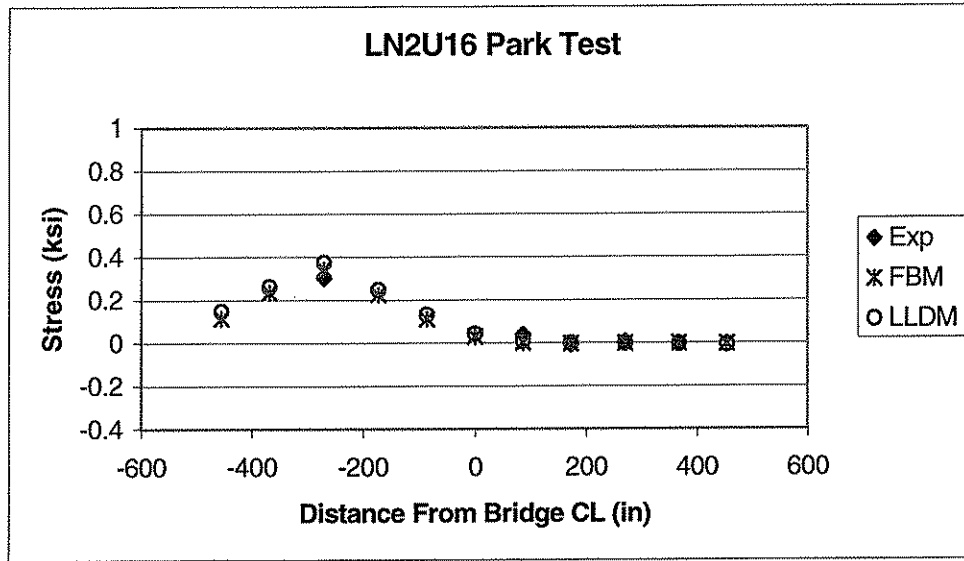
Figure 5.5. FBM – Stringer bottom flange and upper chord bottom web stresses at the center of span between U16 and U18 for a park test in Lane 2 with the centerline of the truck's back axles centered 18 in. north of U16.

111
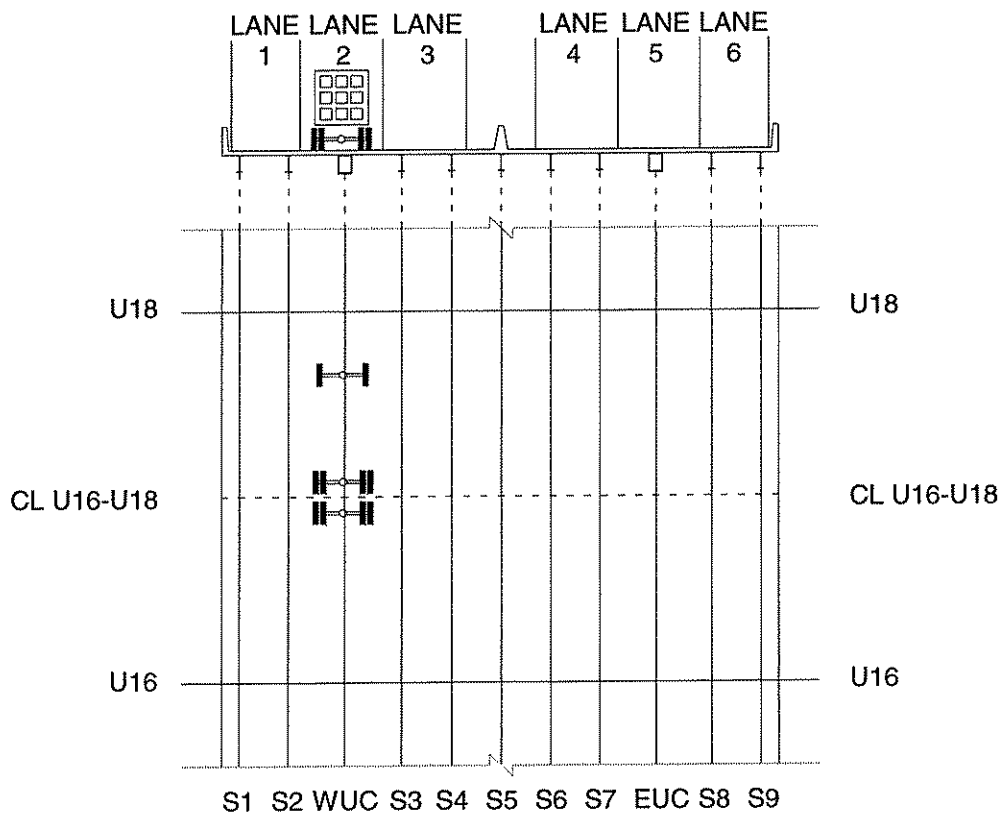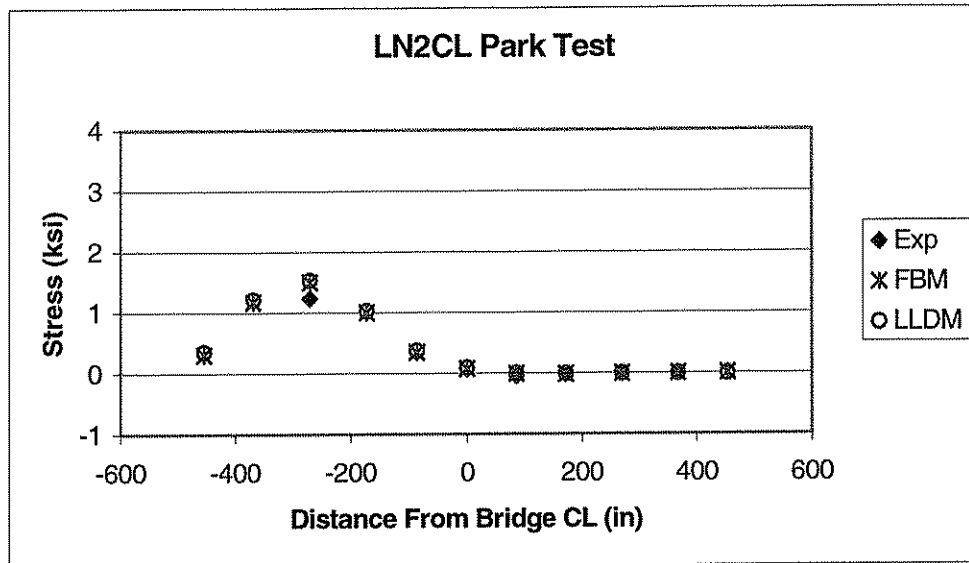
Figure 5.6. FBM – Stringer bottom flange and upper chord bottom web stresses at the center of span between U16 and U18 for a park test in Lane 2 with the centerline of the truck's back axles centered over the center of span between U16 and U18.

112
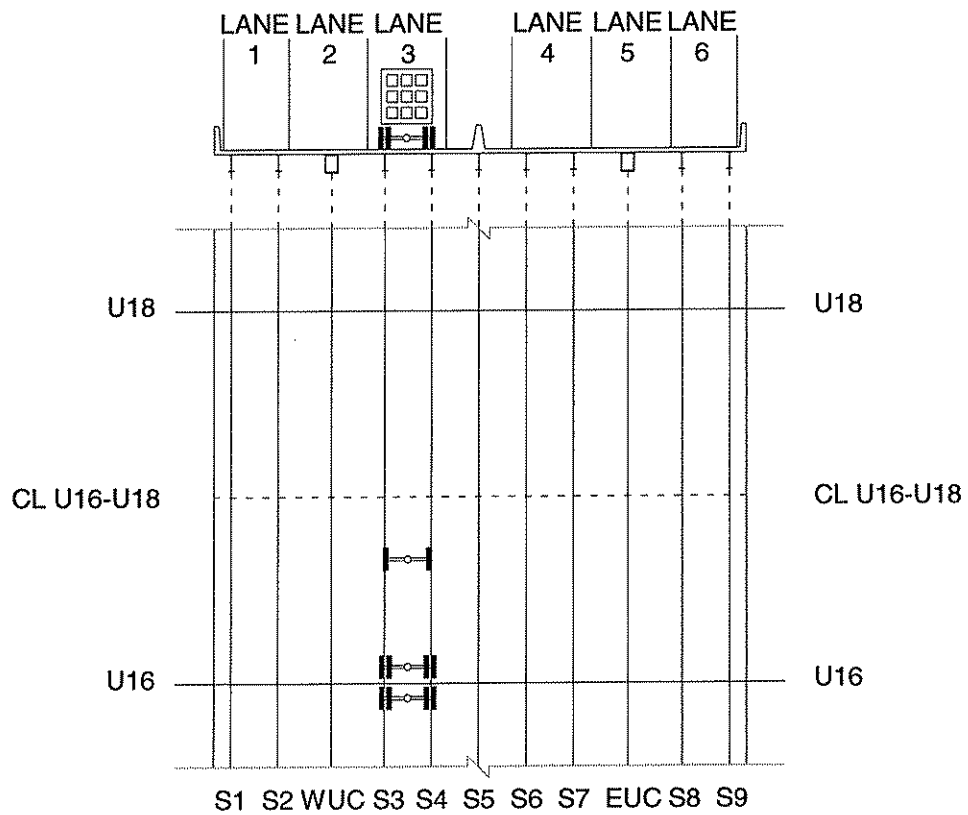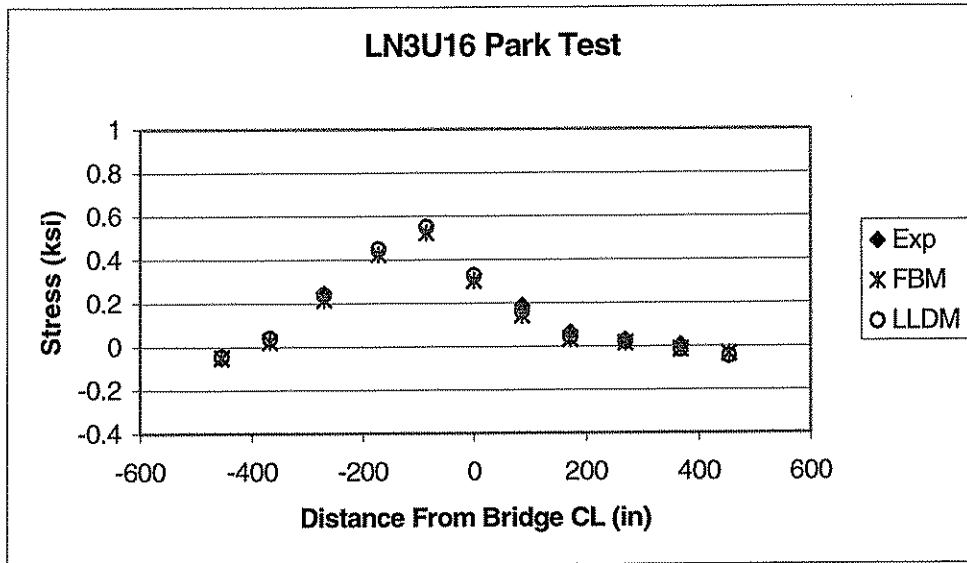
Figure 5.7. FBM – Stringer bottom flange and upper chord bottom web stresses at the center of span between U16 and U18 for a park test in Lane 3 with the centerline of the truck's back axles centered 18 in. north of U16.
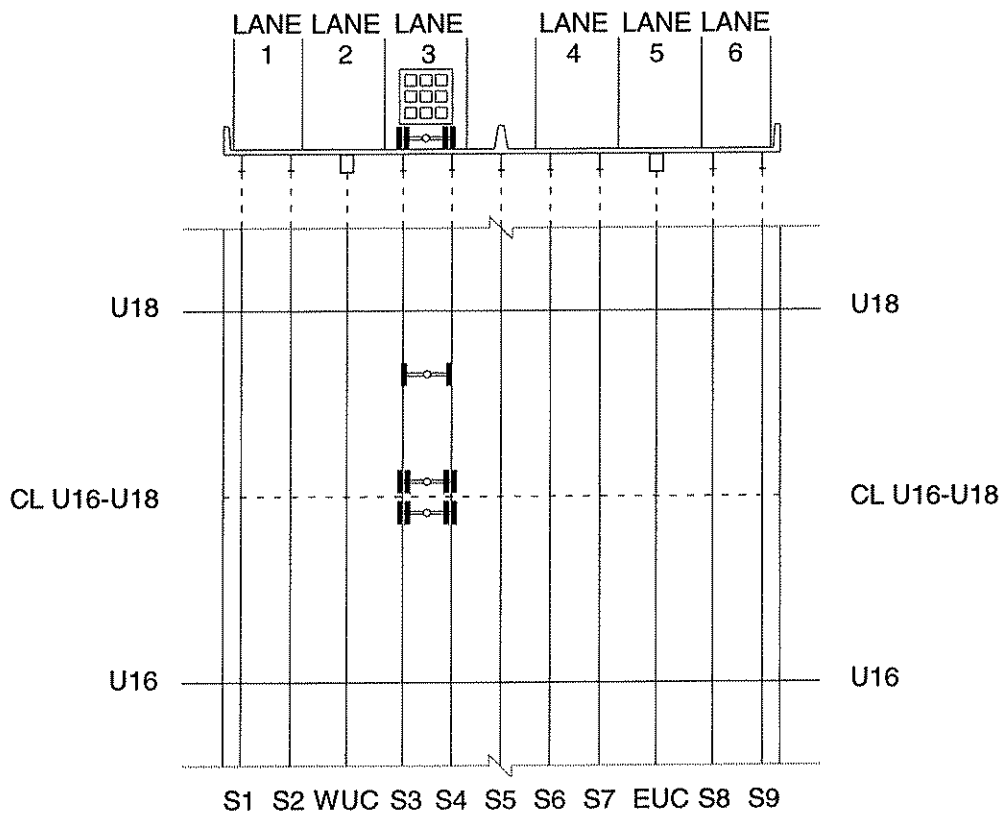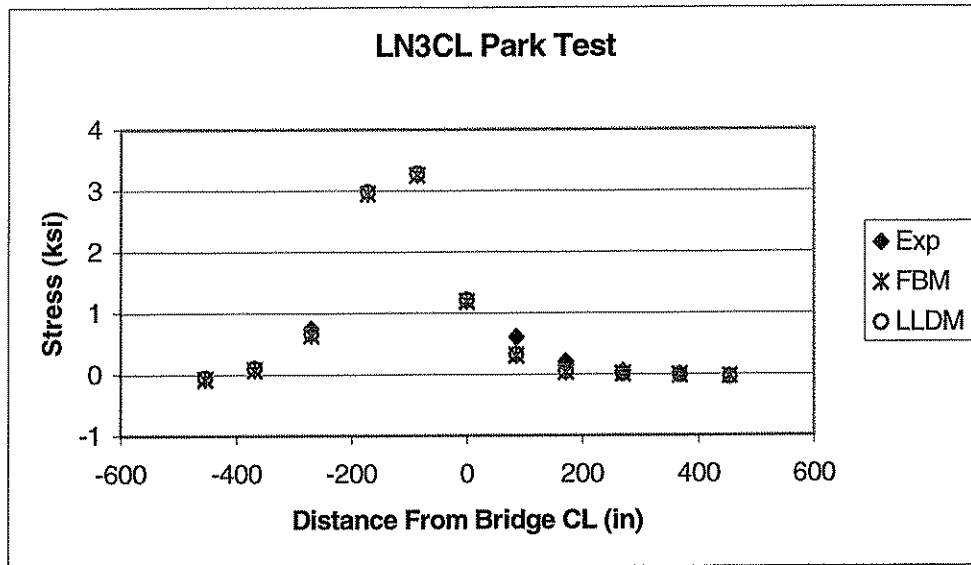
Figure 5.8. FBM – Stringer bottom flange and upper chord bottom web stresses at the center of span between U16 and U18 for a park test in Lane 3 with the centerline of the truck's back axles centered over the center of span between U16 and U18.

114
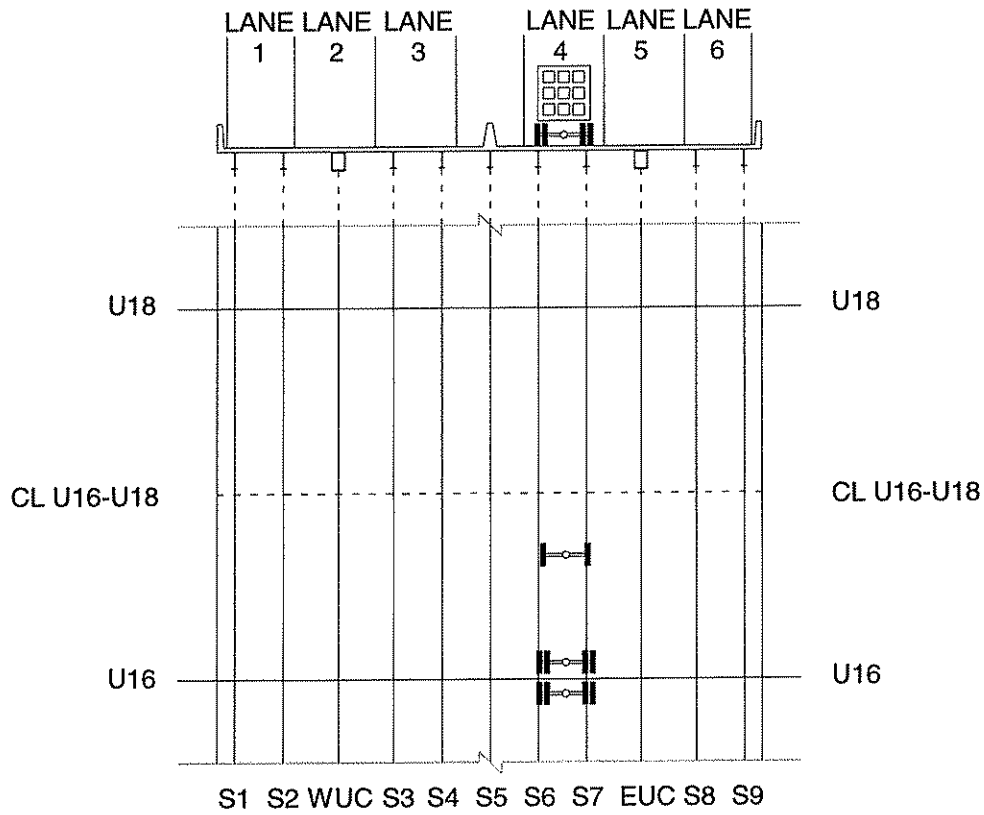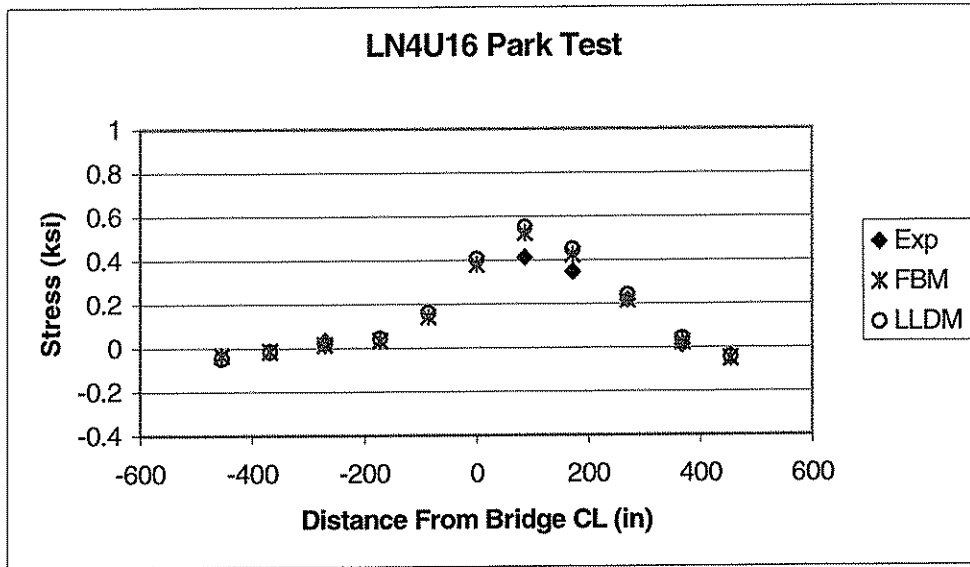
Figure 5.9. FBM – Stringer bottom flange and upper chord bottom web stresses at the center of span between U16 and U18 for a park test in Lane 4 with the centerline of the truck's back axles centered 18 in. north of U16.
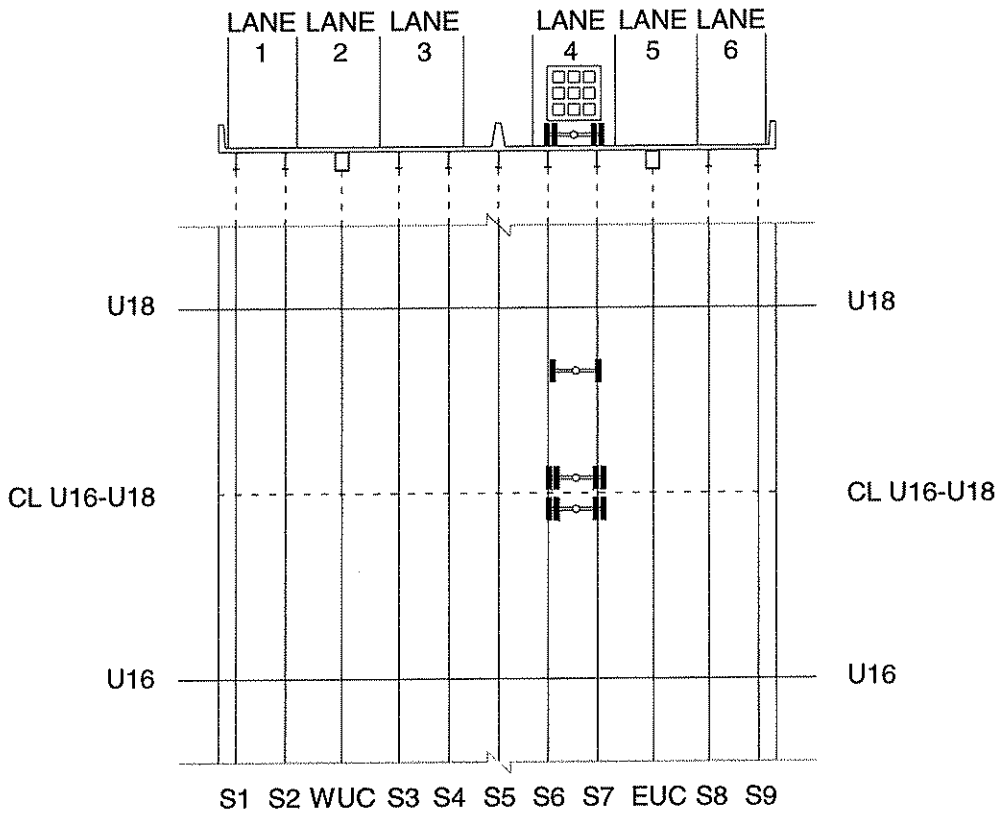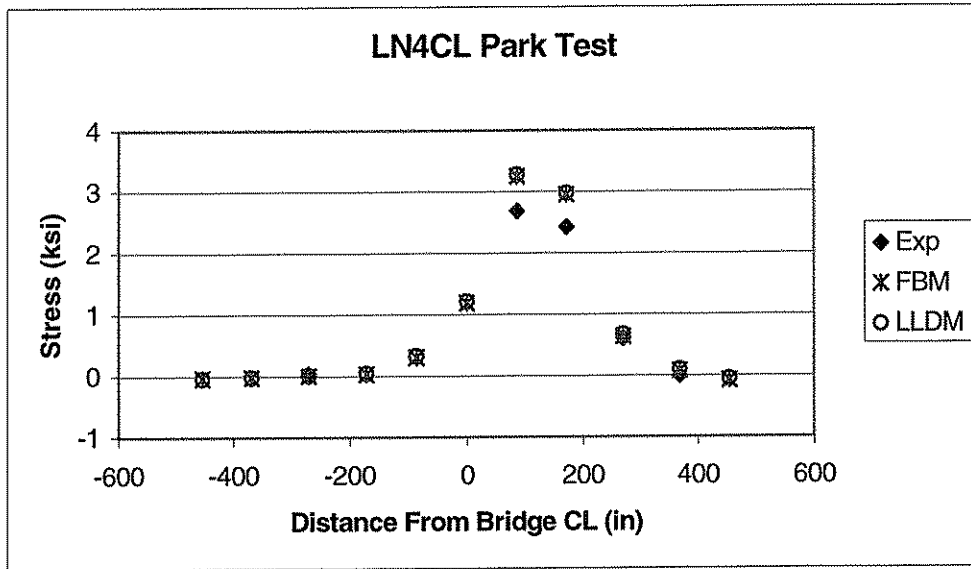
Figure 5.10. FBM – Stringer bottom flange and upper chord bottom web stresses at the center of span between U16 and U18 for a park test in Lane 4 with the centerline of the truck's back axles centered over the center of span between U16 and U18.

116
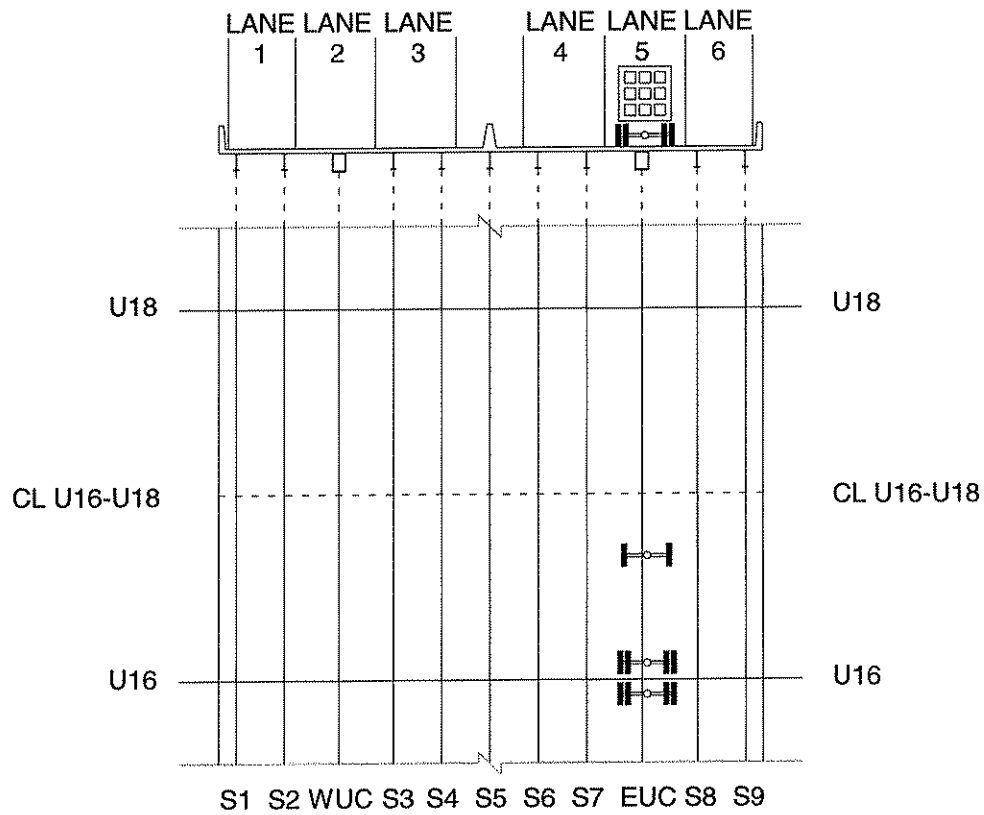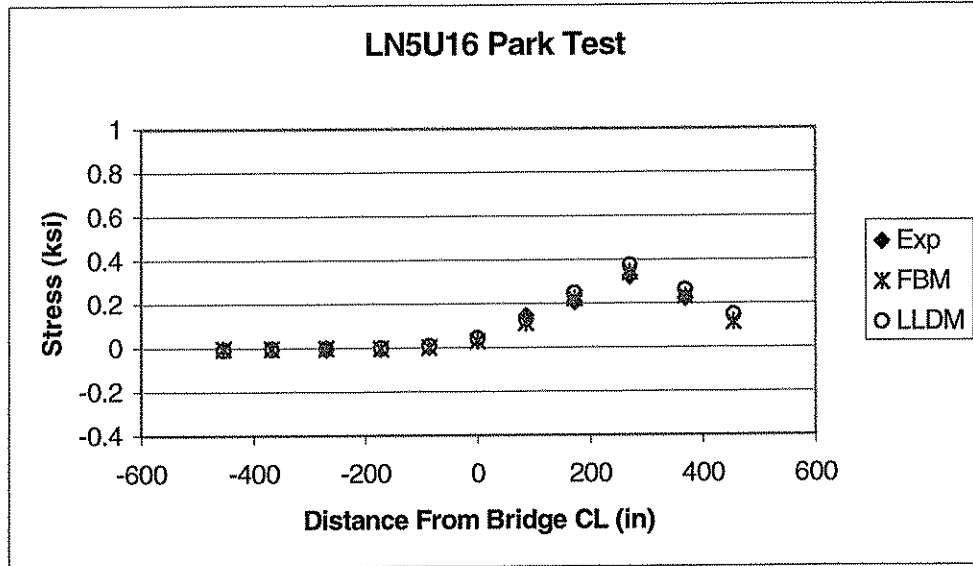
Figure 5.11. FBM – Stringer bottom flange and upper chord bottom web stresses at the center of span between U16 and U18 for a park test in Lane 5 with the centerline of the truck's back axles centered 18 in. north of U16.
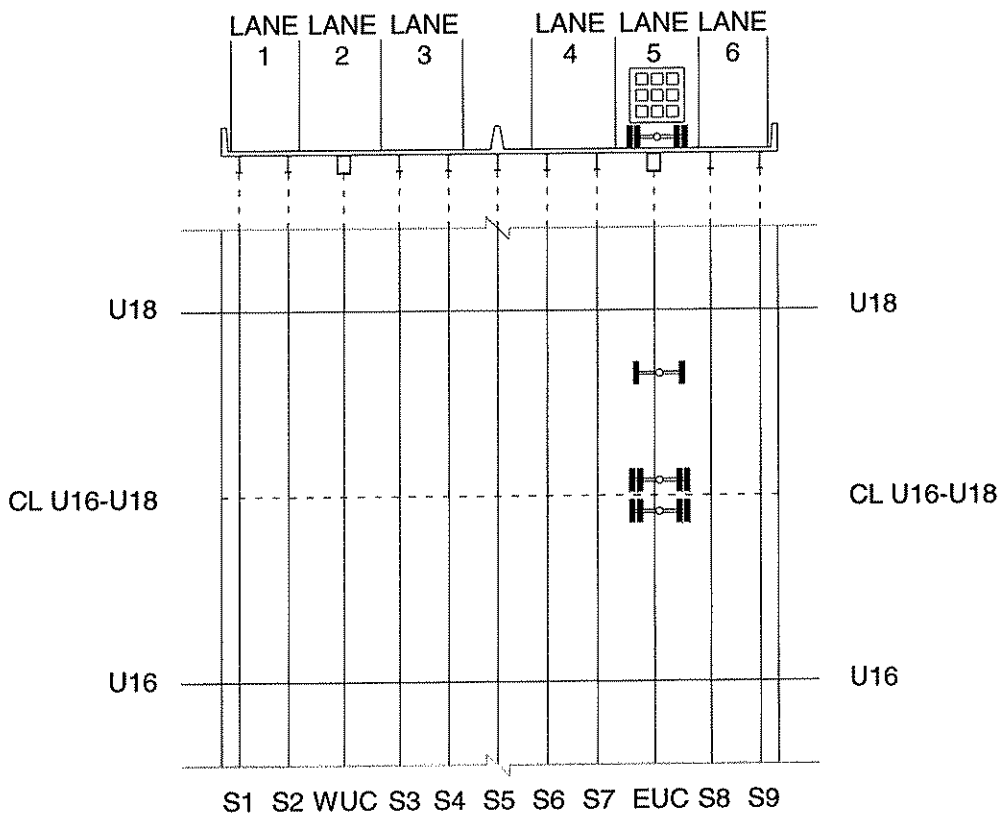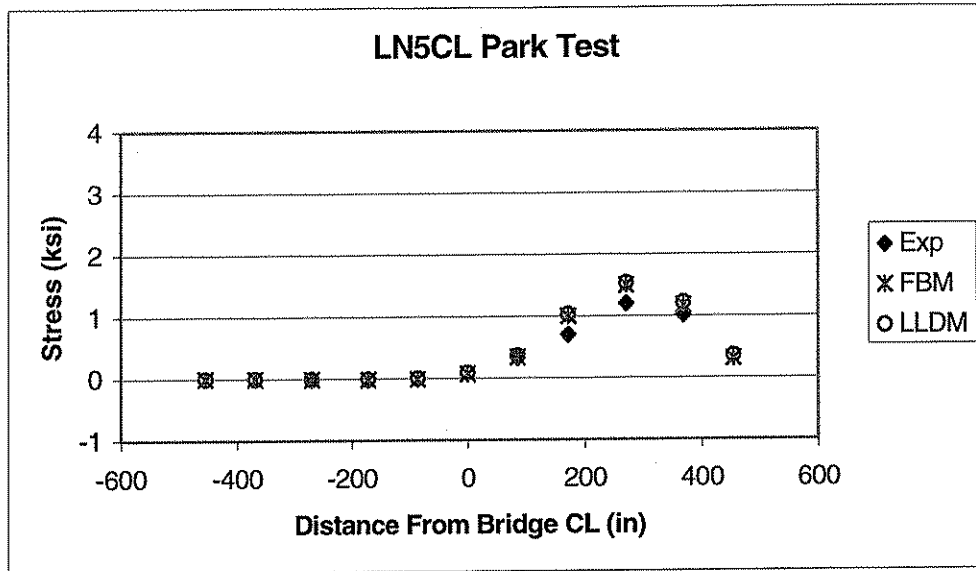
Figure 5.12. FBM – Stringer bottom flange and upper chord bottom web stresses at the center of span between U16 and U18 for a park test in Lane 5 with the centerline of the truck's back axles centered over the center of span between U16 and U18.

118
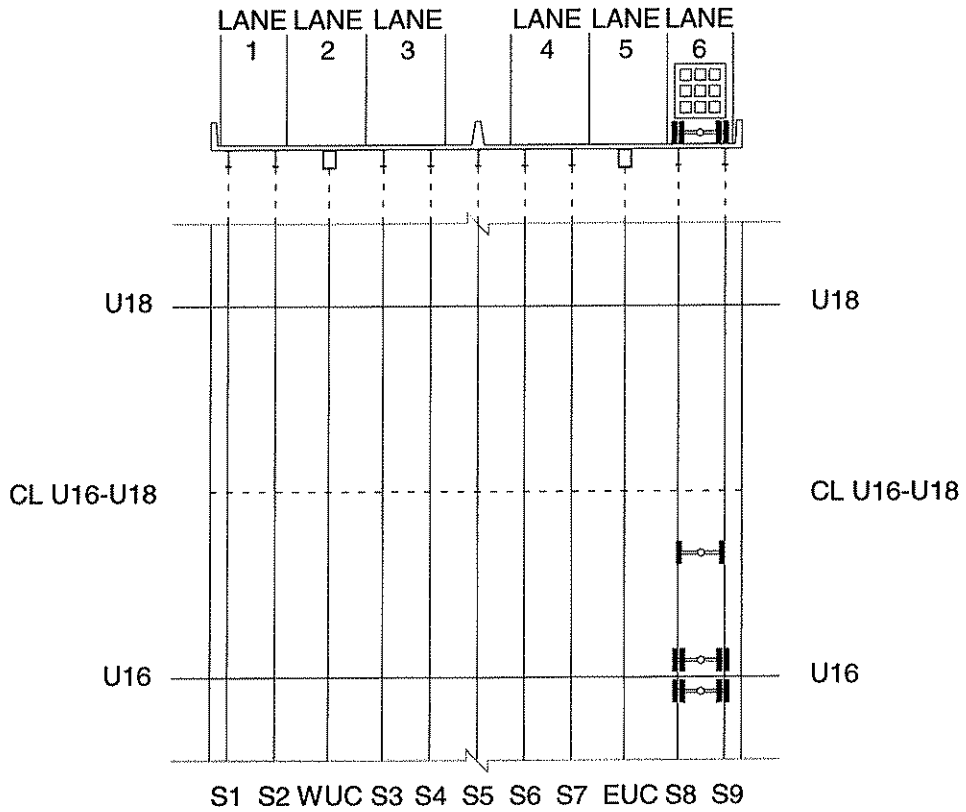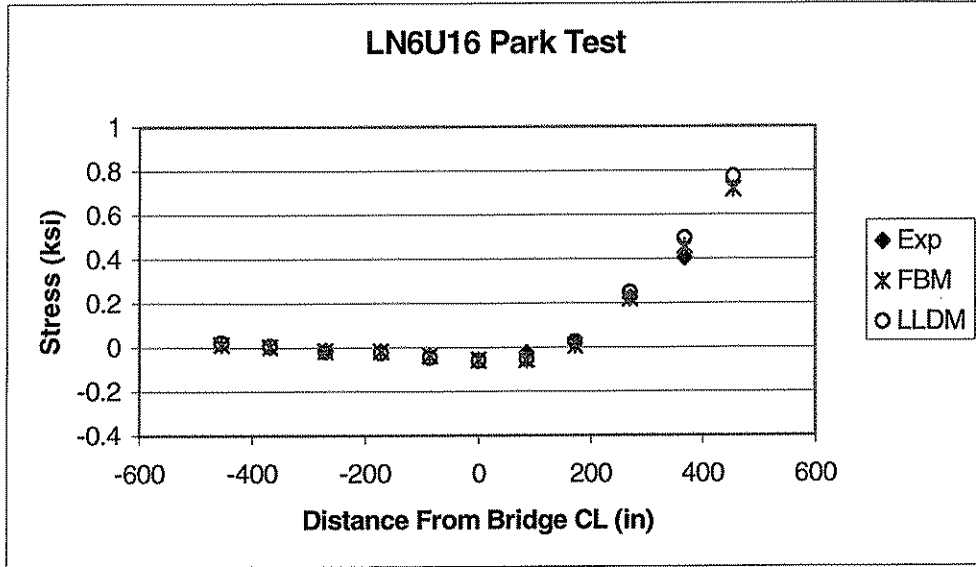
Figure 5.13. FBM – Stringer bottom flange and upper chord bottom web stresses at the center of span between U16 and U18 for a park test in Lane 6 with the centerline of the truck's back axles centered 18 in. north of U16.

119
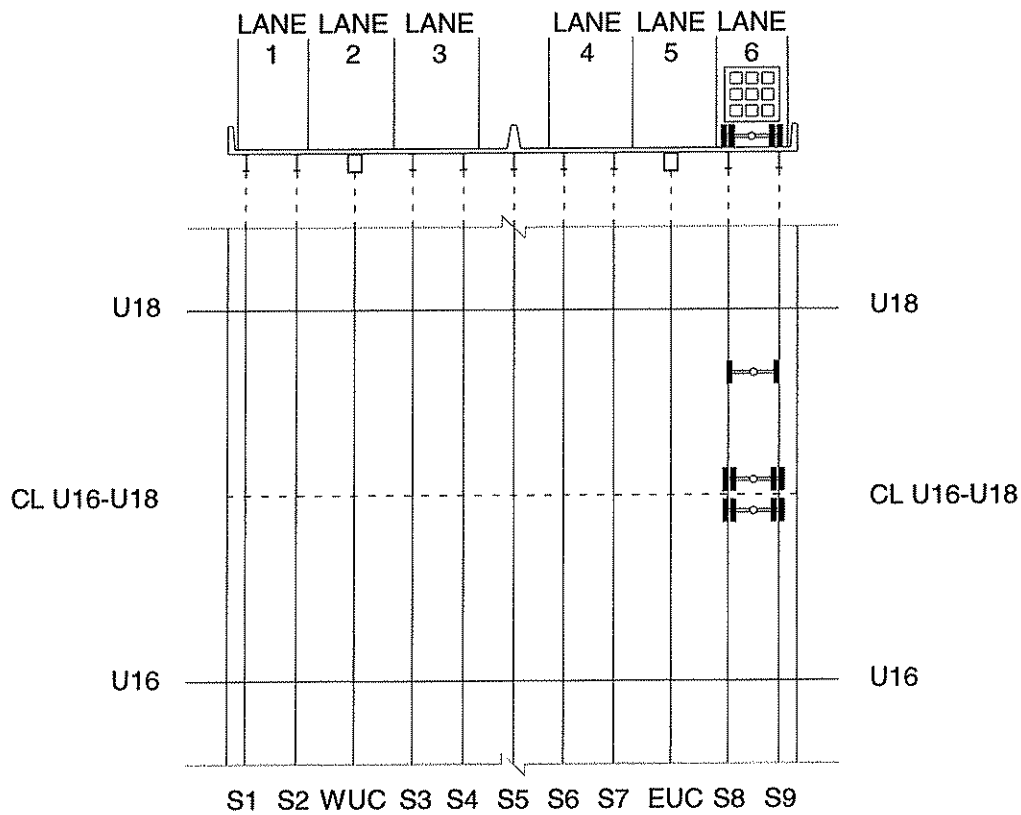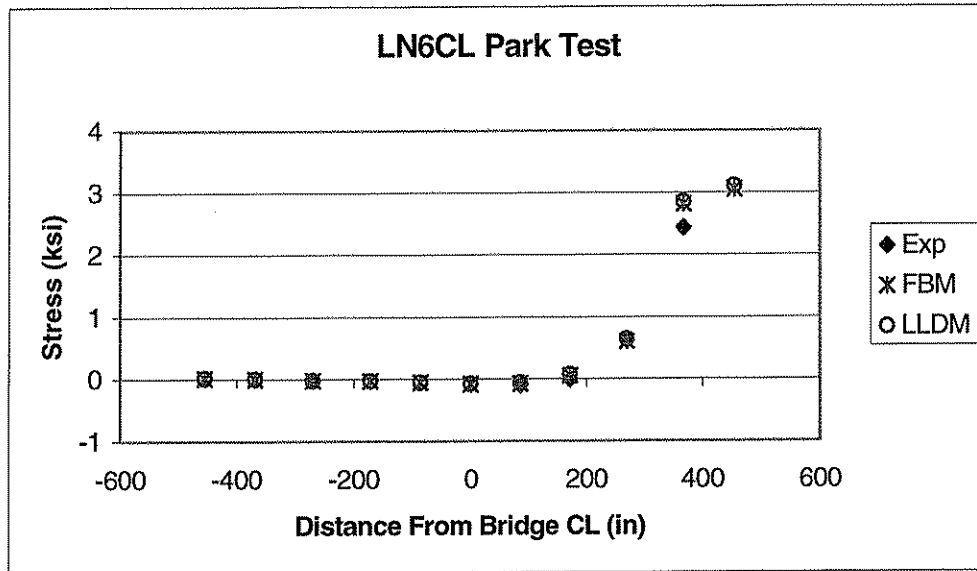
Figure 5.14. FBM – Stringer bottom flange and upper chord bottom web stresses at the center of span between U16 and U18 for a park test in Lane 6 with the centerline of the truck's back axles centered over the center of span between U16 and U18.

120

CHAPTER 6
DESIGN ASSUMPTION COMPARISONS

6.1 INTRODUCTION

This chapter compares design assumptions, experimental results, and analytical results. A discussion follows each comparison.

6.2 LATERAL LOAD DISTRIBUTION FACTORS

As explained in Chapter 2, the steel stringers supporting the reinforced concrete bridge deck were designed in accordance with AASHTO distribution factors. Table 2.1 contains excerpted information from the AASHTO Specifications used to design these members.

Table 2.1 stipulates that for a concrete floor system supported by steel I-beam stringers and a design for two or more lanes, the distribution of wheel loads is S/5.5 for interior members, where S is the average member spacing in feet. The average member spacing for this bridge cross-section was 7.57 ft. Therefore, the above S/5.5 gives a distribution factor of 1.38 for each interior steel stringer at the worst load case, which is assumed to be an all-lanes-loaded condition. For this exercise, the upper chord members of the truss were treated as interior stringers only to provide the correct average spacing (S) value. A code provision does not exist in AASHTO's Table 3.23.1 for such small box girders relative to the size of the bridge deck cross section. Therefore, the members were designed as explained in Chapter 2. As a point of interest however, the interior member distribution value of 1.38 will be compared to the analytical value obtained for these members.

Table 2.1 also stipulates that for a concrete floor system supported by four or more steel stringers, the distribution of wheel loads is S/(4.0 + 0.25*S) for exterior members, where S is the average member spacing in feet. The above S/(4.0 + 0.25*S) gives a distribution factor of 1.28 for the worst load case, which is for an all-lanes-loaded condition.

6.2.1 Experimental and Analytical Result Support

The experimental results related to lateral load distribution are presented in Section 3.5 of this report. These results represent the stress distribution on the bottom flange of each steel member in the deck cross-section between U16 and U18 caused by various park tests conducted during controlled load testing of the bridge. The results were compared to analytical data from both the lateral load distribution model and the full bridge model to be sure that they correlated. This data was found to be mostly consistent.

6.2.2 Lateral Load Distribution Model Lateral Load Distribution

The lateral load distribution model lateral load distribution findings are presented in Table 6.1. These distribution factors were computed for a truck in each lane as suggested in Section 2.3. A linear stress distribution was assumed across each member and the moment in the member was computed utilizing a

calculated neutral axis depth and moment of inertia. The neutral axis depth was calculated using known section properties and then compared to the in-service neutral axis depth from ATLSS Report 02-07. The values were found to be consistent. The fraction that each moment in each member represented of the total moment imposed by the load case on the cross-section was then computed. This value is the distribution factor for that member and specific load case. The distribution factors computed for each member due to each truck loading were then summed to represent a load case where all lanes were loaded. This resulted in the values reported for each member in the "All Lanes Loaded" column of Table 6.1.

It is important to note that the lateral load distribution for Lane 1, noted as LN1CL(OP6) in the table, is taken as the mirror image of the distribution for Lane 6. This was a result of having no experimental data, and therefore no analytical load cases, for loads in Lane 1. It was appropriate to assume a Lane 1 distribution mirrored to a Lane 6 distribution because the results of the analytical model are symmetric about the longitudinal centerline of the model in every other case.

It is also important to note that the distributions presented are only for the load cases that were positioned at the centerline of the span between U16 and U18 (at 27 ft. north of U16). The load cases centered 18 in. north of U16 were not included in the lateral load distribution factor results because the loads in the span for these load cases were not of great magnitude. Therefore a reliable lateral load distribution from these cases was not attainable. Rather, the results from these load cases were utilized in this research to provide more data that were compared to experimental results to prove the accuracy of the finite element models.

A modification to the lateral load distribution factors presented in Table 6.1 was necessary prior to comparison with the distribution factors given by the AASHTO Specifications. Table 6.2 presents the lateral load distribution factors that are compared to the AASHTO distribution factors.

In order to compare the lateral distribution values obtained in Table 6.1 to the AASHTO values, the values in Table 6.1 had to be multiplied by a factor of 2. This is a result of one truck loading being equal to two wheel loadings. Figure 6.1 presents the difference in loading methods and the equivalence of one to the other. The AASHTO values were computed per wheel load, whereas the analytical values were computed per truck load. The disparity in computational methods is solved by increasing the values obtained per truck load by a factor of 2 to represent factors per wheel load.

Table 6.2 presents the final lateral load distribution factors per sets of two wheel loads per load case. The distribution factors for each member due to each load case are added to represent the distribution factor for an all-lanes-loaded condition. This was also done in Table 6.1. Note that each value in Table 6.1 is half of the corresponding value from Table 6.2.

It is inappropriate to consider the values presented in Table 6.2 for each member and individual load case to be the distribution factor that would be

attained from one wheel load. This is true because there are two wheel loads considered per load case and the wheel loads are spaced to represent the actual spacing of wheel loads on the structure. However, it is appropriate to add the factors obtained for each load case to represent an all-lanes-loaded condition. This addition is what is presented in the last column of Table 6.2, and only these values are compared to the AASHTO distribution factors.

The lateral load distribution factor results for an all-lanes-loaded condition in Table 6.2 contain some key characteristics. First, they are perfectly symmetric about the longitudinal centerline of the bridge. Second, the calculated distribution factor for exterior Stringers S1 and S9 is reported as 0.95, which indicates that the AASHTO distribution factor of 1.28 is conservative. Third, the calculated distribution factors for interior Stringers S2 through S8 are reported in a range from 0.40 to 0.72, which indicates that the AASHTO distribution factor of 1.38 is conservative. Finally, the calculated distribution factor for the west and east upper chords, WUC and EUC respectively, is reported as 2.75, which would indicate that the AASHTO distribution factor of 1.38 is unconservative if the upper chord box sections were designed as were their adjacent I-beam stringers.

There is no need for alarm as a result of this last finding (distribution factor of 2.75 versus 1.38 for EUC and WUC) because special attention was given to the upper chord members during design as noted in Chapter 2. The AASHTO distribution factors were derived assuming that all of the stringers in a deck cross-section were evenly spaced and were of the same size cross-section (Newmark, 1948). The distribution value obtained for the upper chord box sections in this research is compared to the AASHTO distribution value given for interior I-beam stringers to point out that when stringers are not all of the same relative size and stiffness, the stiffer members attract more load than the more flexible members.

6.2.3 Full Bridge Model Lateral Load Distribution

The full bridge model lateral load distribution findings are presented in Table 6.3. These distribution factors were computed for a truck in each lane as suggested in Section 2.3. A linear stress distribution was assumed across each member and the moment in the member was computed utilizing a calculated neutral axis depth and moment of inertia. The neutral axis depth was calculated using known section properties and then compared to the in-service neutral axis depth from ATLSS Report 02-07. The values were found to be consistent. The fraction that each moment in each member represented of the total moment imposed by the load case on the cross-section was then computed. This value is the distribution factor for that member and specific load case. The distribution factors computed for each member due to each truck loading were then summed to represent a load case where all lanes were loaded. This resulted in the values reported for each member in the "All Lanes Loaded" column of Table 6.3.

It is important to note that the lateral load distribution for Lane 1, noted as LN1CL(OP6) in the table, is taken as the mirror image of the distribution for Lane 6. This was a result of having no experimental data, and therefore no analytical

load cases, for loads in Lane 1. It was appropriate to assume a Lane 1 distribution mirrored to a Lane 6 distribution because the results of the analytical model are symmetric about the longitudinal centerline of the model in every other case.

It is also important to note that the distributions presented are only for the load cases that were positioned at the centerline of the span between U16 and U18 (at 27 ft. north of U16). The load cases centered 18 in. north of U16 were not included in the lateral load distribution factor results because the loads in the span for these load cases were not of great magnitude. Therefore a reliable lateral load distribution from these cases was not attainable. Rather, the results from these load cases were utilized in this research to provide more data that were compared to experimental results to prove the accuracy of the finite element models.

A modification to the lateral load distribution factors presented in Table 6.3 was necessary prior to comparison with the distribution factors given by the AASHTO Specifications. Table 6.4 presents the lateral load distribution factors that are compared to the AASHTO distribution factors.

In order to compare the lateral distribution values obtained in Table 6.3 to the AASHTO values, the values in Table 6.3 had to be multiplied by a factor of 2. This is a result of one truck loading being equal to two wheel loadings. Figure 6.1 presents the difference in loading methods and the equivalence of one to the other. The AASHTO values were computed per wheel load, whereas the analytical values were computed per truck load. The disparity in computational methods is solved by increasing the values obtained per truck load by a factor of 2 to represent factors per wheel load.

Table 6.4 presents the final lateral load distribution factors per sets of two wheel loads per load case. The distribution factors for each member due to each load case are added to represent the distribution factor for an all-lanes-loaded condition. This was also done in Table 6.3. Note that each value in Table 6.3 is half of the corresponding value from Table 6.4.

It is inappropriate to consider the values presented in Table 6.4 for each member and individual load case to be the distribution factor that would be attained from one wheel load. This is true because there are two wheel loads considered per load case and the wheel loads are spaced to represent the actual spacing of wheel loads on the structure. However, it is appropriate to add the factors obtained for each load case to represent an all-lanes-loaded condition. This addition is what is presented in the last column of Table 6.4, and only these values are compared to the AASHTO distribution factors.

The lateral load distribution factor results for an all-lanes-loaded condition in Table 6.4 contain some key characteristics. First, they are perfectly symmetric about the longitudinal centerline of the bridge. Second, the calculated distribution factor for exterior Stringers S1 and S9 is reported as 0.93, which indicates that the AASHTO distribution factor of 1.28 is conservative. Third, the calculated distribution factors for interior Stringers S2 through S8 are reported in a range from 0.41 to 0.75, which indicates that the AASHTO distribution factor of

1.38 is conservative. Finally, the calculated distribution factor for the west and east upper chords, WUC and EUC respectively, is reported as 2.71, which would indicate that the AASHTO distribution factor of 1.38 is unconservative if the upper chord box sections were designed as were their adjacent I-beam stringers.

There is no need for alarm as a result of this last finding (distribution factor of 2.71 versus 1.38 for WUC and EUC) because special attention was given to the upper chord members during design as noted in Chapter 2. The AASHTO distribution factors were derived assuming that all of the stringers in a deck cross-section were evenly spaced and were of the same size cross-section (Newmark, 1948). The distribution value obtained for the upper chord box sections in this research is compared to the AASHTO distribution value given for interior I-beam stringers to point out that when stringers are not all of the same relative size and stiffness, the stiffer members attract more load than the more flexible members.

6.2.4 Comparison of Experimental, Analytical, and Design Values

Table 6.5 presents a comparison of load distribution factors. The lateral load distribution factors used to design the stringers supporting the reinforced concrete deck were found to be conservative. Design load distribution factors of 1.28 and 1.38 were used for exterior and interior stringers respectively.

These values were greater than the load distribution factors computed based on analytical results for the stringer members. However, they were lower than the load distribution factors computed based on analytical results for the upper chord members. These members were designed as explained in Chapter 2. Therefore, no alarm should be raised by this result.

The results of the analytical models correlate with the experimental results presented in Chapter 3. Therefore they are taken as the actual distribution of loading on the bridge deck.

6.2.5 Discussion

The actual lateral load distribution for fully composite decks systems such as that of the SR 33 Lehigh River Bridge can be determined efficiently though use of finite element modeling. The lateral load distribution factors calculated for this research from analytical finite element results were calculated for a specific cross-section of the bridge deck where previously collected experimental data was taken. The results of experimental controlled load testing were in reasonably good agreement with the results of the analytical finite element models developed during this research. It is reasonable to suggest that the lateral load distribution factors reported in Chapter 6 are generally valid in every span due to the repetitive geometry found in this bridge.

It was found that a relatively small section of the bridge structure was required to produce a good estimate of the actual lateral load distribution on the bridge deck. The results of the lateral load distribution model demonstrate that the lateral load distribution factors for this model are in agreement with the lateral load distribution factors calculated from the results of the full bridge model. As

long as the correct boundary conditions are applied to the smaller and less complicated finite element model, accurate lateral load distribution factors can be attained.

The design assumption related to the lateral load distribution on the bridge deck over-estimated the distribution factors applicable to the stringers incorporated into the composite bridge deck structure. This was a direct result of the presence in the deck cross-section of the upper chord box sections, which are much stiffer than the stringer sections. Thus the AASHTO distribution factors, which are simple to obtain and apply, are a reasonable and conservative approach for design.

The upper chord box sections were not designed utilizing the AASHTO distribution factors because this process would have been unconservative. These members were given special consideration during design as explained in Chapter 2. However, it should be noted that the distribution factor for the upper chord box sections given as a result of this research clearly shows that a member with a relatively greater stiffness than its adjoining members will tend to attract more load.

6.3   DIAGONAL TRUSS MEMBER TWO-DIMENSIONAL DESIGN

As discussed in Chapter 2, a two-dimensional truss model was utilized to design the diagonal truss members. One ramification of this two-dimensional design was that it neglected possible out-of-plane bending in the diagonal members of the truss system.

6.3.1   Experimental and Analytical Result Support

The experimental results related to the diagonal members are presented in Section 3.6 of this report. The plots referenced in this section show that when a load is placed in a position other than directly above the truss line, an out-of-plane bending component is seen to locally affect the diagonal member response. This effect varies in magnitude with the intensity of the load.

These results were obtained from crawl tests conducted on the structure. They are not the result of a static bridge loading, and therefore will not be compared directly to a static loading condition. Instead, the behavior exhibited in the experimental data is compared to behavior found in the analytical results gathered from the full bridge model. This comparison is made in Section 6.3.3.

6.3.2   Three-Dimensional Model Results

The full bridge model was utilized to produce the results related to this design assumption and presented in Section 5.6 of this report. Table 5.2 contains the results collected from diagonal members L19-U20, U20-L21, L23-U24, and U24-L25.

In all cases, these results show that an out-of-plane bending stress exists in the diagonal members when a load is placed inside or outside of a longitudinal truss line. The response is local because this out-of-plane stress only exists if the load is placed in the vicinity of the upper node of any diagonal in question.

126

The out-of-plane bending stress, when present, was shown to be significant relative to the magnitude of in-plane bending and axial stresses in the member.

6.3.3 Comparison of Experimental, Analytical, and Design Values

The two-dimensional model utilized for the diagonal truss member design did not account for out-of-plane stresses induced in the members because it, by nature, did not have this capability. Therefore this out-of-plane bending stress was overlooked by the two-dimensional model.

The experimental results from crawl tests conducted on the bridge deck showed that there was a noticeable out-of-plane bending stress in the diagonal members. This effect was deemed to be local, because the action of the instrumented members was predominantly axial except for when the moving load passed directly over the members. The full bridge model was utilized to demonstrate similar characteristic behavior.

Static loading cases described in Section 5.2.3 were applied to the full bridge model to capture the local out-of-plane bending effect seen in the diagonal truss members. This phenomenon was exhibited and the pertinent analysis results were presented in Table 5.2. The out-of-plane bending stress results were low in magnitude, but tended to be significant relative to the in-plane bending and axial stresses in a given locally affected diagonal member.

The longitudinal truss lines were therefore shown by the experimental and analytical data to exhibit localized out-of-plane bending stresses that were not considered by the two-dimensional model used to design the diagonal truss members.

6.3.4 Discussion

The design assumption related to the use of a two-dimensional analytical model to design the truss members did not consider the possibility of out-of-plane bending stresses in the diagonal members. Local out-of-plane bending stresses exist in the diagonal truss members of the SR 33 Lehigh River Bridge. The experimental and analytical studies performed on this structure show that out-of-plane bending stresses are caused as a load passes over the members. The stresses are low in magnitude, but are significant relative to the in-plane bending and axial stresses, sometimes representing as much as 50% of the axial stress value.

6.4 GLOBAL DECK PARTICIPATION

As explained in Chapter 2, a two-dimensional truss model was utilized to design the truss members. A ramification of this design assumption is that the two-dimensional model did not account for the ability of the steel stringers and composite reinforced concrete deck outside of the assumed 112 in. effective deck width to carry a globally induced load.

127

6.4.1 Experimental and Analytical Result Support

The experimental results related to the bridge deck components are presented in Section 3.6 of this report. The plots referenced for the steel stringers and embedded gages located 27 ft. north of U16 show that when a load is placed out in Span 2 between Piers 2 and 3, a global tension stress results in these members. This phenomenon was also seen to be true for the upper chord members in the same cross-section. Table 3.1 presents the global tension stress in the composite deck cross-section due to a crawl test. The stress results were shown to be small in magnitude, but the cross section over which they act is large. This means that there is a significant amount of load carried by the composite deck as all components act together to resist a global load.

These results were obtained from crawl tests conducted on the structure. They are not the result of a static bridge loading, and therefore will not be compared directly to a static loading condition. Instead, the behavior exhibited in the experimental data is compared to behavior found in the analytical results gathered from the full bridge model. This comparison is made in Section 6.4.3.

6.4.2 Three-Dimensional Model Results

The full bridge model was utilized to produce the results related to this design assumption ramification and was presented in Section 5.7 of this report. Table 5.3 contains the results collected from each member in the deck cross-section at a location 27 ft. north of U16 subjected to a loading (as characterized in Section 5.2.3) in Span 2.

Each member in the cross-section was shown in Table 5.3 to carry a tension stress of 0.08 to 0.09 ksi due to this loading. This means that the components of the cross-section worked together to carry a large tension force, evenly distributing the stress and strain associated with this force across the cross-section. The results indicate that for a loading in Span 2 evenly applied to both truss lines, the entire deck cross-section above Pier 2 in the negative moment region 27 ft. north of U16 is effective.

6.4.3 Comparison of Experimental, Analytical, and Design Values

The two-dimensional model utilized for truss member design only accounted for a 112 in. effective deck width above each longitudinal truss line. The global participation of the composite reinforced concrete deck and steel stringers outside this effective width was not considered. Therefore this tremendous area over which to distribute load was not considered.

The focus of this discussion surrounds the experimental results from the negative moment region above Pier 2. These results were from crawl tests conducted on the bridge deck and showed that there was a noticeable amount of global tension across the entire composite deck structure.

A static load case described in Section 5.2.3 was applied to the full bridge model to capture the global tension effect seen in the deck cross-section located 27 ft. north of U16. This phenomenon was exhibited and the pertinent analysis

128

results were presented in Table 5.3. The global tension stress results were low in magnitude, but did exist.

The entire deck cross-section in the negative moment region above Pier 2 was therefore shown by the experimental and analytical data to exhibit global tension stresses that were not considered by the two-dimensional model used to design the truss members.

6.4.4 Discussion

The design assumption related to the use of a two-dimensional analytical model to design the truss members did not consider the ability of the entire deck structure to carry global forces. The experimental and analytical studies performed on this structure show that when a load placed at the center of Span 2 is evenly applied to the two longitudinal truss lines of the SR 33 Lehigh River Bridge, the entire composite deck structure above Pier 2 is effective in carrying this load. This was observed as an evenly distributed tension strain and the resulting stress distribution on all members in the cross-section. The entire composite deck is behaving as a large top flange for the truss structure.

Member Name	LN1CL (OP6)	LN2CL	LN3CL	LN4CL	LN5CL	LN6CL	All Lanes
S1	0.44	0.04	0.00	0.00	0.00	0.00	0.47
S2	0.25	0.11	0.00	0.00	0.00	0.00	0.36
WUC	0.32	0.72	0.34	0.00	0.00	0.00	1.38
S3	0.00	0.10	0.26	0.00	0.00	0.00	0.36
S4	0.00	0.03	0.27	0.03	0.00	0.00	0.33
S5	0.00	0.00	0.10	0.10	0.00	0.00	0.20
S6	0.00	0.00	0.03	0.27	0.03	0.00	0.33
S7	0.00	0.00	0.00	0.26	0.10	0.00	0.36
EUC	0.00	0.00	0.00	0.34	0.72	0.32	1.38
S8	0.00	0.00	0.00	0.00	0.11	0.25	0.36
S9	0.00	0.00	0.00	0.00	0.04	0.44	0.47
Truck Loads	1.00	1.00	1.00	1.00	1.00	1.00	6.00

Table 6.1. Lateral load distribution model lateral load distribution factors for truck loads.

Member Name	LN1CL (OP6)	LN2CL	LN3CL	LN4CL	LN5CL	LN6CL	All Lanes
S1	0.87	0.07	0.00	0.00	0.00	0.00	0.95
S2	0.50	0.22	0.00	0.00	0.00	0.00	0.72
WUC	0.63	1.44	0.68	0.00	0.00	0.00	2.75
S3	0.00	0.19	0.52	0.00	0.00	0.00	0.72
S4	0.00	0.07	0.54	0.05	0.00	0.00	0.67
S5	0.00	0.00	0.20	0.20	0.00	0.00	0.40
S6	0.00	0.00	0.05	0.54	0.07	0.00	0.67
S7	0.00	0.00	0.00	0.52	0.19	0.00	0.72
EUC	0.00	0.00	0.00	0.68	1.44	0.63	2.75
S8	0.00	0.00	0.00	0.00	0.22	0.50	0.72
S9	0.00	0.00	0.00	0.00	0.07	0.87	0.95
Wheel Loads	2.00	2.00	2.00	2.00	2.00	2.00	12.00

Table 6.2. Lateral load distribution model lateral load distribution factors for wheel loads.

Member Name	LN1CL (OP6)	LN2CL	LN3CL	LN4CL	LN5CL	LN6CL	All Lanes
S1	0.43	0.04	0.00	0.00	0.00	0.00	0.46
S2	0.26	0.11	0.00	0.00	0.00	0.00	0.37
WUC	0.31	0.72	0.33	0.00	0.00	0.00	1.35
S3	0.00	0.10	0.26	0.00	0.00	0.00	0.36
S4	0.00	0.04	0.28	0.03	0.00	0.00	0.34
S5	0.00	0.00	0.10	0.10	0.00	0.00	0.21
S6	0.00	0.00	0.03	0.28	0.04	0.00	0.34
S7	0.00	0.00	0.00	0.26	0.10	0.00	0.36
EUC	0.00	0.00	0.00	0.33	0.72	0.31	1.35
S8	0.00	0.00	0.00	0.00	0.11	0.26	0.37
S9	0.00	0.00	0.00	0.00	0.04	0.43	0.46
Truck Loads	1.00	1.00	1.00	1.00	1.00	1.00	6.00

Table 6.3. Full bridge model lateral load distribution factors for truck loads.

Member Name	LN1CL (OP6)	LN2CL	LN3CL	LN4CL	LN5CL	LN6CL	All Lanes
S1	0.86	0.07	0.00	0.00	0.00	0.00	0.93
S2	0.52	0.23	0.00	0.00	0.00	0.00	0.75
WUC	0.62	1.43	0.65	0.00	0.00	0.00	2.71
S3	0.00	0.20	0.53	0.00	0.00	0.00	0.73
S4	0.00	0.07	0.56	0.06	0.00	0.00	0.68
S5	0.00	0.00	0.21	0.21	0.00	0.00	0.41
S6	0.00	0.00	0.06	0.56	0.07	0.00	0.68
S7	0.00	0.00	0.00	0.53	0.20	0.00	0.73
EUC	0.00	0.00	0.00	0.65	1.43	0.62	2.71
S8	0.00	0.00	0.00	0.00	0.23	0.52	0.75
S9	0.00	0.00	0.00	0.00	0.07	0.86	0.93
Wheel Loads	2.00	2.00	2.00	2.00	2.00	2.00	12.00

Table 6.4. Full bridge model lateral load distribution factors for wheel loads.

Member Name	AASHTO Specification	Lateral Load Distribution Model	Full Bridge Model
S1	1.28	0.95	0.93
S2	1.38	0.72	0.75
WUC	1.38	2.75	2.71
S3	1.38	0.72	0.73
S4	1.38	0.67	0.68
S5	1.38	0.40	0.41
S6	1.38	0.67	0.68
S7	1.38	0.72	0.73
EUC	1.38	2.75	2.71
S8	1.38	0.72	0.75
S9	1.28	0.95	0.93

Table 6.5. Comparison of wheel load lateral distribution factors resulting from the AASHTO Specification and the analytical models created for this research.

LOADS INDUCED BY 6 TRUCK LOADS

(a)

LOADS INDUCED BY 12 WHEELS
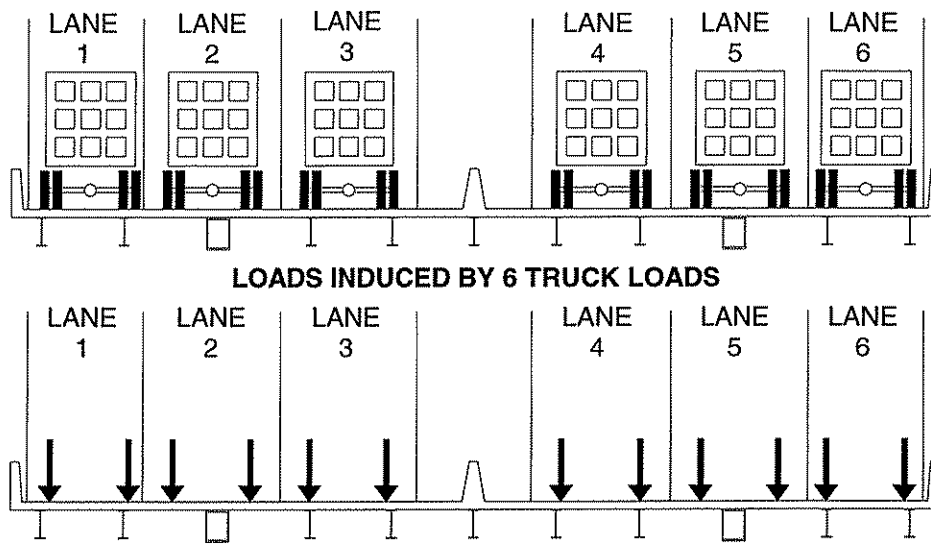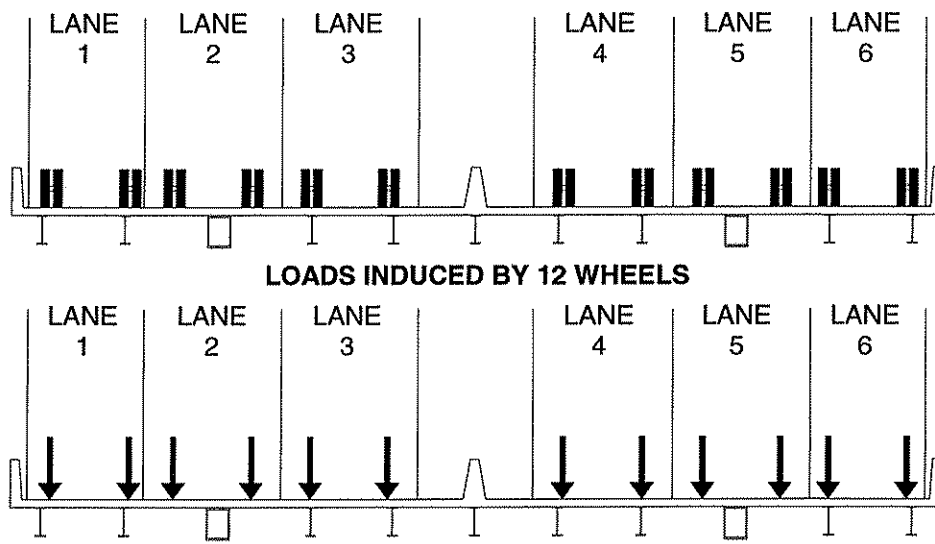
(b)

Figure 6.1. Loading configurations: (a) truck loading; (b) wheel loading.

133

CHAPTER 7
CONCLUSIONS AND FUTURE RESEARCH

7.1 INTRODUCTION

The objective of this research was to evaluate some of the key design assumptions used in the design of the SR 33 Lehigh River Bridge and report on their validity. In order to do this, two of the design assumptions used by URS Corporation to design the bridge were chosen for further study.

The conclusions directly addressing the two design assumptions chosen for study are presented first in Section 7.2. Additional general conclusions based on this research are presented in Section 7.3. Finally, topics for future research are discussed in Section 7.4.

7.2 DESIGN ASSUMPTION CONCLUSIONS

The conclusions directly addressing the two design assumptions chosen for study are the following:

1. The AASHTO distribution factors used to determine the lateral load distribution on the bridge deck were found to be conservative with respect to the stringers incorporated into the composite bridge deck structure.

2. Local out-of-plane bending stresses exist in the diagonal truss members of the SR 33 Lehigh River Bridge. The stresses are low in magnitude, but are significant relative to the live load in-plane bending and axial stresses, sometimes representing as much as 50% of the axial stress value.

3. The entire composite deck structure in the negative moment region of the truss system above Pier 2 was found to be effective in carrying global load cases placed at the center of Span 2. This was observed as an evenly distributed tension strain and the resulting stress distribution on all members in the cross-section.

7.3 GENERAL CONCLUSIONS

The general conclusions based on the results of this research are the following:

1. The results of the finite element analyses of the bridge were in reasonably good agreement with the results of the experimental controlled load tests.

2. If the experimental results are taken as an indication of the *actual* lateral distribution of load for the bridge, then the lateral distribution of load in this system was determined efficiently though use of finite element modeling.

3. For the bridge treated in this study, a relatively small section of the structure (three 54 ft. spans) needed to be modeled to produce a good

134

estimate of the actual lateral load distribution on the bridge deck. The results of the lateral load distribution model demonstrate that the lateral load distribution factors for this model are in agreement with the lateral load distribution factors calculated from the results of the full bridge model. As long as the correct boundary conditions are applied to the smaller and less complicated finite element model, accurate lateral load distribution factors can be attained.

4. The specialized design of the upper chord box sections was found to be valid and of great importance. If these members were designed utilizing the AASHTO distribution factors based on the lateral spacing of members, the design would have been unconservative.

5. The AASHTO lateral load distribution factors were found to be conservative for the stringer members studied in this research.

7.4 TOPICS FOR FURTHER INVESTIGATION

The topics related to this research that require further investigation are the following:

1. The analytical work done for this research and related to lateral load distribution focused on a section of the bridge roadway directly above Pier 2 where there was little chance that relative displacement of the upper truss nodes would occur. Analytical models of this bridge structure should be developed with a refined mesh region in other important locations, such as the third points of Span 2. This would allow the study of any changes in lateral load distribution that may occur do to global truss displacement.

2. Analytical results from this research and related experimental results were able to characterize out-of-plane bending stresses that exist as a local effect in the diagonal members of the truss system. Further analytical modeling and experimental testing should be performed to quantify the effects of this out-of-plane bending, and implications on the fatigue performance of the truss system should be examined.

3. The analytical work done in this research and related to the global participation of the composite deck structure focused on a refined finite element mesh area above Pier 2. A more refined model with the capability to characterize the global composite deck participation at many locations longitudinally along the bridge should be explored. Research related to such a model may be able to give insight into a better estimation of effective deck width for global load cases on structures such as the one studied in this research.

135

REFERENCES

American Association of State Highway and Transportation Officials, (1985) "Guide Specifications for Strength Design of Truss Bridges (Load Factor Design)."

American Association of State Highway and Transportation Officials, (1992) "Standard Specifications for Highway Bridges," 15th Ed.

Cao, C. and Shing, P., (1999) "Simplified Analysis Method for Slab-On-Girder Highway Bridge Decks," *Journal of Structural Engineering*, Vol. 125, No. 1, pp. 49-59.

Connor, R. and Santosuosso, B., (2002) "Field Measurements and Controlled Load Testing on the Lehigh River Bridge (SR-33)," Lehigh University, ATLSS Report 02-07, in preparation.

CSI, Inc., (2000) SAP 2000 Analysis Reference, August, p. 182.

Mabsout, M., Tarhini, K., Frederick, G., and Kesserwan, A., (1999) "Effect of Multilanes on Wheel Load Distribution in Steel Girder Bridges," *Journal of Bridge Engineering*, Vol. 4, No. 2, pp. 99-106.

Macioce, T., Tarquinio, J., and Connor, R., (2002) "Lehigh River Bridge Load Testing and Instrumentation," International Bridge Conference, IBC 02-59, Pittsburgh, PA, June.

Mourad, S. and Tabsh, W., (1999) "Deck Slab Stresses in Integral Abutment Bridges," *Journal of Bridge Engineering*, Vol. 4, No. 2, pp. 125-130.

Newmark, N., (1948) "Design of I-Beam Bridges," *Proceedings, ASCE*, March, pp. 305-330.

O'Connell, H. and Dexter, R., (2001) "Response and Analysis of Steel Trusses for Fatigue Truck Loading," *Journal of Bridge Engineering*, Vol. 6, No. 6, pp. 628-638.

Tarhini, K., and Frederick, G., (1992) "Wheel Load Distribution in I-Girder Highway Bridges," *Journal of Structural Engineering*, Vol. 118, No. 5, pp. 1285-1294.

Tarquinio, J., (2002) Private Correspondence, May.